Critical Thickness in Silicone Thermosets

by

Manish Deopura

Bachelor of Technology, Chemical Engineering
Indian Institute of Technology, Delhi (1997)

Master of Science, Materials Science and Engineering
Massachusetts Institute of Technology (2003)

Submitted to the Department of Materials Science and Engineering
in Partial Fulfillment for the Requirement for the Degree of

Doctor of Philosophy in Materials Science and Engineering

at the

Massachusetts Institute of Technology

February 2005

Author_____
Manish Deopura
Department of Materials Science and Engineering
January 18, 2005

Certified by_____
Frederick J. McGarry
Professor of Polymer Engineering
Thesis Advisor

Accepted by_____
Carl V. Thompson II
Stavros Salapatas Professor of Materials Science and Engineering
Chair, Departmental Committee on Graduate Students

Critical Thickness in Silicone Thermosets

by

Manish Deopura

Submitted to the department of Materials Science and Engineering
January 18, 2005
in partial fulfillment for the requirement for the
Degree of Doctor of Philosophy in Materials Science and Engineering

Abstract

Critical thickness effects are utilized to achieve high fracture toughness in brittle polymers. The postulate of critical thickness, which is: "*Macroscopically brittle polymers deform in a ductile fashion below a critical dimension*" is validated for silicone thermosets and polystyrene using novel "direct" methods by measuring failure strain in thin films.

A discussion on polymer intrinsic deformation mechanisms is presented. Using these intrinsic deformation mechanisms as bases, it is argued that all polymers are ductile at the molecular level. Accordingly, it is suggested that polymer properties below a certain length scale (defined as critical thickness) are dominated by intrinsic deformation characteristics. Two analytical models have been developed which predict critical thickness based on the physical properties of the polymer. The first model is based on an energy criterion according to which crack initiation does not take place if the crack driving force is less than the crack resistance. Such a condition for a brittle polymer is achieved at the critical thickness. The second model is based on a mechanics criterion according to which a minimum film thickness (critical thickness) is required for typical fracture features like crazes to exist within it. Further, using these theoretical models as a basis, the effect of network density, temperature and strain rate on critical thickness is discussed. It is also shown that fracture strain is the characteristic material property to measure film toughness.

A variety of silicone thermosets are studied to demonstrate engineering applicability of critical thickness. The selected polymers include a commercial laminate poly-phenyl-methyl-silsesquioxane resin, an experimental high temperature poly-methyl-silsesquioxane resin and an optical polysiloxane resin. In addition to silicone thermosets, polystyrene is studied as a reference polymer. A bending technique has been developed in order to determine failure strain of thin films (on substrates) of these materials. Using this

technique, the failure strain is evaluated as a function of film thickness. Further, from a plot of failure strain as a function of film thickness the critical thickness is determined.

For polystyrene, a critical thickness value of approximately 0.1μm is observed. The strain to failure of polystyrene films below the critical thickness is >15%, a marked increase over bulk material fracture strain (~2%). For each of the silicone thermosets, a range of curing temperatures is investigated to determine the influence of curing temperature on critical thickness. For the poly-phenyl-methyl-silsesquioxane resin, the optimum thin film properties are observed when it is cured at 225°C. The critical thickness is observed to be ~5μm with a strain to failure of ~13% (bulk strain to failure <2%). Molecular engineering of the poly-phenyl-methyl-silsesquioxane by modifying the chemical structure using functionalized PDMS is shown to increase critical thickness to 10μm. For this PDMS modified poly-phenyl-methyl-silsesquioxane, critical thickness values have been determined over a range of test temperatures from -40°C to 75°C. Results indicate that the test temperature does not influence the critical thickness. For the poly-methyl-silsesquioxane, the critical thickness is observed to be greater than 2.5μm with a strain to failure of 15% when cured at 250°C. Two optical polysiloxane resins are studied. The first resin, commercially called the PF-1202 resin is studied for a single cure temperature and is observed to have a critical thickness of ~0.2-0.3μm. The properties of the second resin, named MP-101, are studied for a range of cure temperatures. The best performance, with 8% strain to failure and a 0.5μm critical thickness, is observed for a 50°C cure temperature.

Infrared spectroscopy measurements in reflection mode are carried out to compare orientation effects in thin (below critical thickness) vis-à-vis thick (above critical thickness) films for polystyrene, poly-phenyl-methyl-silsesquioxane and PDMS modified poly-phenyl-methyl-silsesquioxane. It is observed that both the thick as well as thin films do not exhibit any substantial orientation. A correlation between molecular orientation and fracture properties cannot be made. Infrared spectroscopy has also been used to determine the "nature" of strain (elastic or plastic) these thin films (below critical thickness value) exhibit when stretched to values higher than their bulk counterparts.

Acknowledgements

After a long journey, through good times and tough times, I feel a great sense of satisfaction with the completion of my PhD thesis and to have finally reached "the end of the beginning!" There have been several people - colleagues, family members, friends and at times many unnamed faces - all of whom have been of great help and support throughout my MIT life.

I am greatly indebted to three gifted scholars, teachers and mentors: Prof. Frederick McGarry, Prof. Sam Allen and Prof. Christopher Schuh. All of them have helped shape my career at MIT; without them I would not be what I am today. To Prof. McGarry, I am ever grateful for offering me a PhD project and for suggesting the topic of critical thickness. His words, although few, are filled with a lot of wisdom and experience. It is always a delight to listen to him and learn from him. I am extremely grateful for his guidance and for his patience during times when I needed focus.

I am extremely grateful to Prof. Sam Allen for his help through my entire graduate life at MIT. I am deeply indebted to him, for his standing up for me when the chips were down and I needed help, for his listening to me, for his words filled with wisdom and for his guidance when I have stood at cross-roads. I do not have words enough to express my gratitude for him.

Last but not the least, I would like to thank Prof. Chris Schuh, who was my supervisor during my Master's thesis. Chris took me on as a student when I was going through one of the most difficult phases in my life. I am ever grateful for that. Our professional relationship has continued after I finished my Master's thesis and I am sure it will continue on with new projects as time progresses.

I would like to thank Dr. Bizhong Zhu and Dr. Dimi Katsoulis of Dow Corning Corporation for their valuable discussions as the project progressed. Their critiques, comments and suggestions were key in helping make this project move along at a rapid pace as well as for helping me to focus in on the real issues associated with silicone materials. A special thanks to my colleagues during this project, Andrew Satorius and Dr. Yuhong Wu. Especially Yuhong - for suggesting the McGarry lab as an option to pursue my PhD. The FTIR work performed during this project would not have been possible without the support of Tim McClure. My thanks to him for his help. Both Marjorie Joss and Kathy Farrell, I would like to thank for their administrative support.

I would like to mention a special thanks to my friends Sajan, Mahesh, Charu, Shivanshu, Subarna, Shantoo and Lalit for being extraordinary friends.

Finally, I would like to take a few lines to acknowledge the ones who have been the nearest and dearest for me. My parents for their "long distance" support and for being the wonderful parents they are. My brother, Ashish for being the affectionate and respectful brother he has always been. Rupa for being there for me, for her support and affection. Words are not enough to express the feelings of gratitude and belonging I have for them. Their unconditional support has helped me to emerge victorious in all my endeavors.

Table of Contents

List of Figures

List of Tables

1 Introduction

Polymers [1] are used extensively in many forms for structural applications, [2] optical applications, [3] electronic applications [4, 5] and biomaterial applications. [6, 7] The use of polymers is increasing rapidly and in many applications they are replacing conventional materials such as metals, [8] wood [9] and natural fibers. Polymers offer many favorable properties including a very high strength to weight ratio, low density and ease of processability. Research on polymers over the last several decades has been carried out to synthesize new polymers, to improve properties [10] of existing polymers and to develop new processing [11, 12] as well as characterization [10] techniques. A significant area of research has focused on making high fracture toughness polymers since many synthetic polymers are brittle in their natural form.

In this thesis, the phenomenon of critical thickness is studied. Critical thickness is defined as an absolute thickness dimension below which a macroscopically brittle polymer deforms in a ductile manner. The existence of critical thickness in polymers has been postulated recently. [13, 14] Critical thickness effects can be used as a means to achieve high fracture toughness in polymers. Critical thickness is postulated to be a fundamental material property [13] and is therefore applicable to all polymers, thermoplastics or thermosets. In order to demonstrate applicability of the critical thickness phenomenon, silicone thermosets [15] are selected. Silicone thermosets are extremely brittle and arguably the most difficult to toughen amongst all polymer classes. The anticipated outcome of this thesis is two-fold. The first goal is to demonstrate validity of the critical thickness

postulate and direct it towards engineering applicability. The second goal is to improve fracture toughness in highly brittle silicone resins.

1.1 Current Polymer Toughening Strategies

Toughened polymers[16-18] are used in several applications including structural materials,[19] engineering plastics, matrices for fiber-composite materials[20] and several household items. Polymer toughening is a multi-billion dollar industry with each engineering plastic having several commercially available toughened versions.[21-27] The most common methods to make high toughness polymers include manipulation of inherent molecular composition, alteration of molecular structure and incorporation of second phase particles such as rubbers,[28-30] inorganic fillers[31] and low molecular weight plasticizers.[32] These toughening methods have tremendously broadened the use of many polymers. Some examples of toughened polymers are rubber toughened epoxy resins,[21, 22] plasticized polyvinylchloride,[23] high impact polystyrene (HIPS),[24] polymethylmethacrylate[25, 26] and polycarbonate.[27]

From a micromechanical standpoint, the primary reason for toughening a polymer is to improve its resistance to cracking[16] without significantly decreasing other important mechanical properties like modulus and tensile strength. Resistance to cracking within a material is exhibited when either of the following two conditions is met: first, that no cracks initiate and second that if cracks are already initiated, they do not propagate. In all existing toughening techniques the second methodology, i.e. inhibition of crack propagation, is utilized to improve toughness of polymers. In this section, a brief review

of the physics of crack propagation is presented. Further, various possible methods currently used to inhibit crack propagation in polymers are discussed.

Crack growth within polymers has been studied extensively.[33, 34] Models for crack growth can be derived using two methods: one based on mechanics[35] and the other based on energy analysis.[36] Over the last several decades these models of crack growth have been refined to a great extent. This refinement results from a continuous improvement in the experimental methods devised to substantiate these models. The model of crack propagation which is discussed below is obtained using a principle of potential energy minimization.* Accordingly, the criterion for brittle fracture can be stated as: "the potential energy of an elastically strained body is reduced by the introduction of a crack." Based on this criterion, the generalized mathematical expression for the stress (σ) required to create a crack surface is:

$$\sigma = \sqrt{\frac{2EG}{\pi a}} \qquad \textbf{Equation 1-1}$$

where E is the Young's modulus, G is the sum of energy dissipated per unit area of crack growth and 'a' is the crack length.

Inhibition of crack propagation in polymers can be achieved in several ways, the most utilized of which is introduction of rubber particles.[28, 29] Rubber particles provide an additional stress dissipating mechanism within the system. Mechanistically, addition of these particles allows blunting of the crack tip and therefore inhibits crack growth. Extensive literature is available which document use of rubber toughening in a variety of

* Since both the energy and the mechanics methods provide equivalent results, it is sufficient to elucidate the result from either one for review purposes.

polymers. [28, 29] Rubber toughening can be used provided two conditions are met. First, the polymer matrix needs to have a certain intrinsic ability to deform plastically. Second, the rubber and matrix materials system should be such that adhesion between them is strong so that other mechanical properties like modulus and strength are not adversely affected. When the matrix does not have the ability to plastically deform it needs to be modified by chemical means, a process akin to changing molecular architecture. Thermoset materials, for example silicone resins[37] and certain epoxy resins[38] fall under this class of polymers requiring molecular architectural modification to be used for practical applications. In another toughening approach, plasticization,[32] a compatible organic liquid is added within the matrix to provide more free volume within the polymer. Plasticization has been used most commonly in polyvinylchloride. Other less prevalent methods like cold drawing[39] and phase transformation toughening[40] are material specific and not widely used.

Although abundant literature exists on the subject of polymer toughening and the above described methods have been used successfully for commercial applications there are still several limitations. First, all the above techniques are material specific since polymer modification is required either at the molecular level or through a physical inclusion. The process of polymer modification requires knowledge of materials chemistry since any chemical or physical moieties added to the matrix need to be compatible with it. To devise such methods is extremely challenging, requiring substantial research efforts for each polymer which needs to be toughened. In addition, modification of a material may lead to undesirable consequences such as reduction in Young's modulus or yield strength. Second, explanations of toughening mechanisms are usually retrospective and primarily based on microscopy of fracture patterns. These explanations are usually qualitative.

Therefore development of well defined and generalized polymer toughening rules is severely hindered. Finally, the current techniques focus primarily on inhibition of crack propagation to achieve toughness and not on complete crack elimination. Based on the above information, a new approach to polymer toughening which minimizes material specificity and therefore can be easily applied to brittle polymers would be of much interest.

1.2 Critical Thickness

Until recently, toughness mechanisms and models have been based primarily on macroscopic analyses rather than a bottom-up approach utilizing a molecular level understanding. The first significant advancement in understanding toughness from a molecular point of view is based on experimental work by Kramer.[41] These experiments have focused on deformation within localized regions called crazes. It has been established that the deformation in these localized regions for polystyrene (the polymer chosen for experiments) is at least an order of magnitude higher (>100%) than the bulk material fracture strain value (~3%). However, at this stage, understanding of molecular level toughness had not been envisioned as a means to improve macroscopic toughness.

Taking a cue from these results, VanderSanden[13] postulated the existence of a critical thickness, which is a major advancement in linking molecular level toughness to macroscopic fracture properties. In this postulate, the possibility of utilizing high localized molecular strain levels, for example >100% for polystyrene, as a method to increase macroscopic toughness has been recognized. According to this postulate critical thickness is defined as an absolute thickness dimension below which a macroscopically

brittle polymer no longer exhibits brittle fracture and instead deforms in a ductile fashion. Such a brittle to ductile transition would be observed in one, two or three dimensions. Considering the 1-D case, a film which may be infinitely large in two dimensions and has a thickness less than the critical thickness would undergo ductile deformation. Naturally, this example can be extended to two and three dimensions. Below the critical thickness, strain localization is believed to be absent and therefore the inherent deformation capacity of the polymer is realized. In contrast, the same material in bulk form does not realize its inherent deformation capability since fracture is dominated by cracks which are energetically favorable at low strains.

Indirect experimental results indicate that the critical thickness value for polystyrene is ~0.1μm.[13, 14] Further, VanderSanden and co-workers, in a series of publications,[42- 47] discuss several aspects of the critical thickness phenomenon both using analytical models and experiments. Polystyrene has been used extensively for these experiments. Limited experiments have been carried out on thermoset epoxy materials as well, although a conclusive value of critical thickness for these epoxies has not been determined.[43]

The "critical thickness" postulate and the experimental work carried out to validate and analyze the various aspects of it, provides a foundation for the possible engineering use of critical thickness to achieve high toughness in polymers. However, limited research work on critical thickness has been reported since VanderSanden's investigations in the mid 1990's. Krupenkin presents[48, 49] a detailed theoretical analysis on two dimensional crazing in polystyrene which is helpful to understand the physical origin of critical thickness. Further experimental work has not been reported.

Although use of critical thickness methods can potentially improve toughness in polymers, the engineering use of it requires overcoming of several challenges. First, direct methods to test for critical thickness have to be devised. In previous experimental methods, critical thickness is defined based on locally thinned regions achieved in bulk polymers by making multilayers or through addition of core-shell particles. Direct investigations to determine critical thickness on thin films have not been carried out till now. Critical thickness investigations in thin films require evaluation of film fracture toughness properties. Since measurement techniques for thin film fracture toughness and failure strain are not well developed, a simple and reliable film toughness measurement process needs to be developed. The second major challenge is to devise methods to increase critical thickness values to levels suitable for thin film production. For example, while a 0.1μm ductile film of polystyrene is scientifically significant, producing it may not be possible. If critical thickness can be increased to ~5μm, the use of critical thickness concepts to make high toughness polymers for commercial applications can become a reality because thin film manufacturing at the 5μm and above length scales is feasible. Several applications of such films can be envisioned: multilayer materials, fibers, optical materials and structural plastics.

From a materials engineering perspective, application of critical thickness approach may be more useful in a thermoset than a thermoplastic. Thermosets (crosslinked) as opposed to thermoplastics, are extremely brittle with a strain to failure value of <1%. In fact, there is no known thermoset in bulk form which has a strain to failure value reaching even 2-3%. In contrast, several bulk thermoplastic materials are ductile in their non-modified state. An example is polycarbonate. Therefore a choice of non-modified ductile

thermoplastics is available. For thermoset polymers, on the other hand, toughening is a necessity. A new method which would allow thermosets to achieve a high strain to failure would therefore be extremely useful. A variety of silicone thermosets are being studied to validate as well as capitalize on the critical thickness phenomenon. In addition, polystyrene is being studied as a reference polymer.

1.3 Silicone Resins: Introduction

Silicone polymers are unique materials which combine heat and chemical resistance of inorganic glass with versatility of plastics. In contrast to their organic counterparts, which are long chain carbon molecules, silicone polymers have a silicon-oxygen backbone. The silicone polymers are set apart from carbon polymers by their excellent thermal and oxidation resistance. These superior properties are a consequence of the chemical nature of the backbone. The silicon-oxygen bond is slightly stronger than the carbon-carbon bond leading to excellent thermal stability. Moreover, the silicon-oxygen bond is inert and therefore provides high oxidation resistance. Given their novel properties, silicone materials have been studied extensively (primarily in industrial research laboratories) and put to use for several applications.

There are two categories of silicone polymers: linear and branched. Commercially, over 90% of the worldwide production of silicones is in linear form. Linear silicones have found applications as silicone oils (low molecular weight) and rubbers (high molecular weight). These linear silicones are used for several applications as lubricants, mold release agents, mold materials and fiber adhesives. A common example of a linear silicone is polydimethylsiloxane (PDMS).

In contrast, branched silicones, often denoted as silicone resins, are highly crosslinked brittle materials. Silicone resins have been utilized to a limited extent as coatings,[50, 51] insulation materials for electrical motors, [52] inter-layer dielectrics [53] and ceramics pre-cursors.[54] All these applications in which silicone resins are currently being utilized do not primarily require good mechanical properties. As structural materials, silicone resins, have found limited use because of their low fracture toughness and low resistance to crack initiation and propagation.

Silicone resins are also called polysilsesquioxanes. Polysilsesquioxanes have a chemical structure which can be represented by $(RSiO_{m/2})_n$ where R can denote an H (hydrogen), alkyl group or a phenyl group. The value of m can be two, three or four* with $n \geq 1$. Typically, silicones containing the Methyl silsesquioxane ($MeSiO_{3/2}$) group, phenyl silsesquioxane ($PhSiO_{3/2}$) group and hydrogen silsesquioxane ($HSiO_{3/2}$) group are industrially important. These resins are obtained from hydrolization of oraganotrialkoxysilanes, dialkoxysilanes and tetraalkoxysilanes or a combination of these depending on the eventual desired chemical structure. The crosslinking in these molecules can take place in a number of ways through heat initiation or as a consequence of a condensation reaction. Typical crosslinking reactions are described below:

$\equiv Si\text{-}OH + R\text{-}O\text{-}Si\equiv \rightarrow \equiv Si\text{-}O\text{-}Si\equiv + HOR$ R is an (H or alkyl) group

$\equiv Si\text{-}CH{=}CH_2 + H\text{-}Si\equiv \rightarrow \equiv Si\text{-}CH_2\text{-}CH_2\text{-}Si\equiv$

The poor mechanical properties of silicone resins have been ascribed to the weak inter-chain physical interaction between chain segments as well as the large inter-chain

* m=2 is called a D unit, m=3 is called a T unit and m=4 is called a Q unit.

distance. In order to increase modulus in silicone resins, a relatively high crosslink density is required. In turn, the high crosslink density makes the silicone resin extremely brittle. As an indication of brittleness, the fracture toughness of the toughest commercially available silicone resin is half that of the most brittle epoxy.[37, 55] Further, limited data is available on physical and structural properties of these resins. Besides the standard mechanical properties, like Young's modulus and yield stress, other information like surface tension and details of structural parameters is almost non-existent.

Recently, a Phase-I/Phase-II technique[37, 55-57] has been successfully used to improve fracture toughness of silicone resins. The Phase-I/Phase-II approach[37] is based on the polymer toughening strategies described previously in Section 1.1. Phase-I refers to improvement in the intrinsic deformation ability of the matrix through molecular architecture modification whereas Phase-II refers to inclusion of rubber particles within the silicone matrix. Using PDMS as an additive for both Phase-I and Phase-II, the fracture toughness of a commercial poly-phenyl-methyl-silsesquioxane resin (4-3136) is shown to improve from 0.25 MPa $m^{1/2}$ to 0.55 MPa $m^{1/2}$.[37, 55] For another experimental poly-methyl-silsesquioxane (Methyl-T) resin the fracture toughness value is shown to improve by a factor of approximately 1.5 by similar incorporation of PDMS.[57] The toughness properties of another resin (X1-2672) have also been improved using similar methods.[56] The Phase-I/Phase-II toughening methods have allowed the possibility of silicone resins to be considered for structural applications although the toughness of these materials is still very low.

In this thesis, the critical thickness approach will be applied to several of these silicone resins. Although, the Phase-I/Phase-II approach provides for an increase in the fracture

toughness of silicones, the maximum increase that can be achieved is limited to a factor of approximately two. In essence, even after application of the Phase-I/Phase-II techniques on these resins, they still qualify as brittle materials. The critical thickness method provides for a different approach to increase fracture toughness. Through this approach, these materials are envisioned to reach a ductile state thereby leading to a substantial increase in fracture toughness. Such a result would provide a totally new outlook to the application potential of silicone resins. Three different silicones are being studied in this thesis, a poly-phenyl-methyl-silsesquioxane (4-3136), a poly-methyl-silsesquioxane (Methyl-T) and an optical polysiloxane resin (C-resin).

1.4 Organization of Thesis

This thesis is presented in seven sections followed by the conclusion. Chapter 2 gives an overview of critical thickness. First, a discussion on intrinsic deformation mechanisms of polymers is presented. The two intrinsic deformation mechanisms which have been discussed are extension of fibrils in crazes within glassy polymers and theoretical draw ratio. Second, two analytical models are described, one based on an energy approach and the other being a mechanics based model. Using these models, influence of temperature and strain rate on critical thickness is also examined. Next, a discussion on fracture strain is presented since it is the characteristic property used to evaluate toughness in a thin polymer film. Finally, in this chapter a review of two previous indirect methods of measuring critical thickness is presented.

Chapter 3 describes experimental methods used in this thesis. First, a brief description of thin film sample preparation methods is provided. Next, a description of bending as well

as extension experiments used to determine critical thickness is presented. Following these methods, secondary structural and physical properties are listed. These physical properties include network density, molecular composition, molecular orientation and glass transition temperature. They are being discussed in order to understand whether a change in these properties as a function of thickness can be correlated to the brittle to ductile transition observed at the critical thickness.

Chapters 4-8 are on test results. Chapter 4 is on polystyrene which is the reference polymer. Thin film fabrication conditions are described, followed by bending test observations, critical thickness results and infrared spectroscopy results. In Chapter 5 results are presented for a poly-phenyl-methyl-silsesquioxane resin which is commercially used as a laminate binder. This poly-phenyl-methyl-silsesquioxane is the main focus of this study. For this resin, first the thin film fabrication methods are described, followed by critical thickness test results and infra red spectroscopy results. Chapter 6 describes molecular engineering methods as applied to the poly-phenyl-methyl-silsesquioxane resin. A PDMS is added to the neat resin to achieve molecular modification. Thin film fabrication methods and bending test observations for the modified resin are presented. The effect of test temperature and PDMS concentration on the critical thickness value is also studied. Chapter 7 presents thin film fabrication conditions and critical thickness results for a methyl-T silsesquioxane resin. This resin is a high temperature experimental silicone thermoset. In Chapter 8 two commercially available optical coatings (C-resins) are studied. Thin film fabrication conditions are described followed by critical thickness results.

2 Critical Thickness: Review and Models

For polymers which are macroscopically brittle, critical thickness[13] is defined as an absolute dimension at which a material undergoes a brittle to ductile transition. Below critical thickness, the toughness properties of a polymer are dominated by intrinsic deformation behavior of the material. In contrast, toughness properties of bulk materials are governed by extrinsic fracture features like crazes and cracks. In this chapter, polymer intrinsic deformation mechanisms as relating to critical thickness are examined. Two analytical models for critical thickness are presented. Next, influence of network density, temperature as well as strain rate on critical thickness is reviewed. Finally, physical properties for critical thickness evaluation as well as previously used indirect measurement methods[13] for critical thickness are discussed. Although the discussion is generalized and applicable to all brittle polymers, certain material properties of polystyrene are used to facilitate understanding. Polystyrene is chosen as a representative polymer since extensive information on its physical and structural properties is already available. Moreover, the majority of critical thickness experimental work which has been conducted previously is on polystyrene.

2.1 Basis for Critical Thickness

Critical thickness has been postulated based on molecular level ductility, which is a consequence of the intrinsic deformation ability of a polymer. These intrinsic deformation mechanisms are reviewed below. This discussion is primarily qualitative, emphasizing the conceptual basis for a critical thickness.

2.1.1 Natural Draw Ratio

Typically used to describe the fiber formation process in semi-crystalline polymers, the natural draw ratio[58, 59] quantifies extensibility of a material. The draw ratio (λ) can be expressed as:

$$\lambda = \frac{L}{L_0} \qquad \textbf{Equation 2-1}$$

where L_0 is the original length of the polymer or fiber and L is the length upon extension. Using principles similar to fiber drawing of semi-crystalline materials, toughness in amorphous polymers can be related to the tensile deformation as predicted by the draw ratio. A theoretical maximum draw ratio (λ_{max}) of a polymer strand,[41] assuming no occurrence of chain slippage is given by:

$$\lambda_{\max} = \frac{l_e}{d} \qquad \textbf{Equation 2-2}$$

where l_e is the chain contour length and d is the root-mean square end-to-end distance. After a series of straightforward transformations are applied to Equation 2-2,[41] the draw ratio can be represented as a function of physical parameters of the polymer:

$$\lambda_{\max} = \frac{\rho^{1/2} N_A^{1/2} l_0}{k M_0 \nu_e^{1/2}} \qquad \textbf{Equation 2-3}$$

where ρ is the density, N_A is Avogadro's number, l_0 is the average projected length of the polymer chain, M_0 is the molecular weight, k is a constant and ν_e is the entanglement density.

The theoretical value of draw ratio for amorphous polymers can be as high as 4 (corresponding to an engineering strain to break of 300%),[60] as calculated for a polybutylstyrene. For a densely crosslinked thermoset network, the theoretical value of the draw ratio can be as high as about 1.2 (corresponding to an engineering strain to break of about 20%).[61] In practice, however, experimentally measured strain to failure values are much lower, with polystyrene sustaining a maximum 1-3% strain and thermosets sustaining a maximum 1% strain. The explanation for this discrepancy is attributed to the localization of strain within specific deformation regions.[62, 63] Extensive study of the two commonly observed localized deformation regions, crazing[62] and shear yielding,[63] which occur during brittle fracture have been carried out in the past.

As opposed to a bulk polymer, where fracture properties do not match up to the draw ratio, at reduced lengths scales i.e. below a "critical thickness" it is conceived[13, 14] that the draw ratio may be of significance in determining fracture properties. Extension values comparable to the draw ratio may be achievable below the critical thickness.

2.1.2 Extension of Fibrils in Glassy Polymers

Craze formation is one of the two main deformation mechanisms* in polymers. These craze structures form within a polymer upon tensile deformation (Figure 2-1(a)). Crazes eventually lead to cracking. A craze structure schematic is presented in Figure 2-1(b). Crazes develop in a plane perpendicular to the principal deformation axis. The strain in the material is localized within the craze. The craze is surrounded by unstrained polymer

* The other deformation mechanism in polymers is called shear yielding.[63] It has been proposed that crazing occurs in polymers with network density values less than $9x10^{25}$chains m^{-3}. Polymers with network density values above $9x10^{25}$chains m^{-3} deform primarily by shear yielding. Since the scope of the discussion is limited to extension values achieved within craze structures, a discussion on shear yielding or a comparison between shear yielding/crazing is not particularly relevant and is therefore not presented.

which is in its random coil state. Within the craze, load bearing fibrils exist as depicted in Figure 2-1(b). These load bearing fibrils distinguish a craze from a crack. The size as well as the number of fibrils present within a craze depends on the specific polymer and the amount of stress applied. For example, in polystyrene a typical fibril diameter is in the 5-20 nm range.[64] The typical size of an entire craze can be on the order of several micron.

Experimental studies using optical densitometry as well as transmission electron microscopy indicate that a very high extension[41, 60] is achieved in the craze fibrils prior to craze rupture. These experimentally measured fibril extension values are comparable to the theoretically estimated draw ratio (Section 2.1.1) for several thermoplastics and thermosets.[41, 60] In polystyrene, for example, the fibril extension value is experimentally determined to be approximately 200%.

If strain within the polymer can be delocalized, ductility can be obtained. Such delocalization can be anticipated to occur at reduced length scales i.e. in thin films or ligaments. At these length scales, the deformation mechanisms operative under tensile deformation can differ from the bulk deformation mechanisms.[48, 49] For example, crazes (several micron in size) which are found in bulk polymer may not occur in a film or ligament of the same material in which the thickness is below the typical craze length scale. Therefore it has been postulated that localization phenomena will become absent in polymers when a certain "critical thickness" value is achieved.

2.2 Analytical Models

In this section two analytical models for critical thickness are presented. These models predict a critical thickness value based on the physical properties of the polymer. Although these models are not very exhaustive, they capture the essence of the critical thickness phenomenon. The first model utilizes an energy based approach whereas the second model utilizes a mechanics based approach.

2.2.1 Thin Film Energy Approach

In this approach to model critical thickness in thin films, a linear elastic fracture mechanics analysis is followed. An energy based model for critical thickness in polymer ligaments has been presented previously by Vander Sanden.[14, 42] The fundamental basis for the model presented below as well as the one developed by Vander Sanden is same: brittle failure in a polymer can occur only if the stored elastic energy within the material is larger than the amount of energy required to create brittle fracture. For the purpose of this analysis, it is assumed that cracking is the only failure mode within the film.

The two key parameters[65] for this analysis are crack driving force (G) and crack resistance (Γ_f). The crack driving force is a measure of reduction in elastic energy with advancement in crack. The crack resistance is a measure of energy required to advance the crack. Crack growth is energetically favorable only when the crack driving force equals the crack resistance. An excellent review of the details of crack growth within thin films has been presented by Suo.[65]

Consider a film (infinitely large in two dimensions) with a thickness h atop a substrate.* When a sufficiently high tensile force is applied on the film, a crack will be generated. This crack will start from a flaw within the film. In film thickness direction, the crack can only traverse, at maximum, the film thickness. Laterally the crack length can be several times the thickness of the film. A lateral crack, also called as a channel crack, will only stop extending once it reaches the film edge. Although to model the entire film morphology which includes cracks of various sizes and different growth rates is fairly difficult, it is worthwhile to consider the crack originating from the largest pre-existing flaw. The crack driving force (G)[65] is given by:

$$G = \frac{\beta(1-\nu_f{}^2)\sigma^2 a_c}{E_f} \qquad \textbf{Equation 2-4}$$

where ν_f is the Poisson's ratio, σ is the applied stress, a_c is length of the largest pre-existing crack, E_f is the Young's modulus and β is a shape dependent numerical coefficient. This pre-existing crack grows when the crack driving force equals the crack resistance which can be mathematically expressed as:

$$\frac{\beta(1-\nu_f{}^2)\sigma^2 a_c}{E_f} = \Gamma_f \qquad \textbf{Equation 2-5}$$

Therefore a certain minimum stress is required in order for a lateral crack to form. When the pre-existing crack size is comparable to the film thickness, i.e. a ≈ h, the driving force will attain a value given by:[65]

$$G = \frac{\beta(1-\nu_f{}^2)\sigma^2 h}{E_f} \qquad \textbf{Equation 2-6}$$

* The case of a film-substrate system is considered to reflect the experimental work which has been carried out. To apply this analysis to a free standing film further modifications are required.

Since the largest crack driving force has been considered, it follows that no cracks will form under the following condition:

$$\frac{\beta(1-\nu_f{}^2)\sigma^2 h}{E_f} < \Gamma_f \qquad \textbf{Equation 2-7}$$

In order to obtain a critical thickness value, the stress (σ) is replaced by the yield stress (σ_y) of the polymer in Equation 2-7. The term h, in the above expression, will therefore become the critical thickness h_c. The rationale in imposing this condition is that σ_y is the highest stress state which the polymer can possibly attain. Therefore the expression for critical thickness becomes:

$$h_c = \frac{E_f \Gamma_f}{\beta(1-\nu_f{}^2)\sigma_y^2} \qquad \textbf{Equation 2-8}$$

Crack resistance can be represented as a sum of terms, each of which independently contributes to it. The major contributions for crack resistance arise from surface energy and polymer backbone bond energy. A term for the work of plastic deformation may also be added. The surface energy can be represented by a Van der Waals term (γ); the polymer backbone bond energy can be represented by a $k_1 \nu_e^{1/2}$ term where k_1 is the polymer backbone bond energy (the value of k_1 is similar for all polymers) and ν_e is the network density; the work of plastic deformation can be denoted by φ_p.* Crack resistance is therefore given by:

$$\Gamma_f = \gamma + k_1 \nu_e^{1/2} + \varphi_p \qquad \textbf{Equation 2-9}$$

* In this thesis only γ and $k_1\nu_e^{1/2}$ terms are considered for purposes of calculation of the crack resistance. φ_p has not been used in calculation of crack resistance since an accurate estimate for this term is not available.

Combining equations 2-8 and 2-9, the critical thickness is given by:

$$h_c = \frac{(\gamma + k_1 \nu_e^{1/2} + \varphi_p) E_f}{\beta(1-\nu_f{}^2)\sigma_y^2} \qquad \textbf{Equation 2-10}$$

If the value of the film thickness is below the critical thickness (h_c) brittle fracture will not occur; whereas for film thickness values above the critical thickness brittle fracture will occur.

For polystyrene, taking (γ= 0.04 J/m^2),[10] (k_1 = 7.1 x10^{-15} J chain$^{-1/2}$ m$^{-1/2}$),[41] (ν_e = 4 x10^{25} chains/m^3),[66] (E_f = 3.3 GPa),[10] (ν_f = 0.38),[10] (σ_y = 80 MPa)[10] and assuming β = 1 the value of the critical thickness as predicted by Equation 2-10 is ~0.05μm.

2.2.2 Mechanics Based Approach

This model utilizes a mechanics based approach. A physical model for a craze structure is depicted in Figure 2-2(a). Such a craze feature within a polymer is formed on the application of a tensile stress (S). Typically, in a craze, a series of voids are created (length of void = f_L) which are interspersed with craze fibrils (diameter = D). The void shape is modeled as a rectangle with two semi-circular ends ($r = f_L/2$). The active zone represents the craze boundary of a finite thickness (a).

To calculate critical thickness an assumption is made according to which a minimum of two craze fibrils and one void need to exist for a craze to form (Figure 2-2(b)). A variation* of the model presented below has been earlier published by VanderSanden.[14]

* In the model developed by VanderSanden, critical thickness calculation is based on the assumption that two craze fibrils and two voids exist within the craze structure.

According to this model, the critical thickness $(H_c)^*$ can be computed as (Figure 2-2 (b)):

$$H_c = 2a + 2D + f_L \qquad \textbf{Equation 2-11}$$

The value of 'a' can be determined experimentally.[67] For f_L and D an analytical expression needs to be developed. For this purpose, the craze growth velocity (v_c) is considered. The craze growth velocity[41] is directly proportional to the pressure gradient:

$$v_c \propto \left(\frac{\Delta P}{length} \right) \qquad \textbf{Equation 2-12}$$

where ΔP is the pressure difference between the hydrostatic tension in the active zone (σ_p) and the void (σ_v).[68] Therefore the pressure gradient can be mathematically represented as:

$$\frac{\Delta P}{length} = \frac{\sigma_p - \sigma_v}{(f_L/2)} \qquad \textbf{Equation 2-13}$$

Here it is assumed that the pressure gradient is achieved over a thickness which equals the radius of the semi-circular region of the void. The hydrostatic tension in the active zone can be related to the tensile stress as:

$$\sigma_p = \beta S \qquad \textbf{Equation 2-14}$$

where β is a constant which is nearly equal to 1. The hydrostatic tension in the void is found by using a capillary relation:

$$\sigma_v = \frac{2\Gamma}{f_L/2} \qquad \textbf{Equation 2-15}$$

---

* 'H_c' is used to denote critical thickness in Section 2.2.2. In the energy based model (Section 2.2.1) 'h_c' is used to denote critical thickness. Although both 'H_c' and 'h_c' denote critical thickness, different terminologies in the two sections are used for clarity.

where Γ is the surface tension of the polymer.

Based on the above Equations, the craze growth velocity can be given by the following functional form:

$$v_c \propto \frac{\beta S - \frac{2\Gamma}{f_L/2}}{f_L/2} \qquad \textbf{Equation 2-16}$$

In order to proceed further, an additional constraint is added. To define critical thickness f_L is calculated for the fastest going craze. The f_L value for the fastest growing craze is evaluated by an algebraic minimization of the craze growth velocity (v_c) with respect to the width of the void (f_L):

$$\frac{dv_c}{df_L} = 0 \qquad \textbf{Equation 2-17}$$

Therefore,

$$\frac{2\beta S}{(f_L^*)^2} - \frac{16\Gamma}{(f_L^*)^3} = 0 \qquad \textbf{Equation 2-18}$$

where f_L^* denotes the width of the void within the fastest growing craze. Solving Equation 2-18 one obtains:

$$f_L^* = \frac{8\Gamma}{\beta S} \qquad \textbf{Equation 2-19}$$

Further, S is taken equal to the maximum attainable stress i.e. the yield stress (σ_y). The value of D can be calculated according to the following expression:

$$(f_L + D) = D\lambda^{1/2} \qquad \textbf{Equation 2-20}$$

where λ is the maximum draw ratio.

Simplifying and solving for D, one obtains:

$$D = \frac{f_L}{(\lambda^{1/2} - 1)} \qquad \textbf{Equation 2-21}$$

Finally, combining Equations 2-11, 2-19 and 2-21, critical thickness value is obtained as:

$$H_c = 2a + \frac{8\Gamma}{\beta\sigma_y}\left(1 + \frac{2}{\lambda^{1/2} - 1}\right) \qquad \textbf{Equation 2-22}$$

For polystyrene, (a = 25nm),[67] (Γ = 0.04 J/m^2),[10] (σ_y = 80 MPa),[10] and (λ = 4)[41] and assuming (β = 1), results in a critical thickness value of ~0.06μm.

This model is only applicable to polymers which undergo crazing. Therefore this model is not applicable to thermosets since they do not deform by crazing. The two models certainly have different mathematical forms; however, both these models serve as a good first approximation of critical thickness.

2.3 Critical Thickness as Influenced by Physical Parameters

In this section the influence of network density (intrinsic variable) and the influence of temperature as well as strain rate (extrinsic variables) on critical thickness is discussed.

2.3.1 Influence of Network Density

Based on the analyses presented in Section 2.1 and Section 2.2, critical thickness is shown to be a function of the network density.* In this section, through a quantitative

* Network density has a different definition for thermoplastic and thermoset polymers. For thermoplastics, network density is the polymer entanglement density whereas for thermosets it is the crosslink density.

approach, the effect of network density on critical thickness is discussed. A review on this subject has been presented in previous publications.[14, 42, 43]

First, the influence of network density (ν_e) on the draw ratio (λ) is studied. Below the critical thickness length scale, the draw ratio can be considered to represent the elongation to failure. The Equation describing the draw ratio as a function of network density has been derived in Section 2.1.1 (Equation 2-3) and is again stated below:

$$\lambda_{max} = \frac{\rho^{1/2} N_A^{1/2} l_0}{k M_0 \nu_e^{1/2}} \qquad \textbf{Equation 2-23}$$

From this Equation, it is seen that the draw ratio is inversely proportional to the square root of the network density.

Next, the influence of network density (ν_e) on the critical thickness (h_c) is represented according to the relation described in Section 2.2.1(Equation 2-10):

$$h_c = \frac{(\gamma + k_1 \nu_e^{1/2} + \varphi_p) E_f}{\beta (1 - \nu_f^{\,2}) \sigma_y^2} \qquad \textbf{Equation 2-24}$$

According to this Equation, the critical thickness is a monotonically increasing function of the network density. From the functional dependence of h_c on ν_e in Equation 2-24, it is seen that the relative magnitudes of (γ), ($k_1 \nu_e^{1/2}$) and (φ_p) become important in understanding the influence of network density on critical thickness. In general for thermoplastics, the surface energy (γ) is comparable to the ($k_1 \nu_e^{1/2}$) term (polymer

---

Nonetheless, in relation to critical thickness, it is not necessary to distinguish between the two different terms. In this discussion, network density is used throughout to represent both entanglement density and crosslink density.

backbone bond energy). For thermosets, (γ) would be much less than the ($k_1 \nu_e^{1/2}$) term and the (φ_p) term may become dominant.

Equations 2-3 and 2-10 are graphically represented in Figure 2-3(a) and Figure 2-3(b) respectively. The network density is varied from $4x10^{25}$ to $50x10^{25}$ chains/m^3 which is the typical range of values for thermoplastics.* For thermosets, the network density would be much higher, still the predicted trends are essentially the same as those for thermoplastics.

As a function of increasing network density, the critical thickness value increases whereas the draw ratio decreases. Considering the macromolecular nature of polymers, these trends are not entirely unexpected. A higher network density would constrain tensile deformation and therefore lead to a reduced value of the draw ratio. On the other hand, the bond strength increases as a result of increasing network density which leads to a higher value of critical thickness. In order to best utilize the critical thickness phenomenon, the network density should be optimized so that the two desirable properties, critical thickness and draw ratio are both at acceptable levels. Furthermore, for thermosets a high critical thickness is anticipated since they possess an inherently high network density. As an example, if we consider a thermoset with an extremely high network (crosslink) density (ν_e = 1000 x 10^{25} chains/m^3) the theoretically calculated critical thickness is ~2μm with a strain to failure of ~10%.

* The physical parameter values of polystyrene are used in Equation 2-24 to make these plots. The network density is varied while keeping these parameters fixed.

2.3.2 Influence of Temperature and Strain Rate

Mechanical properties of polymers, in general, are significantly influenced by temperature and strain rate.[1] It is therefore useful to examine how temperature and strain rate would affect critical thickness. A review on this subject has been presented in previous publications.[14, 45]

The energy based model presented in Section 2.2.1 is considered. Critical thickness as a function of the material properties is given by (Equation 2-10):

$$h_c = \frac{(\gamma + k_1 \nu_e^{1/2} + \varphi_p) E_f}{\beta (1 - \nu_f^{\,2}) \sigma_y^2} \qquad \textbf{Equation 2-25}$$

In this equation, yield stress (σ_y) and modulus (E_f) are the two parameters which can exhibit temperature and strain rate dependent behavior. Yield stress typically has a greater dependence on temperature and strain rate as compared to the modulus. Additionally, since critical thickness (h_c) is inversely proportional to the square of yield stress (σ_y) whereas it is only directly proportional to modulus, it is reasonable, as a first approximation, to neglect the effect of variation in modulus as a function of temperature and strain rate.

The yield stress dependence on the strain rate and temperature can be given according to the Eyring theory:[69]

$$\sigma_y = \frac{RT}{v^*} \ln\left(\frac{\dot{\varepsilon}}{A_E}\right) + \frac{\Delta E}{v^*} \qquad \textbf{Equation 2-26}$$

where T is the absolute temperature, $\dot{\varepsilon}$ is the strain rate, R is the gas constant, A_E is a constant, ΔE is an activation energy and v^* is an activation volume. According to Equation 2-26, yield stress decreases with increase in either temperature or strain rate. The yield stress dependence on the temperature (linear function) is greater compared to the strain rate dependence (logarithmic function). Also, critical thickness would become independent of strain rate and temperature under the following condition:

$$RT \ln\left(\frac{\dot{\varepsilon}}{A_E}\right) << \Delta E \qquad \textbf{Equation 2-27}$$

The plot in Figure 2-4 shows the effect of temperature on critical thickness for polystyrene. Below room temperature the critical thickness value is constant and nearly independent of temperature. Above the softening temperature (50°C)* for polystyrene, the critical thickness value increases substantially with increase in temperature. In general, for thermoplastics the yield stress of a material decreases significantly below the softening temperature. Critical thickness is therefore predicted to increase by a large amount above this temperature. Since other mechanical properties deteriorate above the softening temperature, the relevance of a high critical thickness at these temperatures largely diminishes. In contrast, for thermosets a softening temperature is not very meaningful since they are highly crosslinked. Accordingly, Equation 2-26 would predict that the critical thickness value for thermosets varies only slightly with temperature.

* Softening temperature of a material is typically 50°C below the glass transition for a polymer (T_g). The T_g of polystyrene is ~100°C.

2.4 Strain to Failure as a Measure of Fracture Toughness

The phenomenon of critical thickness is associated with a change in fracture properties of a polymer. For bulk materials, fracture toughness of a material is typically quantified using either stress intensity factor (K_{Ic}) or percentage strain to fracture. Typical ASTM standards exist to measure the stress intensity factor as well as the strain to fracture for bulk materials.* However, for thin films no such universal standard exists. Quantifying the stress intensity factor (K_{Ic}) for thin films is extremely difficult and not extensively used. Specialized methods like nanoindentation need to be used to measure K_{Ic} for thin films.[70]

In comparison to the stress intensity factor, the strain to failure is relatively easier to quantify. In this context, it is useful to examine the influence of two characteristic parameters, stress and strain, on fracture property measurement since fracture toughness is a measure of the area under a stress-strain curve. As an example, in Figure 2-5, the stress-strain plot for a brittle polymer (A) is compared to that of a ductile polymer (B). The highest stress attained in polymer A is approximately twice that attained in polymer B; the strain to failure value which polymer B can withstand is several times greater than that for polymer A. The area under the stress-strain curve for material B is clearly more than that for material A. This particular example is in general representative of the stress-strain behavior for almost all polymers. While the ultimate stress value for most glassy polymers is within the 50-100 MPa range and can vary by a factor of two or three, the strain to failure value for a brittle material is approximately 1-2% whereas for a ductile material it can reach 100% or even higher, a variation which is over two orders of

* ASTM D 5045-96 can be used to measure K_{Ic}.

magnitude. Clearly, the area under the stress-strain curve is dependent on the strain to failure value and not on the ultimate stress value. Therefore strain to failure is the characteristic property to distinguish a brittle material from a ductile one.

2.5 Bulk Methods to Identify Critical Thickness

In the past, two methods[13, 14] have been used to experimentally determine critical thickness. In these methods bulk specimens are used. Critical thickness is demonstrated by locally thinning these bulk specimens through addition of core-shell rubber particles or by making mutilayers. Accordingly, these experimental methods are termed as "indirect methods". This terminology also serves to distinguish them from the experimental techniques used in this thesis. The two indirect methods are reviewed briefly.

2.5.1 Alternating Thin Film Layers

In this method[13, 14] of measuring critical thickness, a multilayered sample (schematic in Figure 2-6) is fabricated which consists of alternating layers of the polymer to be tested with a ductile polymer. The ductile polymer is referred to as the sample testing material and is selected such that the level of adhesion between the two polymers is minimal. The multilayer samples can be prepared using co-extrusion methods. In co-extrusion, by varying the proportion of the two materials as well as by a sequential process of folding and re-extrusion a desired layer thickness can be achieved in a particular sample.

Using co-extrusion, several multilayer specimens are prepared with each specimen tuned to a particular layer thickness. Elongation tests on these co-extruded multilayer samples

are performed in order to measure the stress-strain behavior. Using a linear superposition technique, the stress-strain behavior of the individual thin layers in each of the samples is evaluated and thereby the brittle/ductile nature is qualified. The critical thickness equals the layer thickness for the particular bulk sample at which material properties begin to exhibit a ductile behavior. Optical microscopy can also be used to confirm rupture within confined layers.

This technique has been used to measure critical thickness in polystyrene and a polystyrene-polypheneylene ether blend.[13, 14, 42] Polyethylene has been used as the sample testing material since it has minimal adhesion with both polystyrene and polyphenylene ether. A major drawback of using this method is the limitation on the lowest achievable layer thickness. A lower limit exists because of the inherent nature of the co-extrusion process. Below a certain thickness, on the order of 1μm, the layers tend to become discontinuous and hence the method becomes unsuitable if critical thickness value is lower than this limit.

2.5.2 Incorporation of Core Shell Rubber Particles

In this technique[13, 14] local thinning of the polymer is achieved by the introduction of non-adhering core-shell rubber particles as a fine dispersion into a bulk specimen (Figure 2-7). The average distance between the particles (ID), which can be termed as a ligament thickness, can be calculated using the following formula:[71]

$$ID = d\left[\left(\frac{k\pi}{6\phi}\right)^{1/3} - 1\right] \qquad \textbf{Equation 2-28}$$

where d is the particle diameter, φ is the volume fraction of the particles and k is a constant depending on the spatial rubber particle distribution. According to this equation, on changing amount and/or diameter of particles the ligament thickness value can be altered. In order to obtain a critical thickness value, bulk samples are prepared with each sample targeted to a particular value of ligament thickness. Elongation tests are carried out for the various samples to assess the stress-strain behavior and thereby qualify the brittle/ductile nature of each of the samples. The bulk sample with the highest value of ligament thickness for which ductile behavior is obtained defines the critical thickness.

Critical thickness for polystyrene has been estimated using this method.[13, 14] Polymethylmethacrylate (PMMA) core shell rubber particles have been used as addition particles for experimentation since PMMA does not adhere to polystyrene. Since this technique relies on using an average ligament thickness to ascertain a critical thickness value, several experimental errors in measurement can arise. Typically, the critical thickness predicted using this method will be less than the true critical thickness. Other limitations of this method include the requirement of obtaining suitable non-adhering particles to carry out critical thickness measurements.

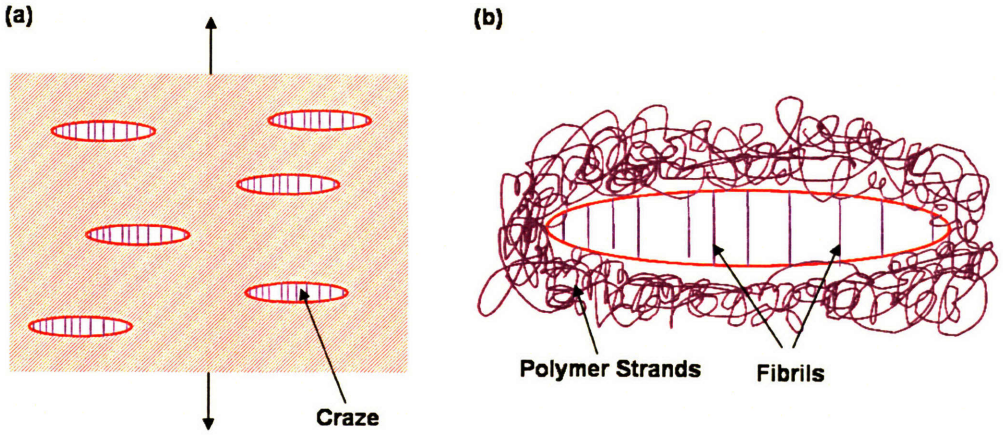

Figure 2-1 (a) Schematic illustration of multiple crazes formed within a polymer upon tensile deformation. (b) Schematic of a single craze structure. The oval shape represents the craze. The vertical lines within the craze represent craze fibrils. The craze is surrounded by unstrained polymer strands in their random coil state. (Note: Both figures are not to scale.)

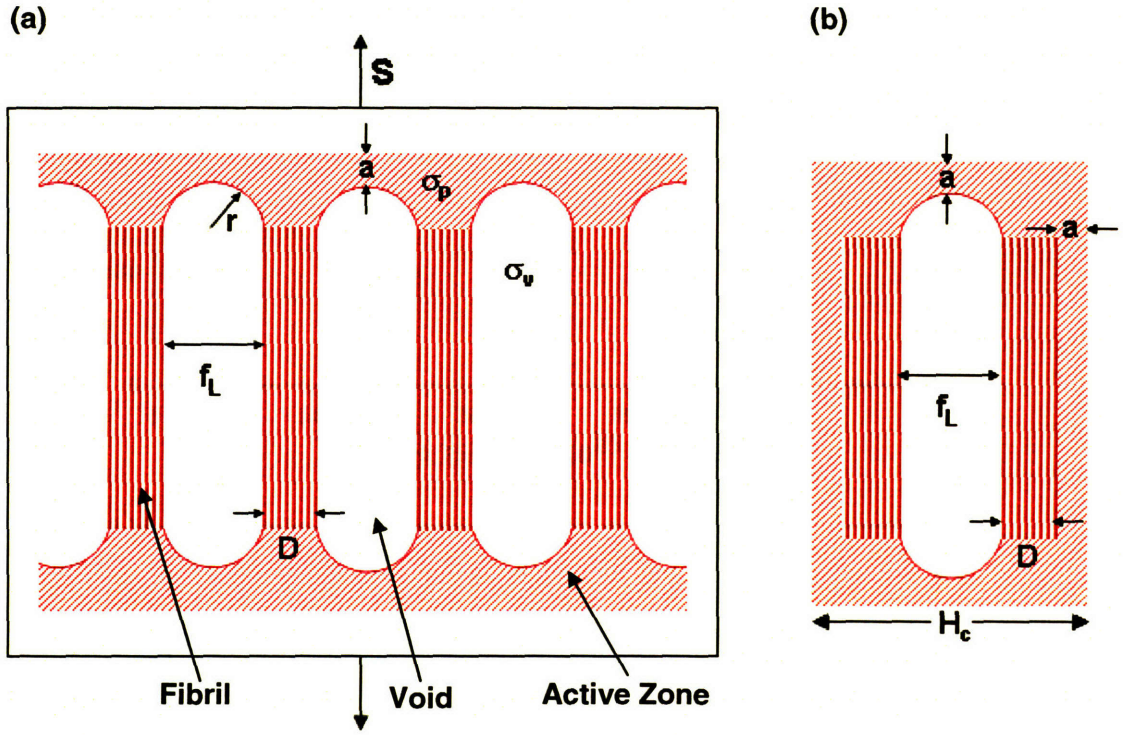

Figure 2-2 (a) A schematic model of a craze structure shows the active zone (dimension 'a'), voids (thickness f_L) and fibrils (diameter D). The hydrostatic tension within the active zone is denoted by σ_p. The surface tension within the void is denoted by σ_v. The end radius of curvature of the void is denoted by r. A tensile stress S is applied on the entire polymer. (b) Model of the smallest possible craze which can exist. Such a craze is depicted to consist of a single void and two fibrils. The craze is bounded by the active zone on all sides.

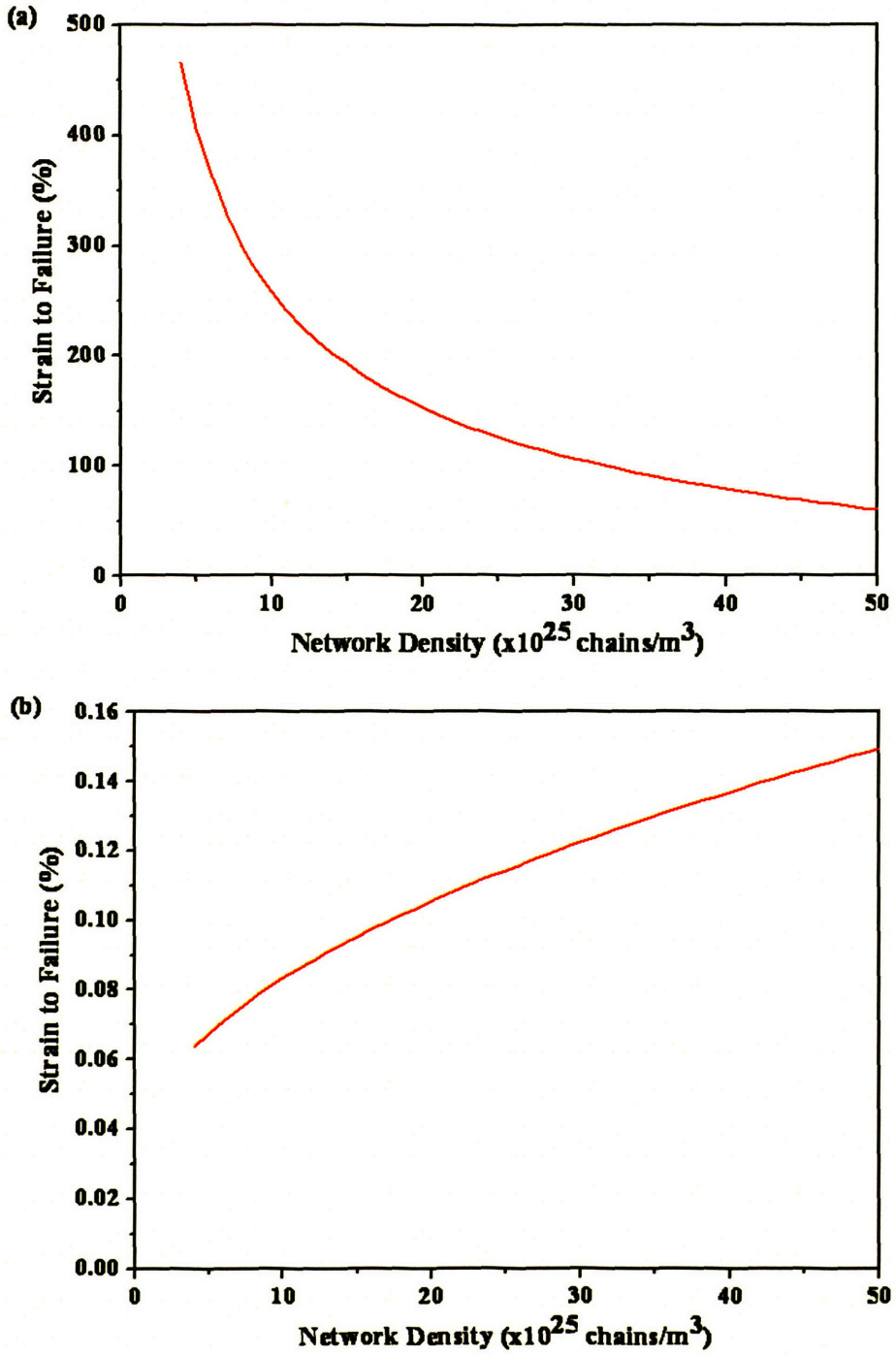

Figure 2-3 Effect of network density variation on draw ratio and critical thickness. (a) Draw ratio as a function of network density as predicted by Equation 2-23. (b) Critical thickness as a function of network density as predicted by Equation 2-24. For both plots, physical parameter values of polystyrene are used. Network density is varied while keeping all other parameters constant.

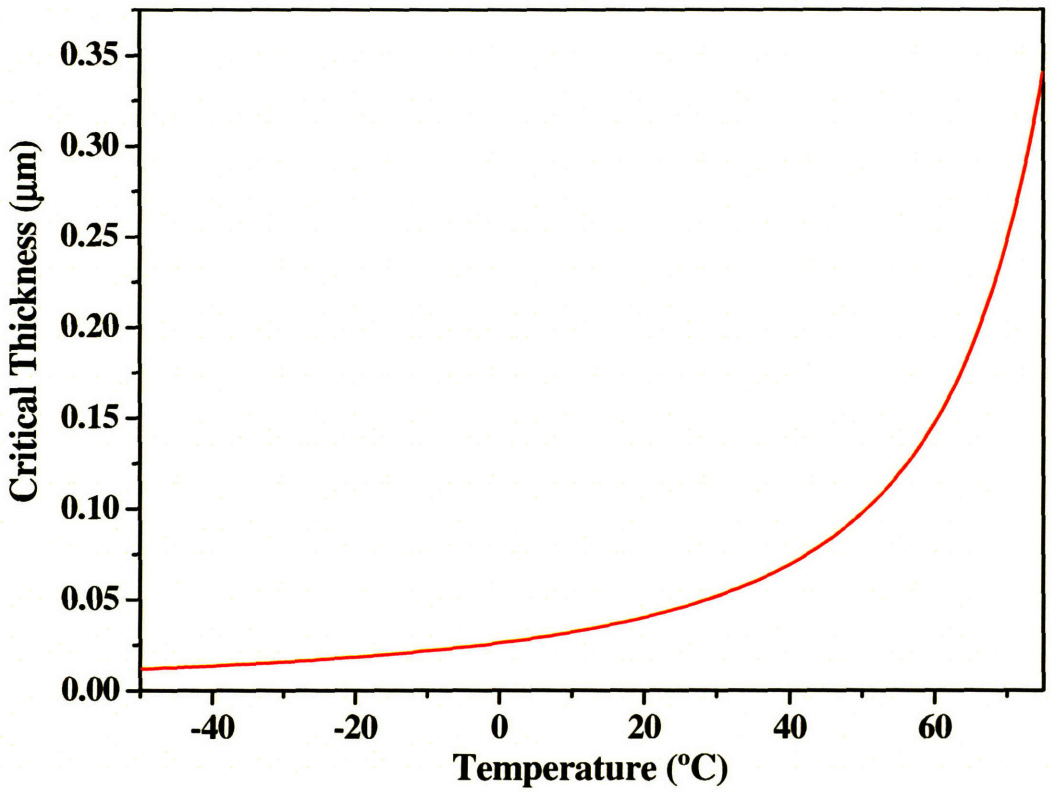

Figure 2-4 Effect of temperature on critical thickness of polystyrene.

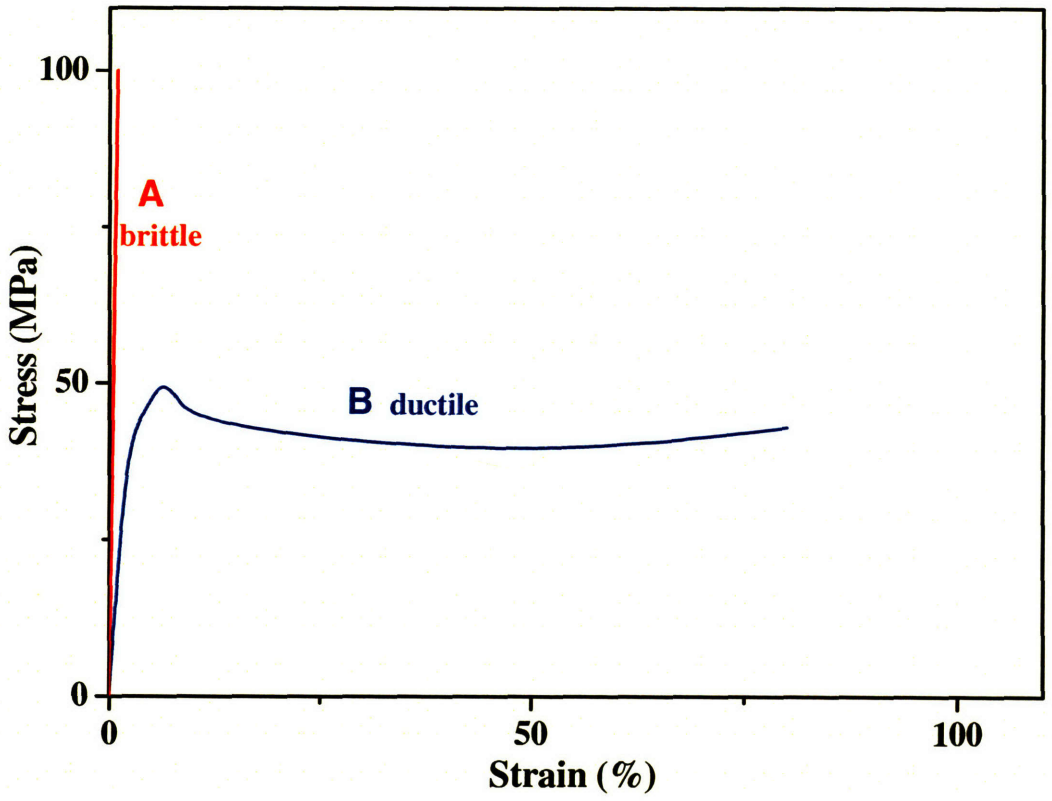

Figure 2-5 Stress-strain plots for two polymers. A represents a brittle polymer and B represents a ductile polymer.

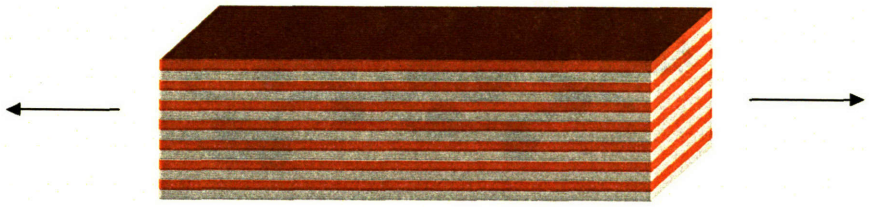

Figure 2-6 Schematic of multilayers made by co-extrusion. The specimen consists of alternating layers of the polymer to be tested with a ductile polymer.

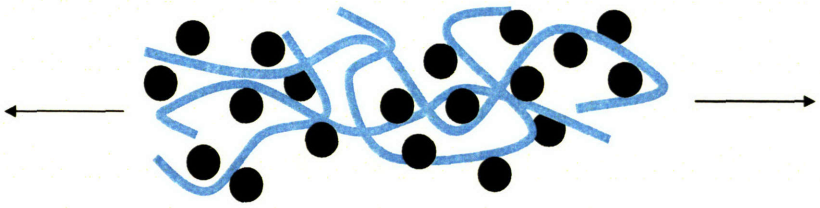

Figure 2-7 Schematic of a bulk polymer which is locally thinned by introduction of core-shell rubber particles. The average distance between two particles is the ligament thickness.

3 Characterization Methods for Thin Films

In this chapter, the characterization methods used to measure thin film properties are presented. Measurement of thin film properties at the micron length scale is a challenging task. In the first section, the procedure used to determine critical thickness is described. Critical thickness involves the determination of failure strains in thin films. Since pre-existing standards for measuring mechanical properties of thin films do not exist, new methods have to be developed. In the next section, several other polymer characteristic properties like molecular orientation, composition and crosslink density are discussed to assess whether these properties may possibly affect or relate to the critical thickness phenomenon. These properties are termed as "secondary properties".

3.1 Procedure to Determine Critical Thickness

In this study, a new method to measure critical thickness is developed. Films of several different thicknesses within a specified thickness range are fabricated using the technique of spin coating. Next, the failure strain is obtained as a function of film thickness. From a visual inspection of the strain to failure plot vs. the film thickness, a critical thickness is determined. A detailed description of the sample preparation procedure, the methods of straining films, optical microscopy techniques to determine failure strain and the method to determine critical thickness from the failure strain data is presented in this section.

3.1.1 Sample Preparation

The thin polymer film is fabricated atop a substrate using the process of spin coating. The spin coating method allows for fabrication of high quality and uniform thickness films.

For spin coating, first the polymer needs to be dissolved in a solvent. Next, several drops of the solution are poured on top of the substrate. Finally, the substrate is rotated so that the solvent evaporates leaving behind a thin polymer film. The polymer concentration in the solution and the rotation speed used in spin coating determine the film thickness. The sample preparation procedure is described below:

1. Substrate Preparation: All substrates are available as large sheets in the desired thickness (1.0mm or 1.5mm). The substrates have a protective coating on the use surface. Using standard machining tools the substrates are cut into the requisite dimensions (~3"x 0.75"). Next, the protective coating from the top surface is removed. The substrate material and substrate dimensions selection criteria are discussed in Appendix A.

2. Prepare Polymer Solution: A measured amount of the solid polymer is added to a known volume of the solvent. The polymer and solvent combination is then allowed to mix for several hours with the aid of a magnetic stir bar to obtain a homogenous solution.

3. Spin Coating: Spin coating is carried out using a Leybold spin coater. The substrate is held on to the base of the spin coater using vacuum pressure. A few drops of the solution are poured on top of the substrate. The substrate is then rotated at the desired spin speed for a specified amount of time. The polymer film is obtained after the rotation procedure is complete.

4. Post spin coating process: The films are processed either by vacuum treatment (as in the case of polystyrene) or by allowing them to cure at a desired

temperature (as in the case of the silicone thermosets). For vacuum treatment, the films are kept within a desiccator and a standard vacuum pump is used to apply vacuum pressure. For curing, the films are kept within a heating oven. A Fischer-Scientific oven is used for the experiments.

3.1.2 Application of Strain on Films: Bending Technique

In order to apply a strain on the film, a bending* technique has been used. Such a technique has been used previously to measure failure strains in metallic glasses, polymer films and flexible electronic circuits.[72-75]

First, the physics of bending of a film-substrate system is discussed (Figure 3-1). By virtue of the bending geometry the top portion of the system will be in tension and the bottom portion will be in compression. Within this film-substrate system, there is one surface which sees no strain. This surface is called the neutral axis. In Figure 3-1, the position of the neutral axis is denoted by a radial co-ordinate r_0. The strain (ε_r) at any location (radial co-ordinate r) within the system is given by:[76]

$$\varepsilon_r = \frac{r - r_0}{R} \qquad \textbf{Equation 3-1}$$

where R is the bending radius. The position of the neutral axis (r_0) is a function of the thicknesses and the Young's moduli of the substrate and the film. Considering the film and substrate are of thicknesses t_f and t_s with Young's moduli E_f and E_s respectively, the position of the neutral axis is given by:[75]

* In the present experiments bending is carried out manually.

$$r_0 = t_f + t_s + R - \left(\frac{t_f + t_s}{2}\right)\frac{(1+2\eta+\chi\eta^2)}{(1+\eta)(1+\chi\eta)}$$ **Equation 3-2**

where $\eta = t_f / t_s$ and $\chi = E_f / E_s$. In the present study, since the film thickness is much less than the substrate thickness, $\eta << 1$ (the highest value of η which has been used is 0.02). Additionally, $\chi \leq 1$, since the Young's modulus of the polymer film is either comparable to that of the substrate (in the case when a polymer substrate is chosen) or less than that of the substrate (in the case when a stainless steel substrate is chosen). Accordingly, for the present case the effect of η and χ in Equation 3-2 is negligible and therefore one obtains the position of the neutral axis as:

$$r_0 = \left(\frac{t_f + t_s}{2}\right) + R$$ **Equation 3-3**

Using Equations 3-1 and 3-3, the strain at the top surface of the film is:

$$\varepsilon_{film,top} = \left(\frac{t_f + t_s}{2R}\right)$$ **Equation 3-4**

The strain at the bottom surface of the film is:

$$\varepsilon_{film,bottom} = \left(\frac{t_s - t_f}{2R}\right)$$ **Equation 3-5**

Since $t_f << t_s$ in the current experiments, $\varepsilon_{film,top} \approx \varepsilon_{film,bottom}$. Accordingly, the strain in the film is nearly uniform throughout the thickness of the film. The strain value which is reported in the results sections of Chapter 4-8 is the average strain in the film given by:

$$\varepsilon_{film,average} = \left(\frac{t_s}{2R}\right)$$ **Equation 3-6**

Further, it is useful to examine how the neutral axis may shift as the bending proceeds to higher strains and whether that impacts the accuracy of the experimental data obtained. For this purpose, an integral form of the equation for neutral axis is considered. Along the neutral axis, the bending moment on any film-substrate cross-section vanishes and therefore one obtains:

$$\int \sigma(r)[r - r_0]dr = 0 \qquad \textbf{Equation 3-7}$$

where the function $\sigma(r)$ denotes the stress at a particular radial co-ordinate. As can be seen from Equation 3-7, the neutral axis would shift upon bending if there is asymmetry in yielding of the material on the tensile side vis-à-vis the compressive side.[72] For the present experiments, the polymer film has a thickness much less than the substrate and does not significantly influence the bending moment. Therefore it is sufficient to consider tensile vs. compressive behavior of the substrate and neglect the effect of polymer film yielding. To estimate the shift in the neutral axis, a stainless steel substrate is considered (most commonly used substrate in this study). In stainless steel, the maximum variation in tensile vis-à-vis compressive yielding is approximately ± 20%.[77] The shift in the neutral axis, as a first approximation, is proportional to the square root of the change in yield characteristics.[75] Therefore the neutral axis would shift by approximately ± 10%. Therefore if a mismatch in tensile vs. compressive yielding of stainless steel is present during experimentation and for calculation purposes the neutral axis is assumed to remain unchanged throughout the bending process, an experimental error in the measurement of strain arises. This error can be predicted by using Equation 3-1. For the present example, the error is ± 10%.

The bending experiments are carried out by flexing the entire film-substrate system against cylindrical metal rods. Strain is applied in increments by using metal cylinders of progressively smaller diameters. A schematic is presented in Figure 3-2. At every level, the film is thoroughly examined for crack initiation using optical microscopy. The lowest strain at which cracks are identified (irrespective of crack size) is established as the strain to failure value.

Instead of bending, an extension technique may be used to apply strain to the film-substrate system. An Instron is used for such experiments. The relative ease of performing the bending experiments makes then preferable to the extension experiments. A limited number of extension experiments have been carried out.

3.1.3 Crack Identification

The process of identifying cracks using optical microscopy can be considered a subjective exercise to a certain extent. Subjectivity can arise because the nature of cracks varies substantially with material, thickness of films, curing temperature and strain value. However, a carefully trained eye and substantial experience in this procedure minimizes uncertainty in crack identification.

Most notably, the nature of cracks varies with film thickness. For films having a thickness greater than critical thickness, the material behaves in a brittle fashion at low strains and cracks are correspondingly large. These cracks are at times visible to the naked eye and easily identifiable under an optical microscope at low magnifications (100x). The typical length scale for such brittle cracks in the plane perpendicular to the film thickness can range from 500μm to 5mm.

On the other hand, when conducting experiments with extremely thin films which are anticipated to crack at very high strain, the nature of the cracks changes and properly identifying cracks becomes challenging. Cracks in thin films may be classified as ductile and are much smaller compared to brittle cracks. The typical length scale for a ductile crack (in a plane perpendicular to film thickness) can range from 5μm to 30μm. In addition to the difficulty associated with optical identification of small cracks another complication arises. Since all the polymer films being studied are transparent, the background substrate features are visible. These background features vary dynamically with strain and become more prominent at higher strain. For example, in deformed stainless steel the grain structure can dominate the view field during microscopy. In order to discern cracks, the focal point has to be repeatedly brought in and out of focus of the top surface of the film as well as the substrate. After repeated steps of bringing the film in and out of focus, the presence of cracks is ascertained.

Furthermore, in some instances, cracks may only be present in certain isolated regions of the films. Such localized differences are not unexpected since there can be slight variations in the thickness of the films across the entire surface. Therefore for each step of microscopy, several different regions are randomly selected to test for presence of cracks. As a side note on thickness variation, one may consider what is described as "lip formation" within a spin coated film. During a spin coating process, a small "lip" region is formed at the edges, with a thickness much more than the inner region of the film. Therefore there exists the possibility of variation in fracture properties at the film edge vis-à-vis the film inner region.

In this thesis, micrographs* of strained samples for a number of specimens are presented to characterize failure strain. Typically, for this purpose two pictures are presented for each sample: one showing the highest strain at which the film does not fail and the other showing the film at the next incremental strain level at which failure is observed. These micrographs need to be interpreted carefully in order to ascertain the presence of cracks. Five selected micrographs are presented which serve as guideline to interpret structural features of the film and distinguish them from the features of the substrate.

The micrograph in Figure 3-3 shows a 1.5μm polystyrene film prior to strain application. Since the film is transparent, features of the stainless steel substrate are visible. Two typical features are noticed, the horizontal lines and dark speckles. For experiments in which stainless steel substrates are used, strain is applied in a direction which is parallel to these horizontal lines on the substrate. Accordingly, the cracks will appear perpendicular to any substrate features allowing us to clearly distinguish cracks within films.

In Figure 3-4, an optical micrograph is shown which depicts brittle cracks in a polymer film. This picture is of a 15μm film of engineered poly-methyl-phenyl-silsesquioxane (on top of stainless steel substrate) strained to 2.3%.† Large brittle cracks which span the entire vertical dimension can be seen. Smaller cracks are also observed. At the top left corner, a dust particle is seen. The stainless steel substrate features are not visible. Typically, upon deformation of a brittle film, large cracks are observed similar to ones seen in Figure 3-4.

---

* In the present experiments, a magnification of 100x – 1000x has been used consistently when examining the films under an optical microscope.

† Direction of strain application is horizontal in all pictures shown.

An optical micrograph is shown in Figure 3-5 which depicts a single ductile crack in a polymer film. This picture is of a 0.4μm methyl-silsesquioxane film strained to 14.5%. Areas in the top left and the bottom right are not in focus. With the substrate being highly bent it is not possible to bring into focus the entire field of view. In the middle portion of the picture, several deformation features can be seen. Stainless steel grains and grain boundaries are also observed. Some details of the grain structure can also be seen. A magnified view of a ductile crack (~20μm wide) within the film is shown in the inset. As described earlier, microscopy has to be carried out extremely carefully in order to clearly distinguish between substrate features from any cracks which may occur in ductile polymer films at large strains.

In Figure 3-6, an optical micrograph of an extremely thin film of C-resin prepared on a polycarbonate substrate is shown. The entire film-substrate system is strained to 7.9%. Small cracks are observed on the right side. In the center, a large dust particle is seen. Due to the presence of the dust particle, a circular region around it does not have a homogenous film thickness. Cracks around this dust particle are observed to be much larger than in the homogenous region of the film. Depending on the experiment, in certain cases, inhomogeneous regions are selected for microscopy studies to ascertain the presence of cracks.

In Figure 3-7, an optical micrograph of the edge region of an extremely thin (0.13μm) polystyrene film is shown. This polystyrene film is prepared on a polysulfone substrate. This picture depicts the lip region. In the top left area of the picture the substrate top surface is exposed. In the bottom right the film is seen. A magnified view of the lip region is also shown. Large cracks are observed in the lip region whereas no cracks are

seen in the inner film region. In certain cases, observations of film edge vis-à-vis film inner region have been used to identify critical thickness.

3.1.4 Critical Thickness Determination

Films of several different thickness values within a specified thickness range are prepared. The bending procedure is carried out to find the strain to failure for each of the films. A low strain to failure (0-3%) will be observed in brittle films whereas a high strain to failure (>10%) will be observed for ductile films. The failure strain data is plotted as a function of film thickness as obtained from bending experiments. By visual inspection of such a plot, a critical thickness can be determined. As an example, a schematic is presented in Figure 3-8. Three possible scenarios are considered. If for a material, the characteristic strain to failure vs. film thickness is of the form as depicted by plot A, it shows that the polymer is brittle across the entire range of film thickness. No critical thickness is therefore observed. For a material with a characteristic plot of the type B where a continual increase in strain to failure is observed, it may be difficult to assign a critical thickness. Plot C shows a unique critical thickness. In such a plot, the critical thickness is determined as the transition point from brittle to ductile behavior (marked on the plot).

In these experiments, the fracture strain in the film is measured while the film is on top of a substrate. Although the fracture properties of the polymer are not dependent on the nature of the substrate it is important to consider the factor of film-substrate adhesion. In order to carry out the experiments according to the bending techniques described above, a minimal amount of adhesion between film and substrate is necessary so that the film does

not delaminate when a strain is applied. For testing of certain polymers, multiple substrates are used for two purposes: first, to examine any film-substrate interactions which may affect critical thickness measurement and second to verify that the methods being used are not dependent on the nature of the substrate. Bending experiments for polystyrene have been carried out using stainless steel, silver and polysulfone substrates. C-resin experiments have been carried out on stainless steel and polycarbonate.

3.2 Secondary Property Testing

It is postulated that the fracture toughness of a polymer changes at the critical thickness. This change in fracture characteristics is ascribed to the mechanism of strain distribution (localized vs. delocalized) and is considered to be a direct consequence of change in thickness. However, it is possible that other physical and structural characteristics of a polymer are modified as a result of thickness change and allow the material to access its inherent deformation capability. In such a case, several possible scenarios exist. The fracture characteristics of the polymer may be correlated to or partly dependent on change in these other physical properties as well. These properties (termed as "secondary properties") include molecular composition, molecular orientation, entanglement density and glass transition temperature.

3.2.1 Molecular Composition (IR Spectroscopy)

This section is only relevant to thermosets. In thermoset materials, since a curing cycle is involved during which chemical reactions take place, it may be possible that chemical composition of the film changes with film thickness. As a result of any compositional

changes, the fracture properties may be affected. Therefore it is useful to monitor the composition of thermosets as a function of film thickness. Fourier Transform Infrared spectroscopy (FTIR) can be used to determine the molecular composition in a thin film. A comparison of the specific molecular peaks in the spectra for films of different thicknesses will indicate if there is a change in molecular composition. Molecular compositional changes are studied in poly-phenyl-methyl-silsesquioxane and engineered poly-phenyl-methyl-silsesquioxane. Reflection spectroscopy is used since the substrate being used for this study, stainless steel, is not transparent to infra red radiation.

3.2.2 Molecular Orientation (Infrared Dichroism)

Molecular orientation is typically known to affect polymer properties, for example in fibers and semi-crystalline polymers.[78] For polymer films which have a thickness in the micron to sub micron regime, in-plane molecular orientation of polymer chains may occur.[79] Characterization of orientation in thin (below critical thickness) vis-à-vis thick (above critical thickness) films would be of importance to test if molecular orientation may have bearing on fracture strain.

In-plane orientation in polymer molecules can be studied by making birefringence measurements or by using infrared dichroism techniques. In the present study, infrared dichroism[80] is used to measure orientation. The general principle[81] of this technique is that in a state of orientation the polymer light absorption characteristics are anisotropic and therefore dependent on the polarization state of incident light. By use of infrared dichroism techniques orientation can be measured for various chemical groups which correspond to the absorption bands in the spectra. To qualitatively evaluate anisotropy,

two infrared spectra are obtained, one with light polarized parallel and the other with light polarized perpendicular to the fixed reference direction. The ratio of the optical densities gives an estimate of the orientation. For this purpose, a dichroic ratio (R) is defined:

$$R = \frac{A_1}{A_2} \qquad \textbf{Equation 3-8}$$

where A_1 and A_2 are the absorption intensities for a particular band in the two polarization directions.* Molecular orientation (in a particular band) is exhibited when $R \neq 1$. For greater accuracy in orientation calculation a dichroic difference (D)† is typically evaluated which is defined as:

$$D = R - 1 \qquad \textbf{Equation 3-9}$$

In the present experiments, reflection spectroscopy has been used since the substrate (stainless steel) on which thin films are fabricated is not transparent to infrared radiation. Since orientation within a material is related to directionality, appropriate measurement geometry with proper light incidence angles needs to be used. For the reflection spectroscopy experiments carried out, the geometry is defined using a schematic as shown in Figure 3-9. In this figure, the three principal measurement directions are shown. With grazing angle incident light, absorption in XZ and YZ planes is measured (for unstrained films XZ and YZ planes are equivalent). Using a near-normal angle incident light, absorption in the XY plane is measured. To measure in-plane molecular orientation

---

* The inverse ratio (A_2/A_1) can also be defined as the dichroic ratio.
† In this thesis, the dichroic difference has been used to assess orientation.

in films (no strain applied), absorption measurements need to be performed in the XY plane using near normal reflection measurements.

Infrared dichroism measurements can also be used to determine the nature of strain (elastic or plastic) exhibited by the thin films (below critical thickness). For this purpose, thin films are extended to high strain (strain used is 10%) and then absorption measurements using the two light polarizations are carried out. If the nature of the strain is elastic, orientation will be observed in the strained films. * A discussion on measurement geometry is essential at this point. Figure 3-9 is considered. Without loss of generality, the straining direction is chosen to be along the Y axis. Accordingly, for orientation study, absorption measurements can be carried out in either the XY plane or YZ plane. The XY plane is selected.

In the experimental procedure, films are prepared on top of stainless steel. When required, the film-substrate combination is strained using an Instron. A Nicolet FTIR instrument is used. For near normal angle incidence absorption measurements, an accessory bench is used. A ZnSe polarizer is used for experiments. Stainless steel is used for background spectrum collection. An experimental detail of extreme importance is that for any particular sample, the two different polarization spectra need to be measured at exactly the same region.[80] For the present experiments, this arrangement is achieved through measurement of the spectra (at the two polarizations) one after the other by rotation of the polarizer by 90 degrees. Molecular orientation effects are studied in

* Time dependent effects can also be anticipated to occur in such measurements i.e. that the orientation in the thin film can change as a function of time. Such time dependent measurements have not been carried out due to equipment limitations. All samples are tested on the FTIR several hours after the elongation procedure is complete.

polystyrene, poly-phenyl-methyl-silsesquioxane and engineered poly-phenyl-methyl-silsesquioxane for both unstrained and strained films.

3.2.3 Network Density

The relation of the network density to the critical thickness is discussed in detail in Section 2.3.1. A change in network density as a function of the thickness can be crucial in understanding the size scale effects on toughness of a polymer. Experimentation to evaluate network density is extremely difficult. Typically, an estimate for the network density is obtained by first calculating the plateau rubber modulus $(G)^*$ of a polymer and then evaluating the molecular weight (M_c) between entanglement nodes using classical rubber elasticity theory:

$$M_c = \frac{\rho RT}{G} \qquad \textbf{Equation 3-10}$$

where ρ is the density, R is the gas constant and T is a reference temperature. Accurate measurement of network density in order to map the network density changes as a function of the polymer thickness is extremely difficult. Such experimentation has not been carried out before and is also beyond the scope of present research.

3.2.4 Glass Transition Temperature

A change in glass transition temperature as a function of film thickness may correlate to any effects the size scale may have on fracture properties. Extensive research is being conducted to study glass transition temperature of thin polymeric films, particularly for

* The plateau rubber modulus is equal to the storage modulus of the polymer at a frequency where the ratio of the loss modulus to the storage modulus is minimum.

polystyrene.[82, 83] Several researchers have claimed that the glass transition temperature is changed when the film thickness is reduced although there is no consensus on this topic. Measurement of glass transition temperature for thin polymer films is extremely challenging. These experiments and are not carried out in the present study.

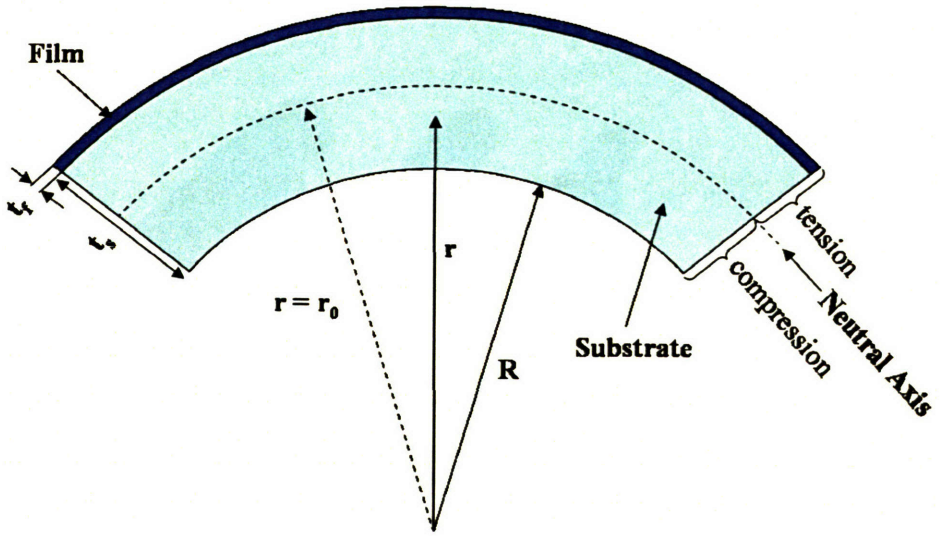

Figure 3-1 Illustration of bending in a film-substrate system. A cross-sectional view is shown. The thickness of the film is t_f and the thickness of the substrate is t_s. The radial co-ordinate is denoted by r. The bending radius is R. The neutral axis (radial position $r = r_0$) does not exhibit any strain and divides the region into two parts. The region above the neutral axis is in tension and the region below it is in compression.

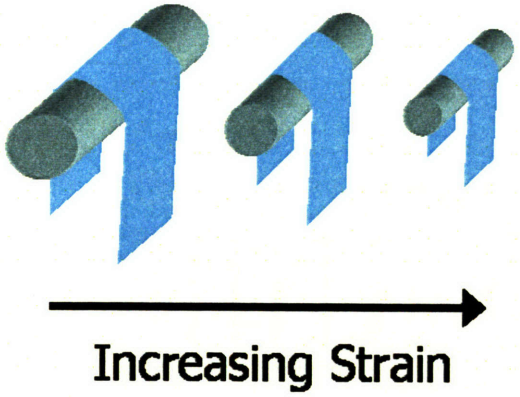

Figure 3-2 Schematic of a typical bending experiment. As the film-substrate system is bent over cylinders with progressively decreasing diameters, the strain in the film increases.

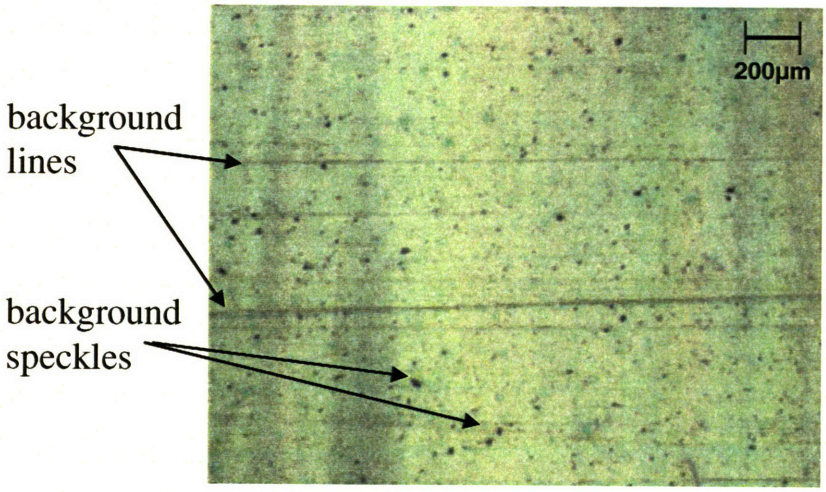

Figure 3-3 Micrograph of a 1.5µm polystyrene film on top of a stainless steel substrate. No strain is applied to the film-substrate system in this case. The substrate features (horizontal lines and speckles) are visible.

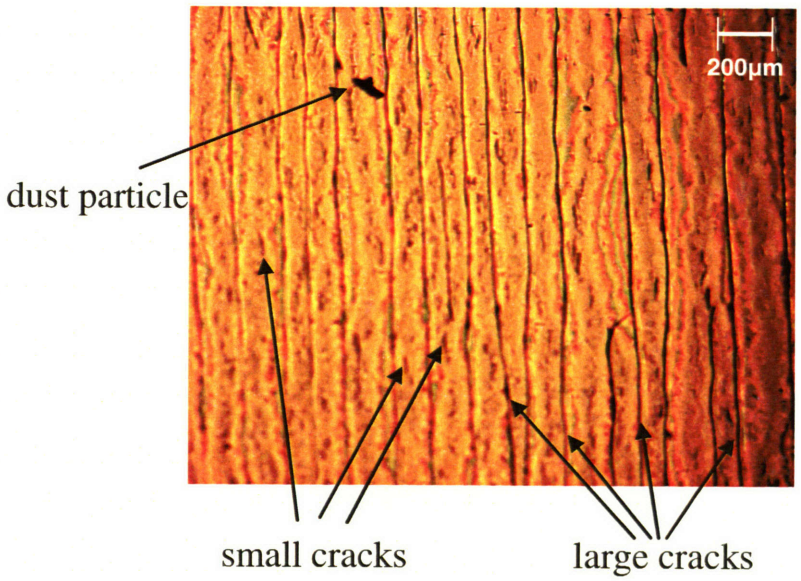

Figure 3-4 Micrograph of a 15μm film of engineered poly-methyl-phenyl-silsesquioxane strained to 2.3%. The substrate is stainless steel. Large brittle cracks in the film are observed which span the entire vertical dimension. Smaller cracks are also observed.

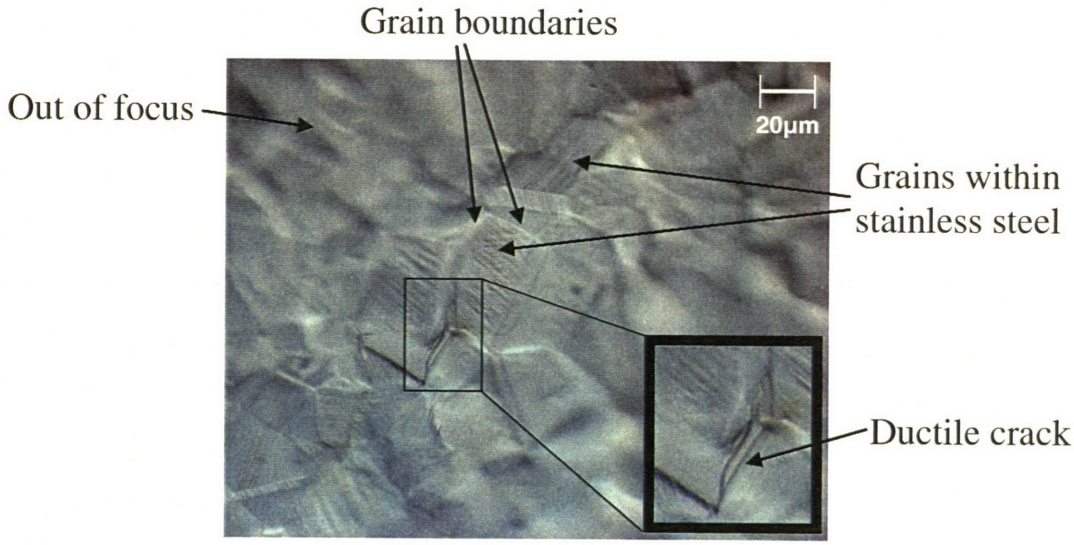

Figure 3-5 Micrograph of a 0.4μm film of methyl-T resin strained to 14.5%. Areas in the top left and the bottom right are not in focus. In the middle portion of the picture, several deformation features of stainless steel substrate are seen. A magnified view of the ductile crack within the film is shown in the inset. The length of the crack is ~20μm.

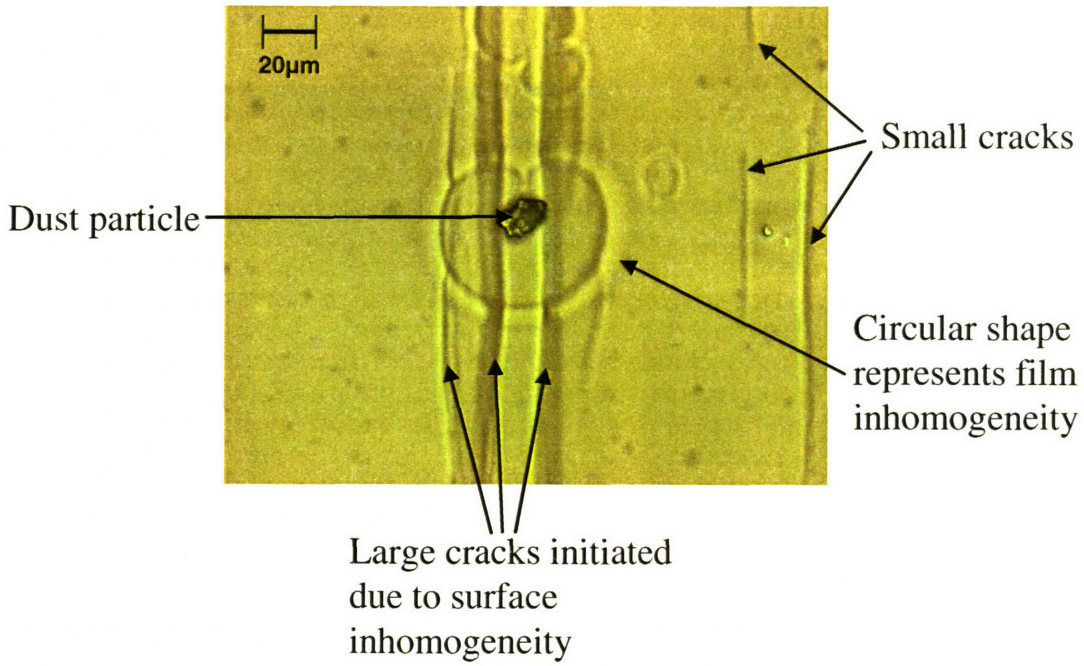

Figure 3-6 Micrograph of an extremely thin film of C-resin prepared on a polycarbonate substrate. The entire film-substrate system is strained to 7.9%. Small cracks are observed on the right side. In the center, a large dust particle is seen. Cracks around the dust particle are much larger than in other regions.

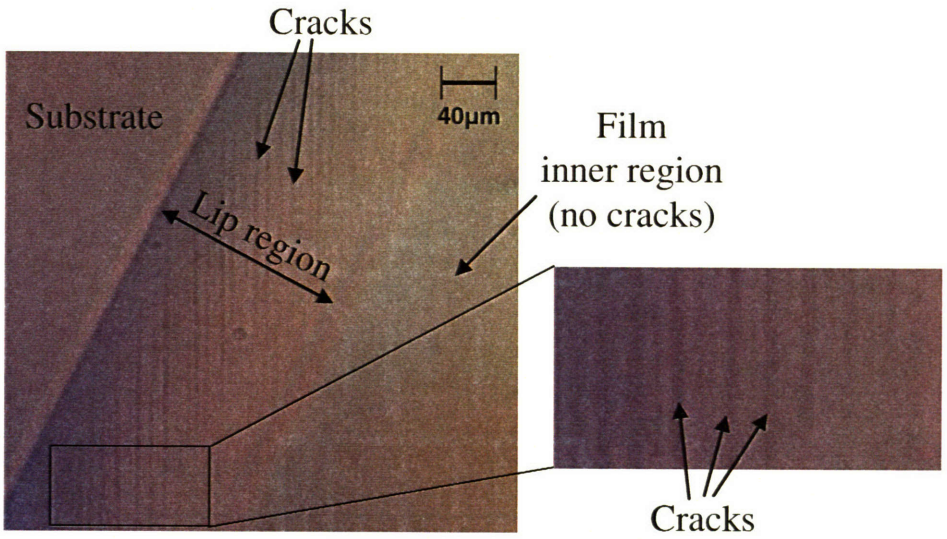

Figure 3-7 Micrograph of film edge depicting the lip region of a 0.13μm polystyrene film. This polystyrene film is prepared on a polysulfone substrate. The entire film-substrate system is strained to 4.8%. In the top left area of the picture the substrate top surface is exposed. In the bottom right the film is seen. In the lip region, which is much thicker than the film, several large cracks are observed. No cracks are observed in the film inner region. A magnified view of the lip region is also shown.

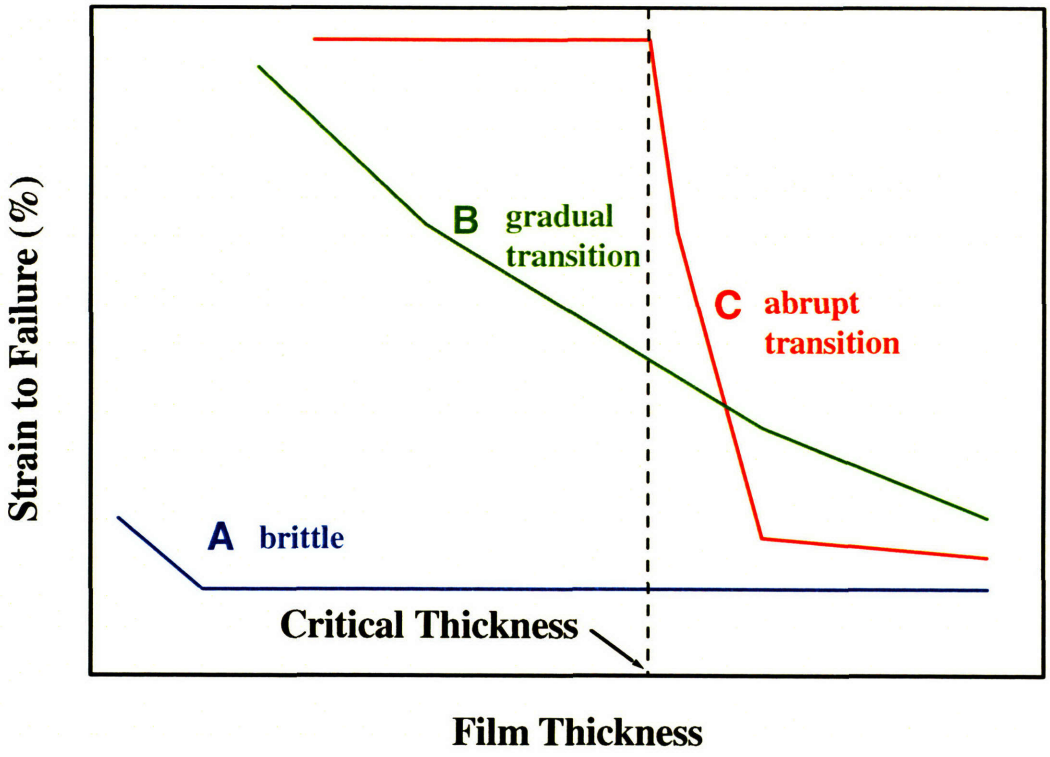

Figure 3-8 Schematic of typical failure strain vs. film thickness plots. Plot A depicts fracture strain for a highly brittle polymer. The fracture strain has a low value over the entire thickness range. Plot B depicts a gradual change in fracture strain as a function of film thickness. Plot C depicts a typical failure strain behavior for a material which exhibits the critical thickness phenomenon. The critical thickness is the transition point from brittle to ductile behavior.

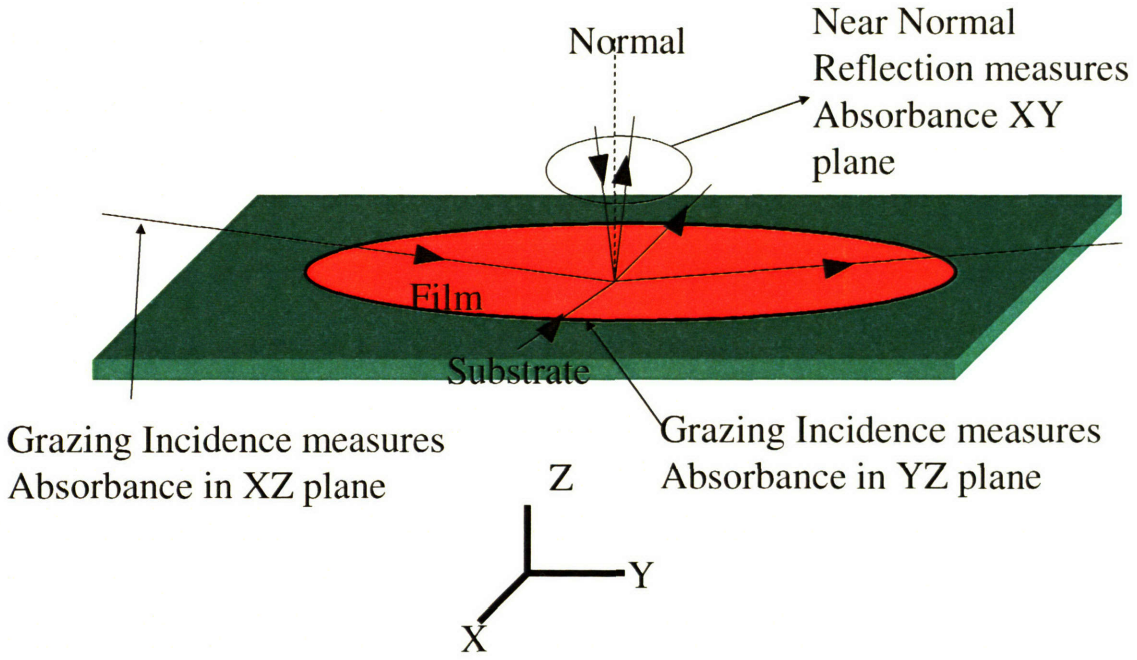

Figure 3-9 Schematic depicting the geometry for reflection spectroscopy experiments. The polymer film is represented as the oval shape. This polymer film is atop a substrate. A X-Y-Z co-ordinate system is marked for reference. This convention is used throughout. Three principal measurement directions are shown. With a grazing angle incidence, absorption in XZ and YZ planes is measured. Using a near-normal angle incidence, absorption in the XY plane is measured. For unstrained films, symmetry dictates that X and Y directions are equivalent. Therefore, XZ and YZ plane absorption measurements are equivalent. To measure in-plane molecular orientation in films (no strain applied), absorption measurements need to be performed in the XY plane using near normal reflection measurements. For the case of absorption experiments on strained films, without loss of generality, the straining direction is chosen to be along the Y axis. For orientation measurements in strained films, absorption measurements can be carried out in either the XY plane or YZ plane. XY plane is used for measurements in strained films.

4 Polystyrene Results

Polystyrene is a hard thermoplastic material. It is a commonly used polymer and is fairly inexpensive. Polystyrene can be processed using a variety of techniques including blow molding, injection molding and extrusion. Common applications of polystyrene include the outside housing of computers - fabricated from a rubber modified polystyrene, foamed polystyrene for packaging (Styrofoam), model cars, and clear plastic drinking cups. Although used extensively in its rubber modified versions, virgin polystyrene is extremely brittle and not suitable for practical applications.

Structurally, polystyrene is a vinyl polymer, with a carbon backbone and has one phenyl group attached to it on every other carbon atom. The typical structure of a polystyrene molecule is:

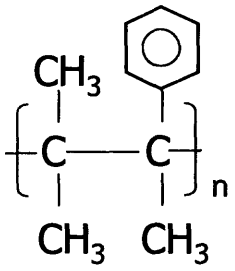

In bulk form polystyrene undergoes failure at a strain of less that 2-3%. As discussed in Section 2.1.2, premature fracture of polystyrene is a consequence of the uncontrolled crazing process which occurs due to strain localization within the polymer.

To demonstrate validity of critical thickness, polystyrene has been chosen as a model polymer. Extensive studies have been carried out in past to investigate the micro-mechanical deformation mechanisms in polystyrene thin films.[41, 60] Further, indirect

experiments as described in Section 2.5, have been carried out to measure critical thickness of polystyrene. Analytical models have been used previously to predict critical thickness for this polymer. In this chapter, the results of bending experiments are presented and a critical thickness value is determined. Further, infrared spectroscopy results on polystyrene thin films vis-à-vis thick films are presented. The polystyrene chosen is a commercially available Dow Styron grade with a molecular weight of 80,000.

4.1 Critical Thickness Results

4.1.1 Thin Film Fabrication

Polystyrene films of different thicknesses in the range from 0.1μm – 1.5μm have been prepared on three substrates: stainless steel, polysulfone and silver.* The solvents used are toluene (for stainless steel substrate) and methyl-isobutyl-ketone (for polysulfone and silver substrates). Spin coating is carried out for one minute at a spin speed of 1300 RPM for films prepared on stainless steel substrate. For films prepared on polysulfone and silver substrates a 2500 RPM spin speed is used. An acceleration of 425 revolutions/min^2 is utilized in both cases. The film thickness is measured using a profilometer; the values for film thickness and the corresponding solution concentrations are presented in Appendix B.

4.1.2 Bending Test Results

First, bending test results for polystyrene films fabricated on a stainless steel substrate are presented. In Figure 4-1(a-1) a picture of a 1.5μm film prior to strain application is

* ~5μm film of silver is deposited on top of flexible polycarbonate.

shown. The horizontal lines and speckles are due to the stainless steel. Application of a 2.3% strain to this film (strain in horizontal direction)* results in large vertical cracks as seen in Figure 4-1(a-2)). These cracks are approximately 0.2–1mm across and are noticeable even with the naked eye. In Figure 4-1(b-1) a 0.28μm film prior to strain application is shown. Stainless steel substrate features are visible. Upon application of a 2.3% strain to this film, small cracks are observed (Figure 4-1(b-2)). These cracks are approximately 20μm in length. These cracks are much smaller in size compared to the cracks observed in the 1.5μm film. Next, results for a 0.21μm film are presented in Figure 4-1(c-1, c-2). At 5.3% strain the film does not crack as depicted in Figure 4-1(c-1). When this film is strained to a value of 6.o% cracks appear (Figure 4-1(c-2)). The cracks are most readily observable in the inset in Figure 4-1(c-2). Therefore a change in polystyrene toughness properties is already being observed. Whereas a film of 0.28μm can sustain only a 2.3% strain, a 0.21μm film can sustain a strain of 5.3%. Finally, bending results on a 0.11μm film are presented in Figure 4-1(d-1) and (d-2). At both 6.8% and 15% strain no cracks are observed which suggests ductile nature of the thin film. In the last two figures, the stainless steel bands and grain structure becomes more prominent.

In Figure 4-2, the bending test results for polystyrene films fabricated on polysulfone substrate are presented. In Figure 4-2(a-1), the edge of a 0.3μm film prior to strain application is shown. This 0.3μm film cracks at a 3.9% strain (Figure 4-2(a-2)). These cracks are fairly large and extend several millimeters across. Figure 4-2(b) shows a 0.13μm film with a lip region, a typical characteristic of a spin coated film. In the lip region, the thickness of the film is much more (four to five times) compared to the inner

* For all the optical micrographs which show bending test results in this thesis, the direction of strain application is horizontal.

region. In this 0.13μm film, cracks are observed only in the lip region and not in the inner film. The cracks which are observed span the entire lip region and arrest at the film. This observation provides a good comparison of fracture toughness of polystyrene in thin vis-à-vis thick film form. In the film region which is thin, cracking resistance is much higher as compared to the lip region which is thick. Further experimentation using this film is not carried out since the substrate is observed to crack if the strain is increased. In Figure 4-3, a 0.15μm thick film of polystyrene on a silver substrate strained to a 6.8% is shown. Again cracks are only observed in the lip region and not in the inner film. Similar to the case of polystyrene film on polysulfone substrate, further experimentation of polystyrene on a silver substrate is not carried out since the substrate begins to crack.

In Figure 4-4, the strain to failure value is plotted as a function of film thickness according to the bending tests. Two plots are shown for bending tests carried out using stainless steel and polysulfone substrates. The lower plot (in solid line) depicts the highest strain that is achieved at a particular film thickness. The dashed line depicts the next incremental strain level at which failure is observed. For bending tests carried out on a silver substrate only the solid line is shown. From these plots, it is clear that strain to failure increases as film thickness reduces. A rather abrupt change in strain to failure is observed at around the 0.1-0.2μm thickness. Therefore the critical thickness is ~0.1μm. From these results it is seen that polystyrene thin films below the critical thickness can sustain >15% strain. This value of strain is attained for films fabricated on stainless steel. The green region denotes the range of film thickness for which eventual failure in films is not attained because of substrate limitations.

4.1.3 Comparison of Experimental Results to Models

The experimentally obtained value of critical thickness for polystyrene is ~0.1μm. According to the energy based model presented in Section 2.2.1 the predicted value of the critical thickness is 0.05μm. The mechanics based model presented in Section 2.2.2 predicts a critical thickness of 0.06μm. While the three values do not match up exactly, the experimental value is of the same order of magnitude as the analytically determined values. Considering the rather simplified nature of the models, the experimental and theoretical values match up fairly reasonably.

4.2 IR Dichroism

As discussed in Section 3.2.2, in the present experiments, a dichroic difference is used to assess orientation in polystyrene. As a reference, prior to presentation of experimental results, a discussion on reference dichroic difference values for oriented materials is carried out. Ideally, for a perfectly oriented material, the dichroic ratio will either be infinity or zero. A more useful reference for practical considerations is taken from literature. The dichroic ratio for a 100% elongated uniaxially oriented polypropylene is estimated to be approximately 2.5.[80] This value would correspond to a dichroic difference of approximately 150%. Assuming linearity,* a 10% extension would correspond to a dichroic difference of approximately 15%.

Two films of different thickness values are considered. These two films are designated as thick film (above the critical thickness) and thin film (below the critical thickness). The

* Although the mathematical forms of the orientation functions are rather complex and not linear, as a first approximation, a linear correlation between elongation and orientation is assumed.

thick film chosen is ~2μm and the thin film chosen is 50nm. In Figure 4-5, spectra obtained for the two polarizations and the dichroic difference result are presented for a thick polystyrene film (no strain application). From the dichroic difference, it is clear that no orientation is observed in the thick film. In comparison, the dichroic difference result for a thin film of polystyrene in Figure 4-6 also shows no substantial orientation effects. Therefore, it can be inferred that orientation in films does not correlate with fracture strain change for the thin vs. the thick film.

Further, to assess the nature of strain, a thin film (50nm) of polystyrene which is elongated to 10% is considered. In Figure 4-7, the results for the thin stretched film are presented. The peak observed at ~3000 cm^{-1} where orientation is observed corresponds to stretching in the benzene ring. Besides this peak, no other absorption peak shows any substantial orientation. The dichroic difference (<1%) is much less than what is observed according to the reference (~15%). Accordingly, it is inferred that the extra extension in thin films is attributable to plastic strain.

4.3 Summary

According to the bending test results, polystyrene has a critical thickness of approximately 0.1μm. This value is comparable to previous results obtained using the indirect test methods performed by VanderSanden and co-workers as well as to the numerical value predicted using the analytical models. Further, according to the results, at the critical thickness length scales polystyrene behaves in a ductile manner with a strain to failure of at least 15%. Additionally, use of the different substrates for critical thickness measurement has shown that the fracture strain value of polystyrene for

different thicknesses is largely independent of the nature of the substrate material. In the future, experimental methods which could test extension values substantially greater than 15% need to be designed since the draw ratio predicts an extension of >100% in polystyrene.

Direct validation of critical thickness for polystyrene is a crucial step in utilization of this phenomenon for applications. Since the analytical models accurately predict a critical thickness for polystyrene, for other materials extensive experimental investigations may not be necessary since these can be used to predict critical thickness. For polystyrene in particular, thin films below critical thickness can be used directly in applications like coatings. Commercial polystyrene materials without the standard rubber toughening protocols can be envisioned to be used in practical applications: for example, foamed structures and thin film applications.

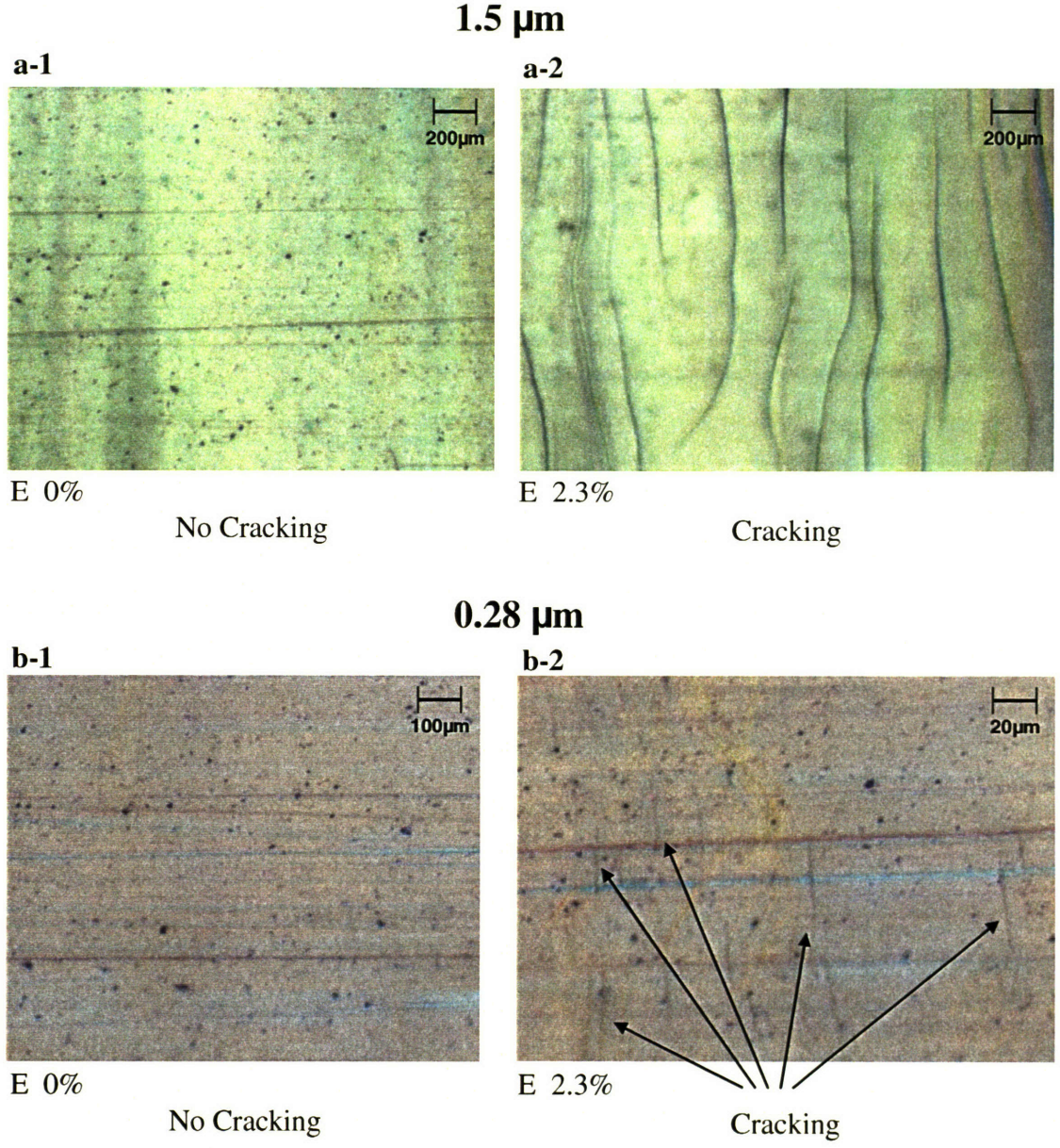

Figure 4-1 Microscopy results for bending tests carried out on polystyrene films which are prepared on a stainless steel substrate. (a-1) 1.5µm thick film prior to strain application is shown. Speckles and horizontal lines observed are characteristic substrate features. (Note: This micrograph has been presented before in Section 3.1.3.) (a-2) Brittle cracking observed in a 1.5µm thick film at 2.3% strain. Most cracks span the entire vertical dimension of the picture. Cracks are several mm across. (b-1) A 0.28µm film prior to application of strain. Speckles and horizontal lines are characteristic of stainless steel. (b-2) Cracking observed in a 0.28µm film at 2.3% strain. Several cracks have been labeled. Cracks are ~20-30µm across.

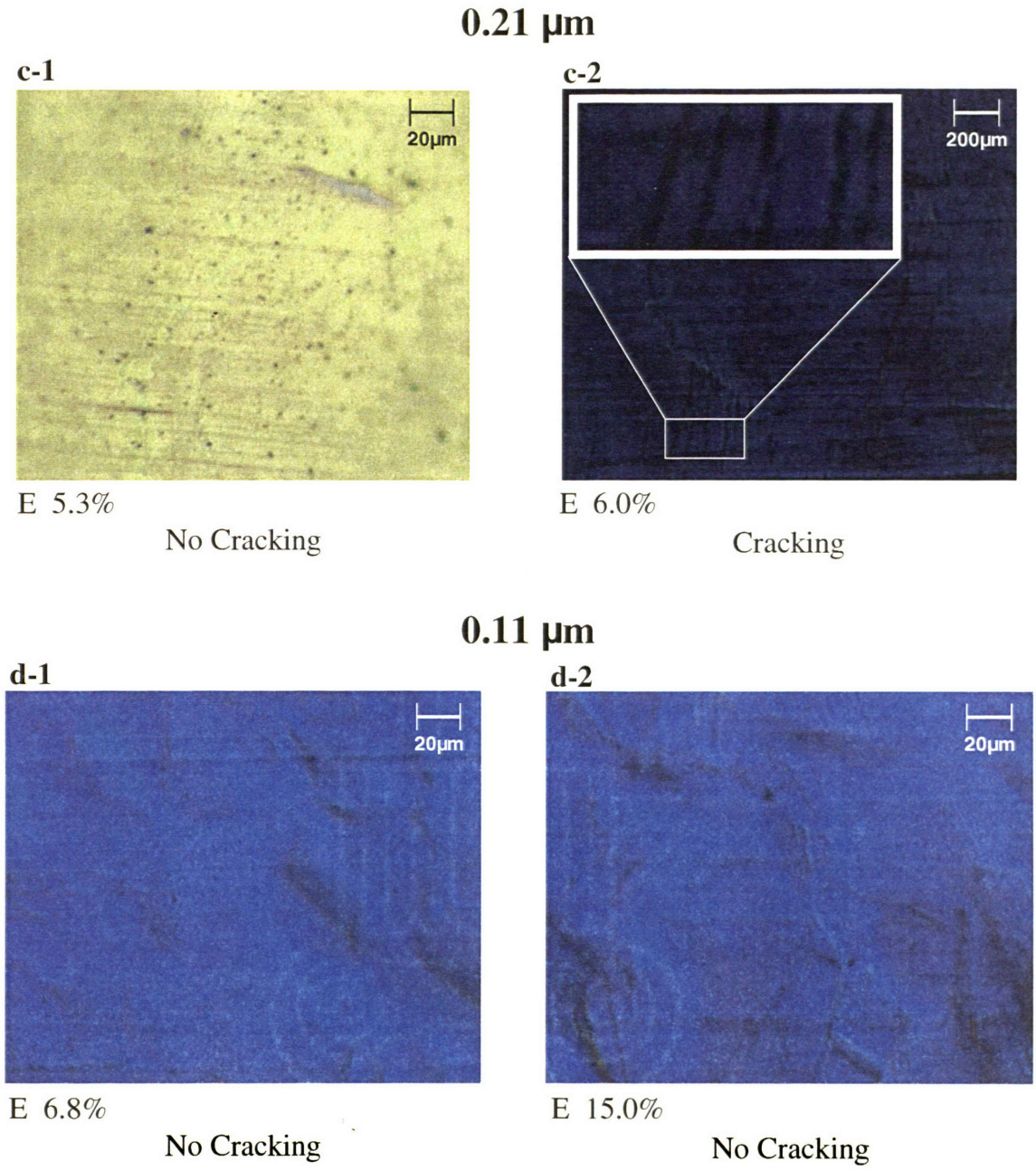

Figure 4-1 Polystyrene films on stainless steel. (c-1) No cracking in a 0.21μm thick film under 5.3% strain. Speckles and horizontal lines are characteristic of stainless steel. (c-2) Cracking observed in a 0.21μm thick film at 6% strain. Several cracks are observed throughout the film. A magnified region is shown in the inset. Grain structure of the deformed stainless steel is also visible. Typical crack length is ~200μm. These cracks seem to have a character which cannot be classified as purely brittle or ductile. (d-1) No cracking is observed in a 0.11μm thick film at 6.8% strain. Grains of the stainless steel are visible. (d-2) No cracking observed in a 0.11μm thick film at 15% strain. Characteristic grain structure of stainless steel dominates the view field.

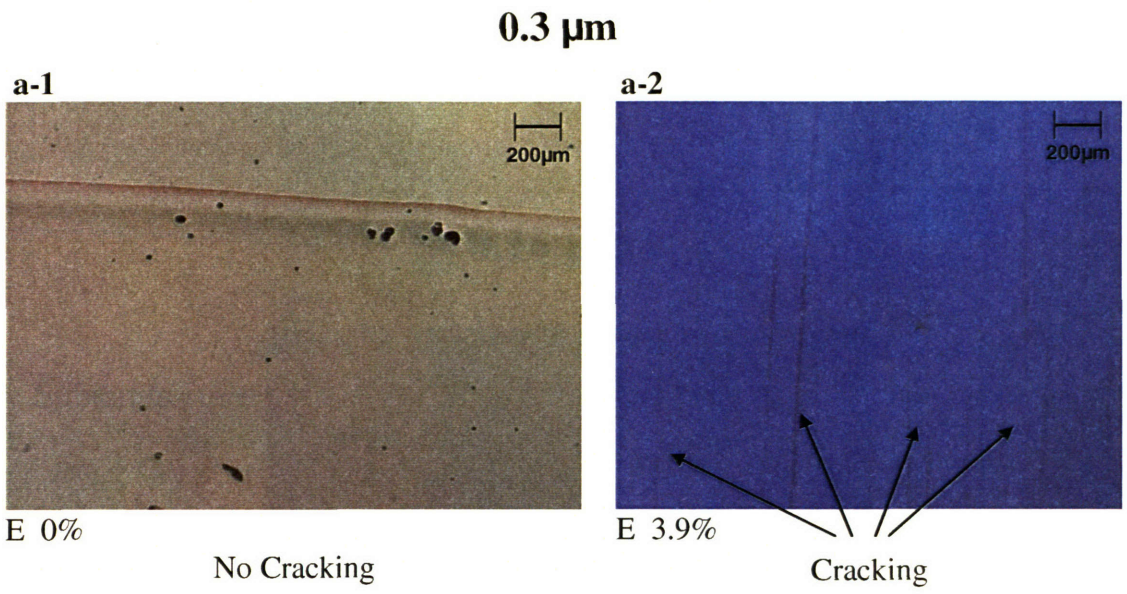

Figure 4-2 Micrographs from bending tests carried out on polystyrene films which are on top of a polysulfone substrate. (a-1) A 0.3µm thick film prior to strain application is shown. The film edge is visible. Several dust particles are observed (black spots). (a-2) Brittle cracking is observed in a 0.3µm thick film at 3.9% strain. Several of these cracks are labeled. The cracks are over several mm in length. (b) A 0.13µm film is shown at 4.8% strain. Cracking is observed in the lip region. No cracking is observed in the inner region of the film. (Note: this micrograph has been previously presented in Section 3.1.3.)

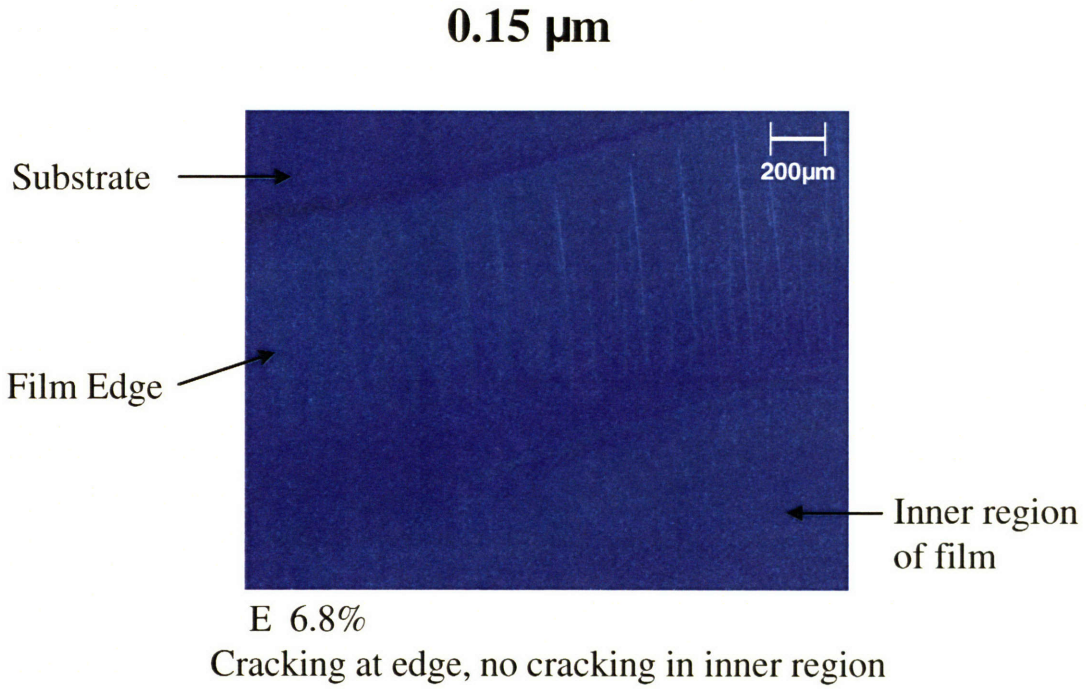

Figure 4-3 Micrograph from bending test carried out on polystyrene which is on top of a silver substrate. A 0.15µm film is shown at 6.8% strain. Cracking is observed in the lip region. No cracking is observed in the inner region of the film. The cracks are ~500µm wide extending throughout the lip region. (Note: this micrograph is similar to the one presented in Section 3.1.3. Interpretation of structural features within the micrograph is on lines similar to that discussed for Figure 3-7.)

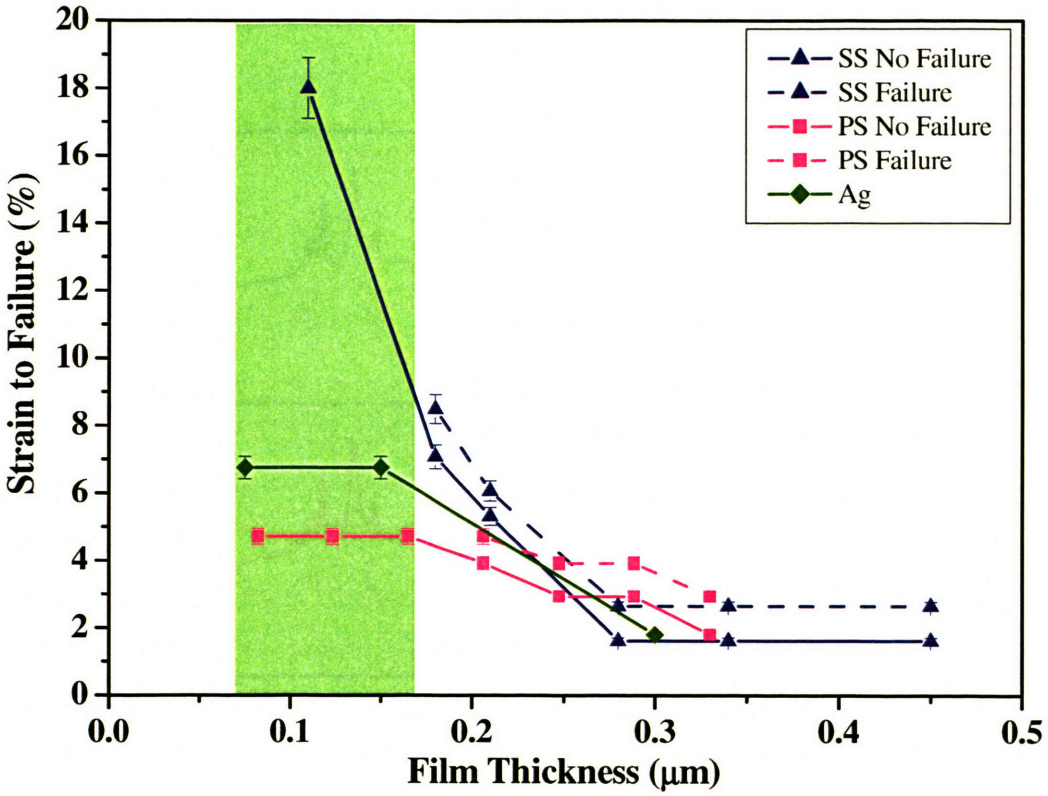

Figure 4-4 Plot of strain to failure as a function of film thickness for polystyrene obtained from bending test results. Two lines are shown for bending tests carried out on polystyrene films prepared on top of stainless steel and polysulfone substrates. The solid line depicts the highest strain sustained at a particular film thickness. The dashed line depicts the next incremental strain level (at which failure is observed). For bending tests carried out on a silver substrate only the solid line is shown. In all cases, an abrupt change in strain to failure is observed at around the 0.1-0.2μm thickness. For polystyrene thin films on stainless steel substrate (below critical thickness) a strain of >15% is sustained. This value of strain is attained for films fabricated on stainless steel. The green region denotes the range of film thickness for which eventual failure in films is not attained because of substrate limitations. (Error bars for all plots are according to the analysis presented in Section 3.1.2. Error bars for data points corresponding to low strains are not visible since they are buried in the marks that indicate the average value.)

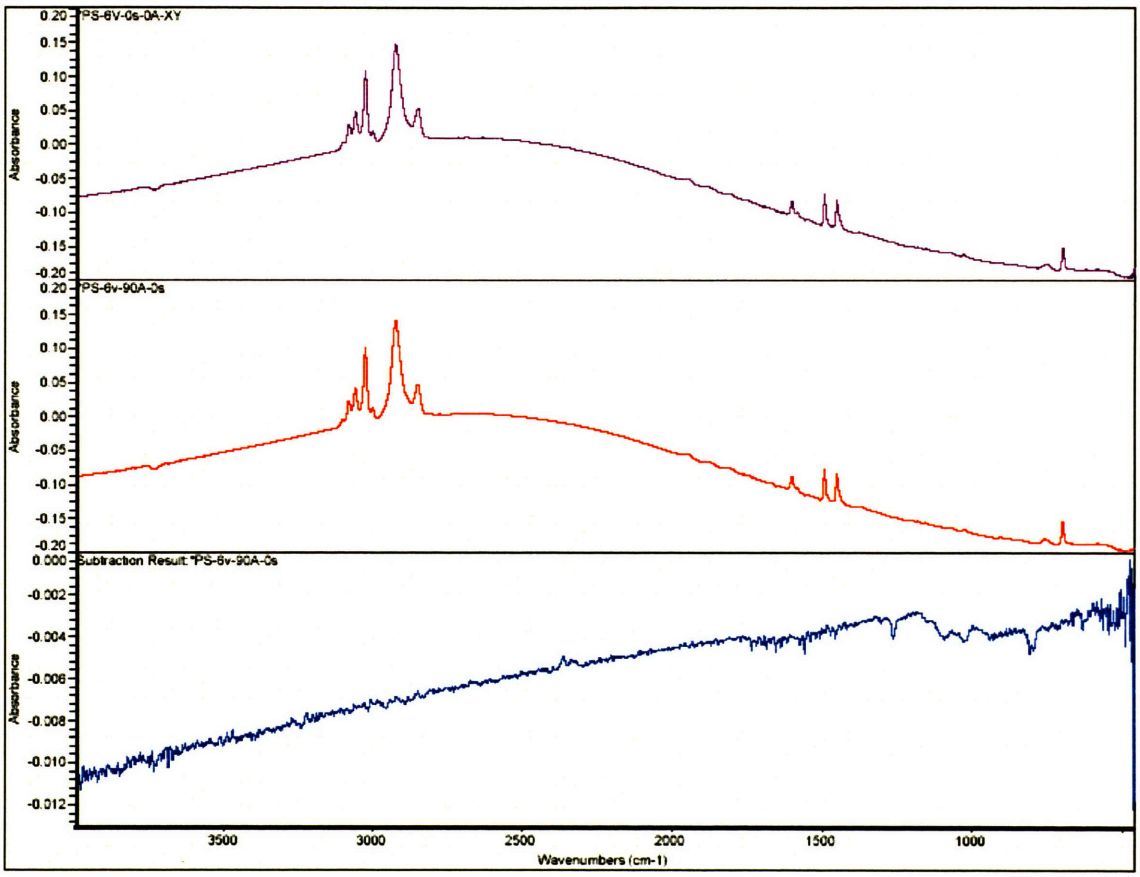

Figure 4-5 Results of orientation study carried out on a polystyrene thick film (2.0μm). No strain is applied. The top two graphs show the IR spectra for the two different polarizations. The bottom curve is the resultant difference obtained upon subtraction of the first graph from the second.

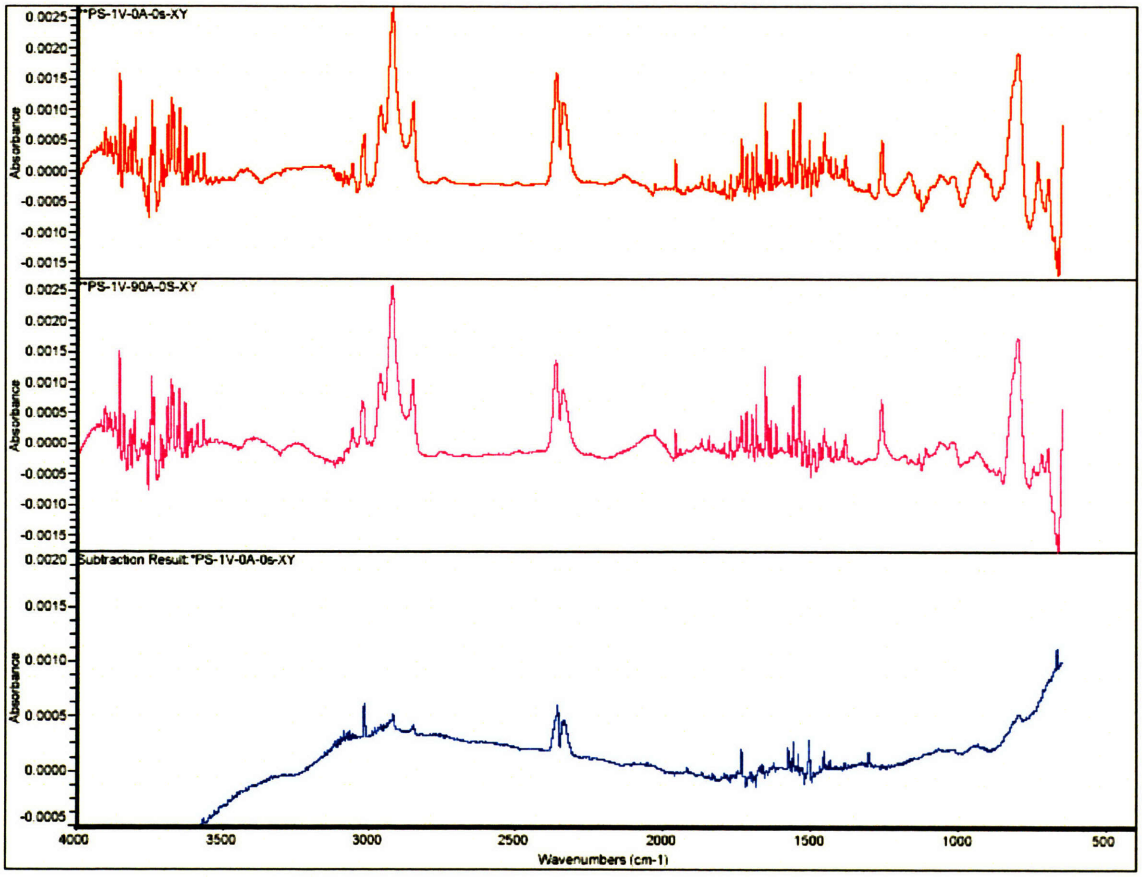

Figure 4-6 Results of orientation study carried out on a polystyrene thin film (50 nm). No strain is applied. The top two graphs show the IR spectra for the two different polarizations. The bottom curve is the resultant difference obtained upon subtraction of the first graph from the second. Peak at 2300 cm^{-1} is due to carbon-di-oxide.

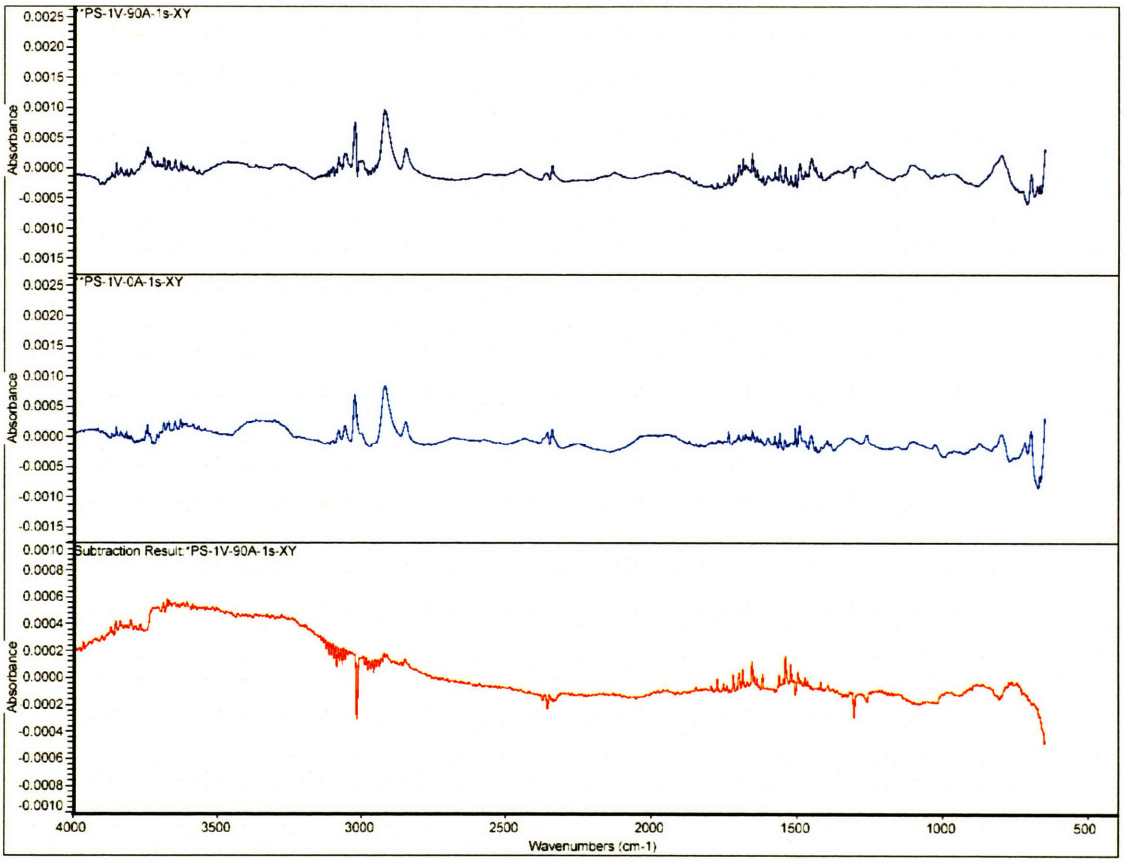

Figure 4-7 Results of orientation study carried out on a polystyrene thin film (50nm) at 10% elongation. The top two graphs show the IR spectra for the two different polarizations. The bottom curve is the resultant difference obtained upon subtraction of the first graph from the second.

5 Poly-phenyl-methyl-silsesquioxane*

The poly-phenyl-methyl-silsesquioxane chosen for this study is a commercially available condensation cure resin called 4-3136 † which is manufactured by Dow Corning Corporation. 4-3136 resin is a laminate binder and has been successfully used in composites as a matrix material. In this study, 4-3136 is chosen due to three reasons: First, this silicone resin has superior mechanical properties compared to many other condensation cure silicone resins. Second, mechanical properties including fracture toughness and physical properties of this material have been experimentally investigated in detail previously.[37, 55] Finally, experimental work to toughen this resin in bulk form using a Phase-I/Phase-II method[37, 55] has been carried out in past. Critical thickness tests have also been carried out on 4-3136 in the McGarry lab previously.[84] 4-3136 is therefore a suitable candidate for critical thickness investigation since a fair amount of information is already available on this resin.

The composition of 4-3136 resin is $(PhSiO_{3/2})_{0.40}(MeSiO_{3/2})_{0.45}(Ph_2SiO)_{0.10}(PhMeSiO)_{0.05.}$ 4-3136 is synthesized by cohydrolisis of a stoichiometric mixture of phenyltrichlorosilane, methyltrichlorosilane, diphenyldichlorosilane and phenylmethyldichlorosilane in presence of excess amounts of water and acid. The reaction is carried out to obtain a pre-polymer with a number average molecular weight of approximately 1500. The pre-polymer is highly branched and has several unreacted silanol ends which are utilized to form a crosslinked material during the curing cycle.

---

* Bending experiments carried out in collaboration with Mr. Andrew Satorius.
† In the text the condensation cure resin is identified by the commercial name 4-3136.

5.1 Critical Thickness Results

5.1.1 Thin Film Fabrication

4-3136 resin films samples of different thicknesses (thickness range 0.1μm – 20μm) are prepared on stainless steel substrates using spin coating. The solvent used is methyl-isobutyl-ketone. A catalyst, tin tetra butoxide, commercially available as Y-177 catalyst, is added in a 0.05 wt% ratio of the pre polymer. Spin coating is carried out for one minute at a spin speed of 1300 RPM. An acceleration of 425 revolutions/min^2 is used. The film thickness is measured using a profilometer. The values for film thickness and the corresponding solution concentrations are presented in Appendix C.

After this step the films undergo a curing cycle. Multiple curing temperatures are utilized to investigate how the curing temperature affects the mechanical properties. For the curing cycle, first the temperature is increased from room temperature to 70°C at a rate of 10°C/min. At 70°C the film is allowed to pre-cure for 30 minutes. Next, the temperature is increased at 5°C/min to reach the final cure temperature. The films are then allowed to stay at the cure temperature for one hour. Subsequently, the film is allowed to cool to room temperature at a rate of 3°C /min.

5.1.2 Bending Test Results

Five curing temperatures for 4-3136 are selected for experimentation: 177°C, 200°C, 225°C, 250°C and 300°C. The curing temperature selection is based on prior information available for 4-3136 resin curing in bulk form.[37, 55] These previous publications indicate that a cure temperature in the 200-225°C range results in the best performance for 4-3136

resin. Additional cure temperatures for present study are selected in order to explore their effect on mechanical properties. Optical micrographs are presented for bending tests carried out on 4-3136 samples cured at three chosen temperatures: 177°C, 225°C and 250°C.

First, optical micrographs from bending tests carried out on 4-3136 samples cured at 177°C are presented in Figure 5-1. In Figure 5-1(a-1), a 2.4μm film is shown at 1.9% strain, the lowest strain attainable prior to cracking. In Figure 5-1(a-2) it is shown that this 2.4μm film cracks at 3.0% strain. These cracks are observed to be brittle. They are optically visible and at least 250μm in length. When the film thickness is reduced from 2.4μm to 2.2μm a dramatic shift in fracture strain value is observed. Figure 5-1(b-1) shows the 2.2μm film without cracking at 13.6% strain. At 17.9% strain, the film cracks in a ductile manner as shown in Figure 5-1(b-2). The ductile cracks in this figure are ~20-30μm in length. In these last two pictures, the grain structure of the stainless steel dominates the entire view field. Based on these bending tests, the critical thickness for 4-3136 cured at 177°C is determined to be 2.2μm.

Next, the sequence of optical micrographs for tests carried out on 4-3136 samples cured at 225°C temperature are presented in Figure 5-2. For a 7.3μm film, the highest strain at which no cracks are observed is 1.2% (Figure 5-2(a-1)). Large brittle cracks which are at least 250μm in length appear at a strain of 1.9% strain (Figure 5-2(a-2)). As compared to a 7.3μm film, a 5.7μm film shows no cracks at a 9.5% strain (Figure 5-2(b-1)). Cracks appear at a strain of 13.6% (Figure 5-2(b-1)). These cracks are observed to be ductile and much smaller than the brittle cracks observed in thicker films. The crack length is

~20-30μm. Based on these bending test micrographs, a critical thickness value of ~5.7μm is determined for 4-3136 cured at 225°C.

Finally, results for the 250°C cure temperature are presented in Figure 5-3. A gradual decrease is observed in strain to failure value as a function of increasing film thickness. A film of 19.5μm is observed to crack at 3.8% strain (Figure 5-3(a)). The crack length is over 1mm. A 5.5μm film is observed to cracks at 9.6% strain as shown in Figure 5-3(b). The crack length is ~200μm.

The results of the bending tests are summarized in Figure 5-4. For films cured at 177°C the critical thickness value is ~2.2μm. A strain to failure of 13% is observed for films below critical thickness compared to the failure strain of 2% observed for films above critical thickness. For 4-3136 cured at 200°C a critical thickness of ~4μm is observed. At critical thickness, the strain transition is from 2% to 13%. The highest critical thickness of 5.7μm is observed for 4-3136 when the material is cured at 225°C. Data for 250°C and 300°C cured 4-3136 films indicates a departure from critical thickness behavior. The films cured at 250°C show a gradual increase in failure strain from 3% for a 20μm film to a failure strain of 10% for a 4-5μm film. For 4-3136 cured at 300°C it is observed that brittle fracture occurs for the entire range of film thickness. It is presumed that film properties at 250°C and 300°C deteriorate because of atmospheric oxidation of the material at these high temperatures.

5.1.3 Comparison of Experimental Values to Models

In order to compare the experimental value of the critical thickness for 4-3136 to an analytical prediction, Equation 2-10 is used:

$$h_c = \frac{(\gamma + k_1 \nu_e^{1/2} + \varphi_p) E_f}{\beta (1 - \nu_f^{\,2}) \sigma_y^2} \qquad \textbf{Equation 5-1}$$

For most polymers the material properties required in Equation 5-1 to predict an analytical value for critical thickness would be easily available in literature. However, for silicone thermosets it is not so. Even with 4-3136 resin which is one of the most studied silicone resin, amongst the parameters in Equation 5-1 only the modulus (E_f = 1 GPa)[37] and yield stress (σ_y = 80 MPa)[37] have been measured previously. Values of other parameters need to be assumed. Surface tension (γ) of polymers is typically in the 0.03-0.05 mJ/m^2 range. Therefore, an average value of (γ= 0.04 mJ/m^2) is assumed for 4-3136. In the crack resistance term ($\Gamma_f = \gamma + k_1 \nu_e^{1/2} + \varphi_p$) it is assumed that ($k_1 \nu_e^{1/2}$) term dominates.* The crosslink density is assumed similar to that of an epoxy and therefore it is taken to be (ν_e = 250 x 10^{25} chains/m^3), the constant k_1 is nearly same for all polymers and equal to (7.1 x 10^{-5} J chain$^{-1/2}$ m$^{-1/2}$).[41] For most materials, the Poisson's ratio is close to 0.3 and therefore this value is chosen for the 4-3136 as well (ν_f = 0.3). Assuming β = 1 the analytically predicted value of critical thickness for 4-3136 is ~1μm. Clearly, several assumptions have been made in determining the critical thickness. The numerically predicted value of 1μm is the same order of magnitude as the experimentally obtained values. As suggested in Section 4.1.3, further refinement in the model is required.

* An estimate for the φ_p term is not available.

Further, it is useful to analytically examine the influence of curing temperature on critical thickness using Equation 5-1. Experimentally it has been observed that an optimal cure temperature (225°C) allows for the highest value of critical thickness in 4-3136. Below this optimal temperature, the crosslinking reaction does not go to full completion. Therefore the optimal crosslink density (ν_e) would not be achieved and hence according to Equation 5-1, the critical thickness is predicted to be low. Above the optimal cure temperature the critical thickness is anticipated to decrease because of material degradation.

5.2 IR Dichroism

In this case, two films of 4-3136 are selected for comparison: a thick film (4μm) and a thin film (0.5μm). In Figure 5-5, the orientation results for 4-3136 thick film are shown (no strain applied). In Figure 5-6, the orientation results for 4-3136 thin film are shown (no strain applied). Comparing the nature of the two curves, specifically the broad peak in the 1200–1000 cm^{-1} region which corresponds to the silanol group, the shape of the peak is different for thick vis-à-vis thin films. This compositional variation may be related to a change in the network density of the material and consequently affect the fracture properties. Additionally, the orientation effects in the thick vis-à-vis thin film are compared. No significant orientation is observed in the thick film (Figure 5-5). In the thin film, orientation is observed to a very limited extent (~1%) at the 1250 cm^{-1} peak (Figure 5-6). This level of orientation is much less than the reference orientation level as discussed in Section 4.2. Most likely, orientation is not influencing the fracture strain when a thin film is compared to a thick film.

In Figure 5-7 orientation results for a thin film (0.5μm) elongated to 10% are shown. Similar to the unstretched film, orientation is observed to a limited extent at the 1250 cm^{-1} peak. The nature of strain is classified as plastic.

5.3 Summary

According to the bending test results, the 4-3136 resin is observed to have a critical thickness of ~2.2μm when cured at a temperature of 177°C with a strain to failure of ~12%. For a 200°C cure, the observed critical thickness is ~3.7μm with a failure strain of ~12%. For a 225°C cure, the observed critical thickness is ~5.7μm with a strain to failure of ~12-13%. In all these cases, the fracture strain is observed to increase substantially in comparison to bulk material fracture strain (~2-3%). Based on these results, 4-3136 essentially qualifies as ductile in thin film form. As the cure temperature is increased, the fracture properties of 4-3136 deteriorate. For a 250°C cure, a gradual transition in fracture strain of 4-3136 is observed as a function of film thickness. Further, for a 300°C cure, the fracture strain reduces substantially across the range of film thickness tested. The deterioration in fracture properties at high temperatures is most likely associated with chemical degradation of the material. With a critical thickness in the 3-5μm range, 4-3136 can be used for applications such as coatings. In order that 4-3136 has greater application potential it would be useful to increase the critical thickness value. Such a technique has been described in the next Chapter.

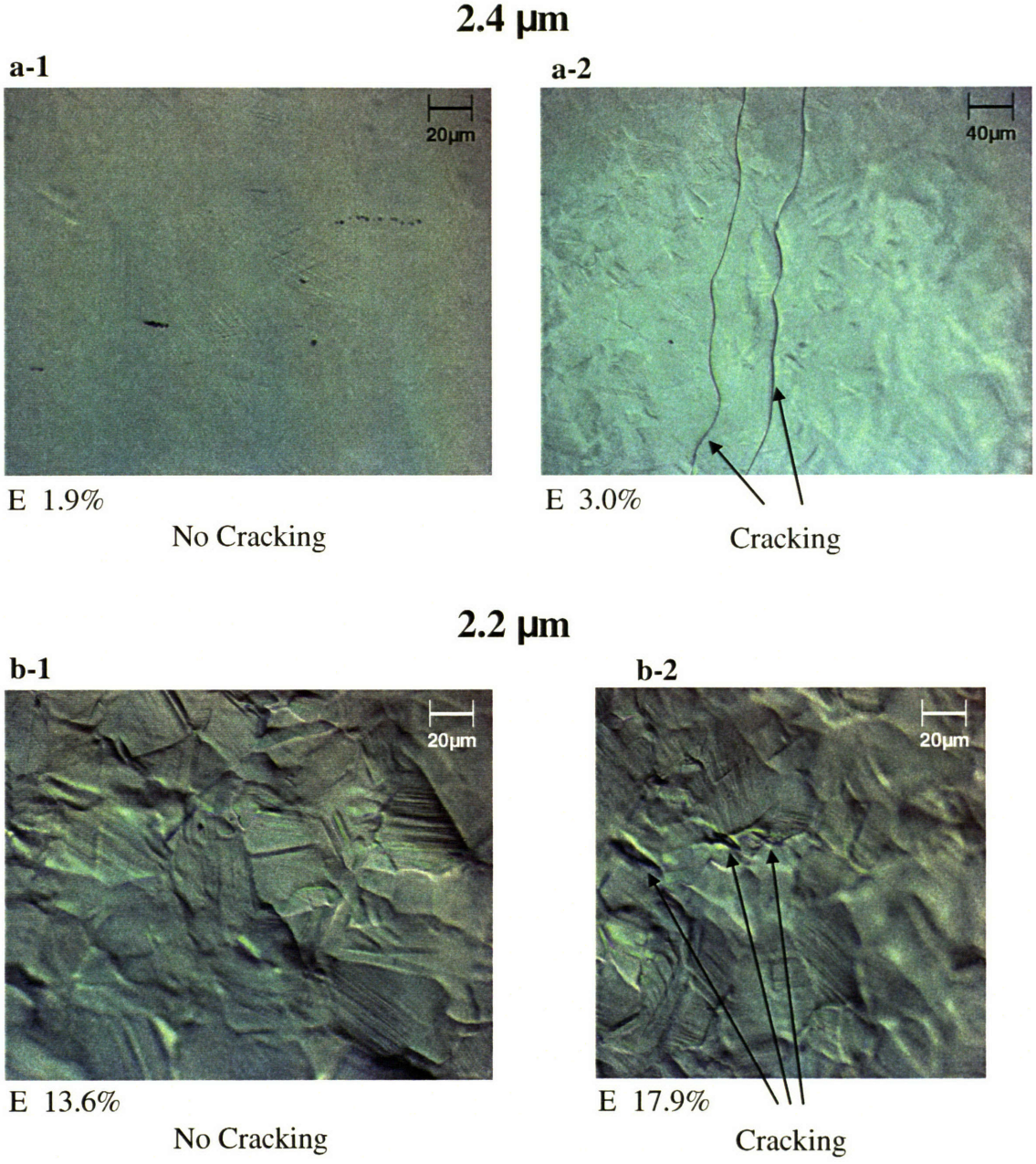

Figure 5-1 Micrographs from bending tests carried out on 4-3136 films cured at a temperature of 177°C. Stainless steel substrate is used. (a-1) No cracking in a 2.4µm thick film at 1.9%. Structural features of the deformed stainless steel can be seen. (a-2) Brittle cracking observed in 2.4µm thick film at 3.0% strain. The two cracks which are in the view field are labeled. The length of the crack is over 250µm. (b-1) No cracking in a 2.2µm film at 13.6% strain. Stainless steel grain structure dominates the view. (b-2) Ductile cracking observed in a 2.2µm film at 17.9% strain. The three cracks have been labeled. The crack size is ~20-30µm. The film cracks are clearly distinguishable from the substrate features.

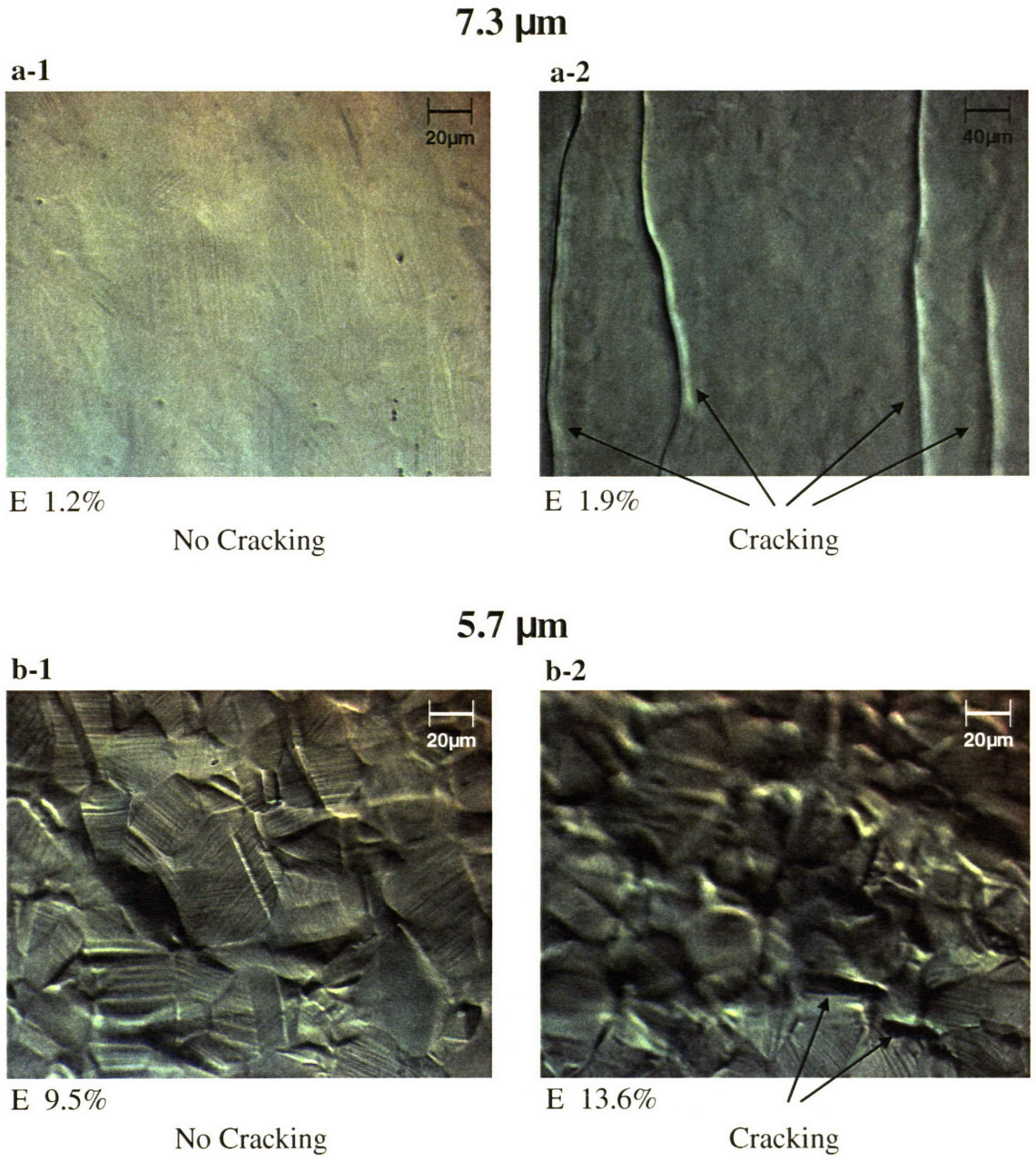

Figure 5-2 Micrographs from bending tests carried out on 4-3136 resin cured at a temperature of 225°C. Stainless steel substrate is used. (a-1) No cracking is observed in a 7.3µm thick film at 1.2% strain. Structural features of the deformed stainless steel can be seen. (a-2) Brittle cracking observed in a 7.3µm thick film at 1.9% strain. The cracks are over 250µm in length. (b-1) No cracking observed in a 5.7µm film at 9.5% strain. View field is dominated with deformation features of the stainless steel. (b-2) Ductile cracking observed in 5.7µm film at 13.6% strain. The cracks are marked by arrows. Two cracks are labeled. These cracks are ~20-30µm in length.

19.5 µm

a

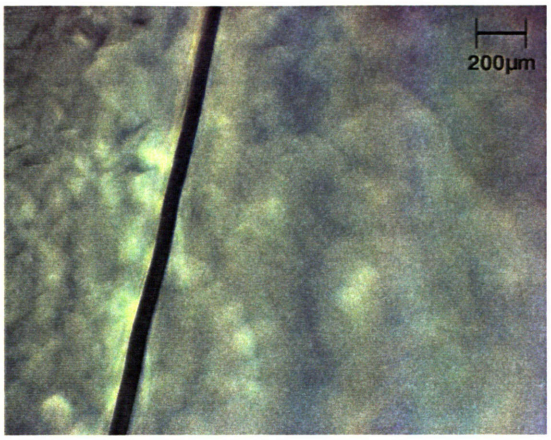

E 3.8%
Cracking

5.5 µm

b

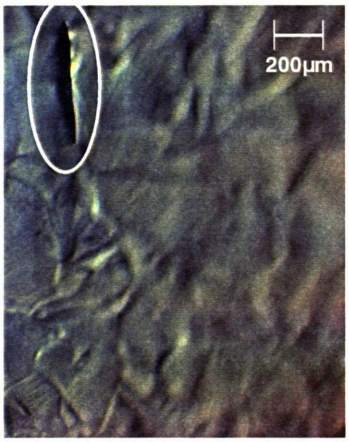

E 9.6%
Cracking

Figure 5-3 Micrographs from bending tests carried out on 4-3136 resin cured at a temperature of 250°C. Stainless steel substrate is used. (a) Brittle cracking observed in a 19.5µm thick film at 3.8% strain. The crack is at least 1 mm in length. (b) Cracking observed in 5.5µm film at 9.6% strain. The crack is about 200µm in length. Grain structure of the stainless steel substrate is visible.

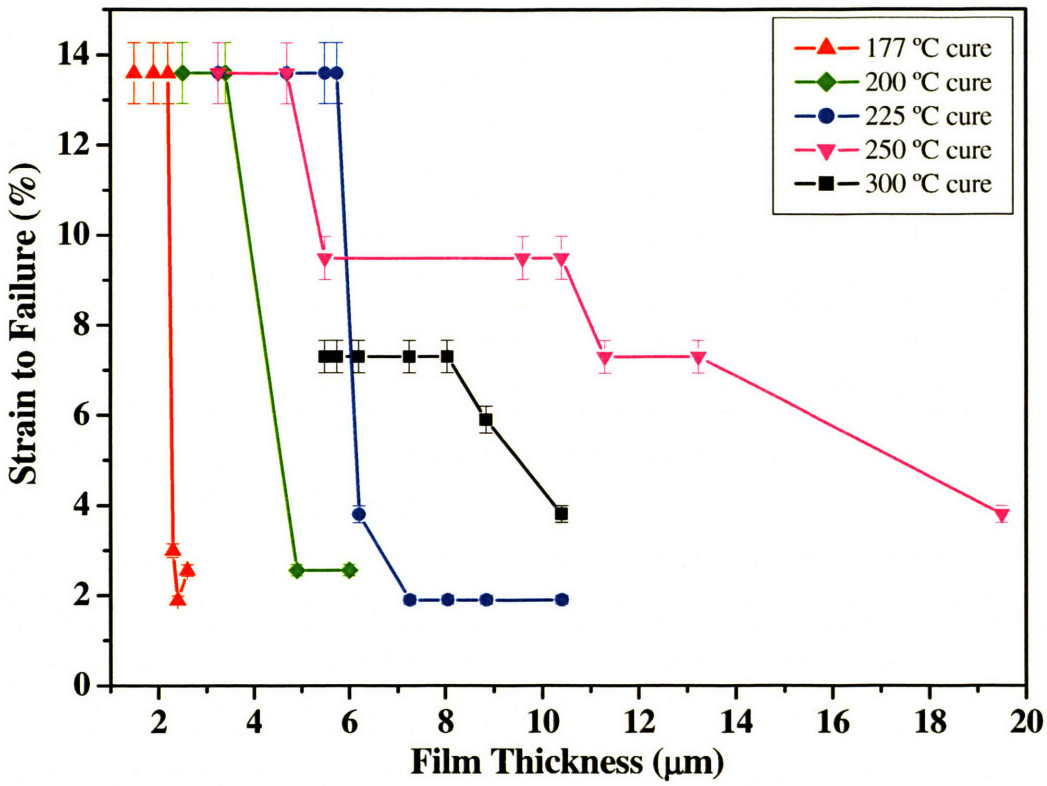

Figure 5-4 Strain to failure as a function of the film thickness for 4-3136 cured at five temperatures. A critical thickness value of 2.2μm is observed for films cured at 177°C with a strain to failure of 13% below critical thickness. For a cure temperature of 200°C the critical thickness is observed to be 4μm with a failure stain of 13%. A critical thickness of 5.7μm is observed when the material is cured at 225°C. The 250°C cured films show a gradual increase in failure strain from 3% for a 20μm film to a failure strain of 10% for a 4-5μm film. For films cured at 300°C the strain to failure reduces substantially for the entire range of film thickness. (Error bars for all plots are according to the analysis presented in Section 3.1.2.)

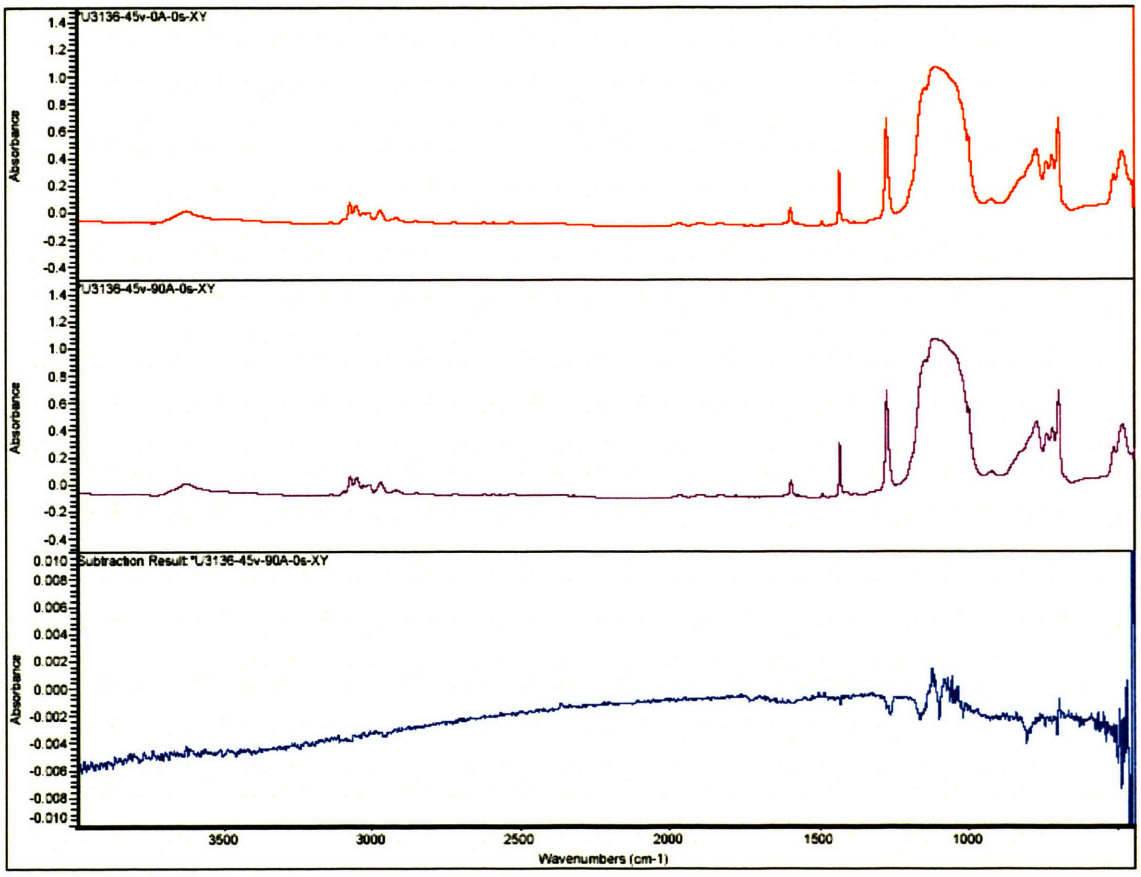

Figure 5-5 Results of orientation study carried out on a 4-3136 resin thick film (4μm). No strain is applied. The top two graphs show the IR spectra for the two different polarizations. The bottom curve is the resultant difference obtained upon subtraction of the first graph from the second.

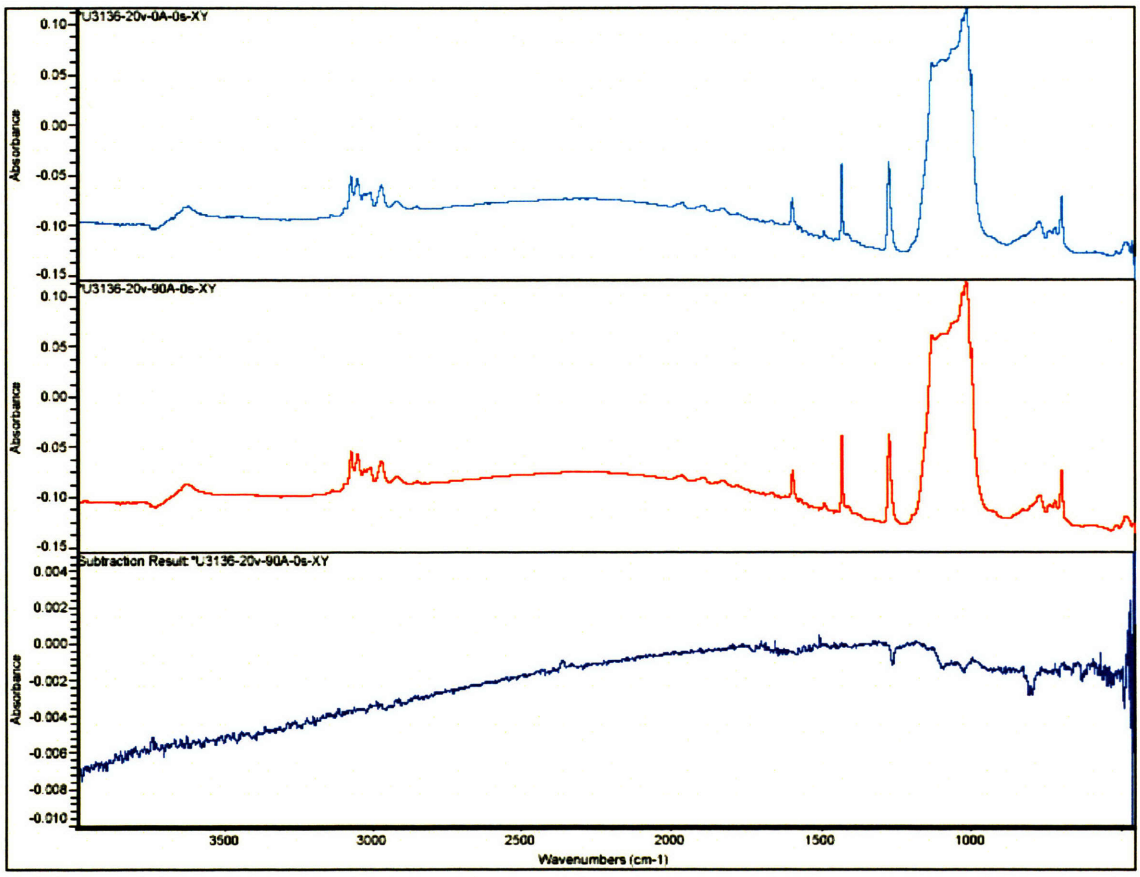

Figure 5-6 Results of orientation study carried out on a 4-3136 thin film (0.5μm). No strain is applied. The top two graphs show the IR spectra for the two different polarizations. The bottom curve is the resultant difference obtained upon subtraction of the first graph from the second.

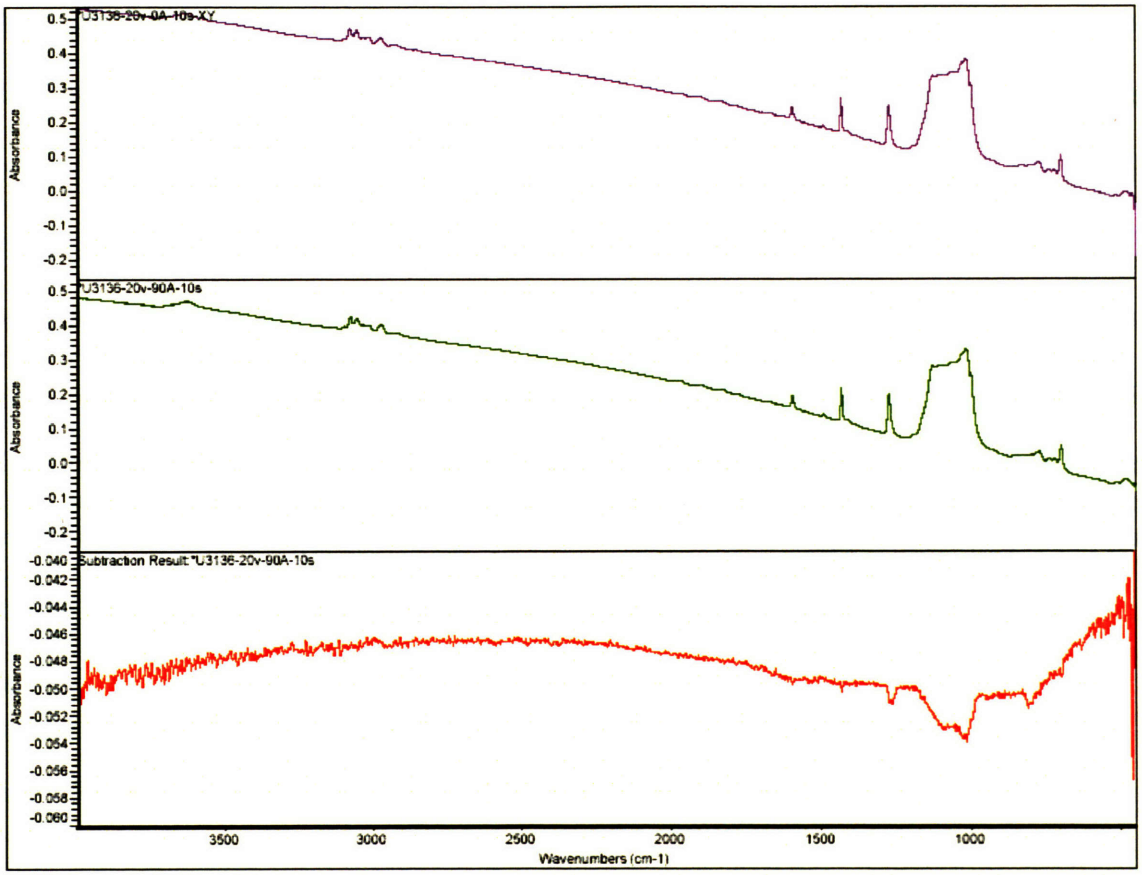

Figure 5-7 Results of orientation study carried out on a 4-3136 resin thin film (0.5μm). The film is at 10% elongation. The top two graphs show the IR spectra for the two different polarizations. The bottom curve is the resultant difference obtained upon subtraction of the first graph from the second.

6 Molecular Engineering in Poly-phenyl-methyl-silsesquioxane (4-3136)

A molecular engineering approach to improve fracture properties of 4-3136 resin is presented in this chapter. While a critical thickness of ~3-4μm with an allowable failure strain of ~12-13% for a silicone thermoset is a useful engineering result (as in 4-3136), it would be desirable to further increase the critical thickness value. Even a marginal increase in critical thickness will allow for much greater utility of 4-3136 in practical applications. To increase critical thickness it is necessary to increase the intrinsic deformation capability of the material. Chemical modification of the polymer at the molecular scale can possibly result in such an increase. Such an approach is employed for the 4-3136 resin. The process is described below followed by test results on the modified resin.

6.1 Molecular Engineering: Chemical Modification

Chemical modification of polymers, although not trivial, has been utilized in several instances to attain desirable mechanical properties. In particular, improvement in bulk fracture toughness properties of silicone resins[37, 55] including the 4-3136 resin has been carried out using a Phase-I/Phase-II approach through addition of polydimethylsiloxane (PDMS). Phase-I modification is achieved by chemical reaction of the pre-polymer with PDMS to increase intrinsic deformation capability of the resin. Phase-II modification is the second step, in which PDMS is incorporated into the polymer as fine particles. For molecular modification of 4-3136 a PDMS can be employed according to the Phase-I methods described in literature.

To chemically modify 4-3136, a suitable process step prior to curing has to be identified so that PDMS can be reacted into the resin. Chemical modification of fully cured material is not possible since it is crosslinked and therefore not chemically reactive. Since the pre-polymer has several unreacted silanol ends, the PDMS can be reacted into it at this stage. Upon reaction the PDMS will chemically attach to the pre-polymer through these silanol bonds. The following factors need to be considered in order to select the proper PDMS: first, the chosen PDMS should react with 4-3136. Second, other desirable properties of 4-3136 like modulus, strength, high temperature properties, dielectric properties and optical properties should be retained upon this chemical change.

A PDMS with a DP (Degree of Polymerization) of 57 is selected based on prior Phase-I toughening work in bulk 4-3136.[37, 55] This PDMS, typically referred to as KPE, is reported to improve bulk fracture toughness of 4-3136 by a factor of three when added in to the resin in a 1:10 ratio. The KPE PDMS can be synthesized by reaction of KP-80 fluid, available commercially from Dow Corning Corporation, and tetraethoxysilane to form a triethoxysilyl end capped PDMS according to the following reaction:

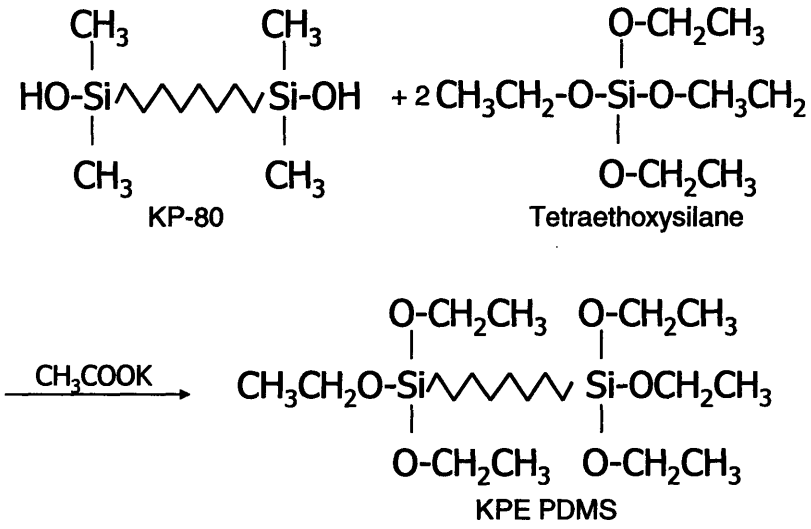

Once synthesized, the KPE PDMS is reacted into the 4-3136 pre-polymer.* For this reaction, the ratio of the KPE to the 4-3136 is chosen as 1:10. This coupling reaction is carried out in a 38 wt% solution of toluene at 95°C for several hours.† A standard round bottom flask is used to carry out the reaction while stirring the entire solution using a magnetic stir bar. After the reaction is completed, the product is dried until all toluene is evaporated. The chemically modified pre-polymer, called as engineered 4-3136‡, at this stage is in a form which can be used to make films.

6.2 Critical Thickness Results

6.2.1 Thin Film Fabrication

Engineered 4-3136 films of different thicknesses (thickness range 1μm – 20μm) are prepared on stainless steel substrates using spin coating. The solvent used is methyl-isobutyl-ketone. A catalyst, tin tetra butoxide, commercially available as Y-177 catalyst, is added in a 0.05 wt% of the pre polymer. Spin coating is carried out for one minute at a spin speed of 1300 RPM. An acceleration of 425 revolutions/min^2 is utilized. The film thickness is measured using a profilometer; the values for film thickness and the corresponding solution concentrations are presented in Appendix D.

After this step, the films undergo a curing cycle. Multiple curing temperatures are utilized to investigate how the curing temperature affects the mechanical properties. For the curing cycle, first the temperature is increased from room temperature to 80°C at a rate of

* This experimental procedure has been carried out by the author at the Dow Corning research laboratory in Midland, Michigan in collaboration with Dr. Bizhong Zhu.
† Overnight reaction is carried out.
‡ Chemically modified 4-3136 polymer with KPE PDMS is referred to as "engineered 4-3136" in the text.

10°C/min. At 80°C the film is allowed to pre-cure for 30 minutes. Next, the temperature is increased at 5°C/min to reach the final cure temperature. The films are then allowed to stay at the cure temperature for one hour. Subsequently, the film is allowed to cool to room temperature at a rate of 3°C /min.

6.2.2 Bending Test Results

The range of curing temperature studied for engineered 4-3136 is 177°C to 400°C. Optical micrographs of bending test results carried out on engineered 4-3136 prepared at four selected curing temperatures are presented. These temperatures are 200°C, 300°C, 350°C and 400°C.

In Figure 6-1, optical micrographs from bending test carried out on engineered 4-3136 cured at a temperature of 200°C are presented. Figure 6-1(a-1) shows a 7μm film prior to strain application. This film is observed to undergo brittle cracking (Figure 6-1(a-2)) at 2% strain with the crack length of ~40-60μm. In Figure 6-1(b-1), a 4μm thick film is shown which sustains a strain up to 4% without undergoing fracture. The same film when strained to 4.5% is observed to undergo fracture (Figure 6-1(b-2)). The crack length is ~20μm. In comparison, a 3.2μm film sustains a strain of 15% (Figure 6-1(c-1)) and fails in a ductile manner at a strain > 15% (Figure 6-1(c-2)). The length of the ductile cracks is observed to be ~20μm. Based on these bending experiments, the critical thickness for engineered 4-3136 cured at a temperature of 200°C is ~3.2μm.

In Figure 6-2, the optical micrographs from bending tests carried out on engineered 4-3136 samples cured at 300°C are presented. A 16μm thick film does not undergo any

fracture at 3.1% strain (Figure 6-2(a-1)) and fractures at a 3.9% strain with the presence of brittle cracks (Figure 6-2(a-2)). The crack length is at least 1mm. A 12μm film sustains a higher strain of 4.5% (Figure 6-2(b-1)) and fractures at 6.3% strain (Figure 6-2(b-2)) with smaller cracks. The cracks in this case are observed to be ~100μm in length. A thinner film of 10μm sustains a much greater strain of 10.5% (Figure 6-2(c-1)) and fractures at 15.5% strain (Figure 6-2(c-2)). According to these bending test results, a critical thickness of ~10μm is determined for engineered 4-3136 cured at 300°C.

In Figure 6-3, the optical micrographs from bending tests carried out on engineered 4-3136 samples cured at 350°C are presented. A 16μm film does not fracture at 4.5% strain (Figure 6-3(a-1)) whereas it fractures at 5.3% strain (Figure 6-3(a-2)). The crack length is at least 1mm. A 12μm film sustains 6.3% strain (Figure 6-3(b-1)) and undergoes fracture at 7.9% strain (Figure 6-3(b-2)). The crack length is ~1mm. A 10μm film is more ductile which sustains a strain of 7.9% (Figure 6-3(c-1)) and fractures at 10.5% strain (Figure 6-3(c-2)). The length of the crack is ~100μm. A 5μm thick film attains 10.5% strain (Figure 6-3(d-1)) and fails at 15.7% strain (Figure 6-3(d-2)). The length of the crack as observed is ~50μm. For films less than 5μm thick the fracture strain remains constant at 15.7%. Although with decrease in thickness a gradual increase in the fracture strain is observed, a critical thickness of 5μm can be assigned to engineered 4-3136 cured at a temperature of 350°C.

In Figure 6-4 the optical micrographs for bending tests carried out on engineered 4-3136 samples cured at 400°C are presented. The strain to failure is 1.2% for a 16μm film (Figure 6-4(a)). For a 4μm film, the strain to failure remains at 1.2% (Figure 6-4(b)). The

cracks in both the cases extend the entire vertical dimension of the picture and are at least 1mm in length.

The results for the fracture properties of the engineered 4-3136 resin are summarized in Figure 6-5. The critical thickness value for engineered 4-3136 cured at 177°C is 3μm with a strain to failure of ~15%. The critical thickness increases to ~4μm for engineered 4-3136 cured at 200°C with a strain to failure of 15%. For the range of cure temperatures 225°C - 300°C a much higher critical thickness of ~10μm is attained with a strain to failure of 15%. As the cure temperature is increased to 325°C the fracture properties of engineered 4-3136 deteriorate slightly. A gradual increase in the strain to failure from 4% for a 15μm film to 15% for a 5μm film is observed in this case. Bending test results for engineered 4-3136 cured at a temperature of 350°C are similar to bending test results for a 325°C cure temperature. When cured at 400°C the material loses its characteristic toughness properties and behaves in an extremely brittle manner over the entire thickness range. An analysis along the lines of what is presented in Section 5.1.3 can be used to understand the influence of cure temperature on critical thickness of engineered 4-3136.

6.3 IR Dichroism

For this study two films are chosen: one above the critical thickness denoted as the thick film (~15μm) and another below the critical thickness denoted as the thin film (~7.5μm). In Figure 6-8, the orientation results for the thick film are presented. No significant orientation is observed according to the curve for the dichroic difference. In Figure 6-9, ~2% orientation is calculated for the peak corresponding to the 1250 cm^{-1} band. This result is similar in nature to that obtained for the unmodified 4-3136 resin. In Figure

6-10, FTIR dichroism results the thin film elongated to 10% are shown. No significant orientation is observed. Therefore the nature of strain is classified as plastic.

6.4 Effect of PDMS Concentration

In this section the effect of PDMS concentration on fracture properties of 4-3136 is studied. In addition to unmodified resin and modified resin (10% PDMS) a third 4-3136 containing 5% PDMS is tested. A cure temperature of 225°C is used for this study. Strain to failure as a function of film thickness is shown in Figure 6-6. The results indicate that the critical thickness value increases as the PDMS concentration increases. While the unmodified 4-3136 resin has a critical thickness of 5μm, the value increases to 6-7μm for a 5% PDMS modified 4-3136 and to 8-9μm for a 10% PDMS 4-3136. Therefore the introduction of PDMS improves the intrinsic deformation ability of the 4-3136. It is useful to examine whether such a trend in fracture toughness is as predicted by models. For this purpose Equation 2-10 is considered:

$$h_c = \frac{(\gamma + k_1 v_e^{1/2} + \varphi_p) E_f}{\beta(1-{v_f}^2)\sigma_y^2} \qquad \textbf{Equation 6-1}$$

Previous experimentation[37] carried out on bulk 4-3136 indicates that the Young's modulus (E_f) decreases slightly as the PDMS concentration increases. Yield stress (σ_y) for these materials has not been obtained, however the trend in flexural stress may be considered in lieu. The flexural stress is shown to increase slightly with increase in PDMS concentration. These trends in Young's modulus and yield stress as a function of PDMS concentration do not explain why critical thickness should increase. In fact, if

only the Young's modulus and yield stress variation is considered the critical thickness value, according to Equation 6-1, is predicted to decrease as a function of increase in PDMS concentration. Therefore other terms in Equation 6-1 need to be considered. It is unlikely that the surface energy (γ) would change substantially so as to explain an increase in critical thickness as a function of the PDMS concentration change. The polymer backbone energy term k_1 has a similar value for almost all polymers and therefore cannot contribute to an increase in critical thickness. The crosslink density (ν_e) is unlikely to be impacted by PDMS incorporation. The Poisson's ratio (ν_f) is not expected to change either. Most likely, in this case the φ_p term which denotes the work of plastic deformation will be the one which is significantly impacted by PDMS incorporation into 4-3136. This inference is reasonable since neat PDMS typically extends to very large amounts and therefore can increase the plastic deformation capability of the entire system.

6.5 Effect of Test Temperature

The effect of test temperature on the modified 4-3136 (10% PDMS) is studied in order to determine the range of temperature for which the resin can be used in practical applications. Two cure temperatures, 225°C and 300°C, are selected for this study. This selection is made since the modified 4-3136 resin shows the highest critical thickness value when cured within this temperature range (tested at room temperature).

Three test temperatures are selected: -40°C, room temperature and 75°C. The strain to failure as a function of film thickness is presented in Figure 6-7. The plots for the 225°C cure show that the critical thickness value is ~8μm and is largely independent of test

temperature. Similarly, for the 300°C temperature cured films the fracture properties and critical thickness are also largely independent of the test temperature. A slight increase in critical thickness is observed with increase in test temperature for both cases (225°C and 300°C cures). Since the increase is minimal, it does not serve as a means to validate the discussion of the influence of test temperature on critical thickness presented in Section 2.3.2. Nonetheless, the trend predicted by the analytical study does match the experimental results obtained for engineered 4-3136.

6.6 Summary

It is shown that by chemical modification of the 4-3136 using 10% KPE rubber the critical thickness of 4-3136 can be improved significantly. This technique of increasing critical thickness falls in the paradigm of molecular engineering. The critical thickness of engineered 4-3136 when cured at 177°C is 3μm. The critical thickness at 200°C cure temperature is 4μm with strain to failure of >15%. Most remarkably, as the temperature goes in the 225-300°C range the critical thickness increases to 10μm with a strain to failure of >15% (bulk fracture at 2-3%). The engineered 4-3136 clearly has superior fracture properties over neat 4-3136 with a critical thickness which is twice that observed in neat 4-3136. Further, engineered 4-3136 resin shows a high critical thickness value for test temperatures from -40°C to 75°C. These results demonstrate that the 4-3136 resin can be essentially qualified as a ductile material. For thin films of engineered 4-3136, with a 10μm critical thickness and a 15% strain to failure, the potential for use in practical applications is greatly enhanced. Besides the current application as a laminate binder, the material can now be used for coatings in structural materials. In addition,

4-3136 family of materials can be used for practical applications like inter layer dielectrics, structural materials and optical filters. In future, to access superior properties further experimentation using molecular engineering techniques by PDMS incorporation can be pursued.

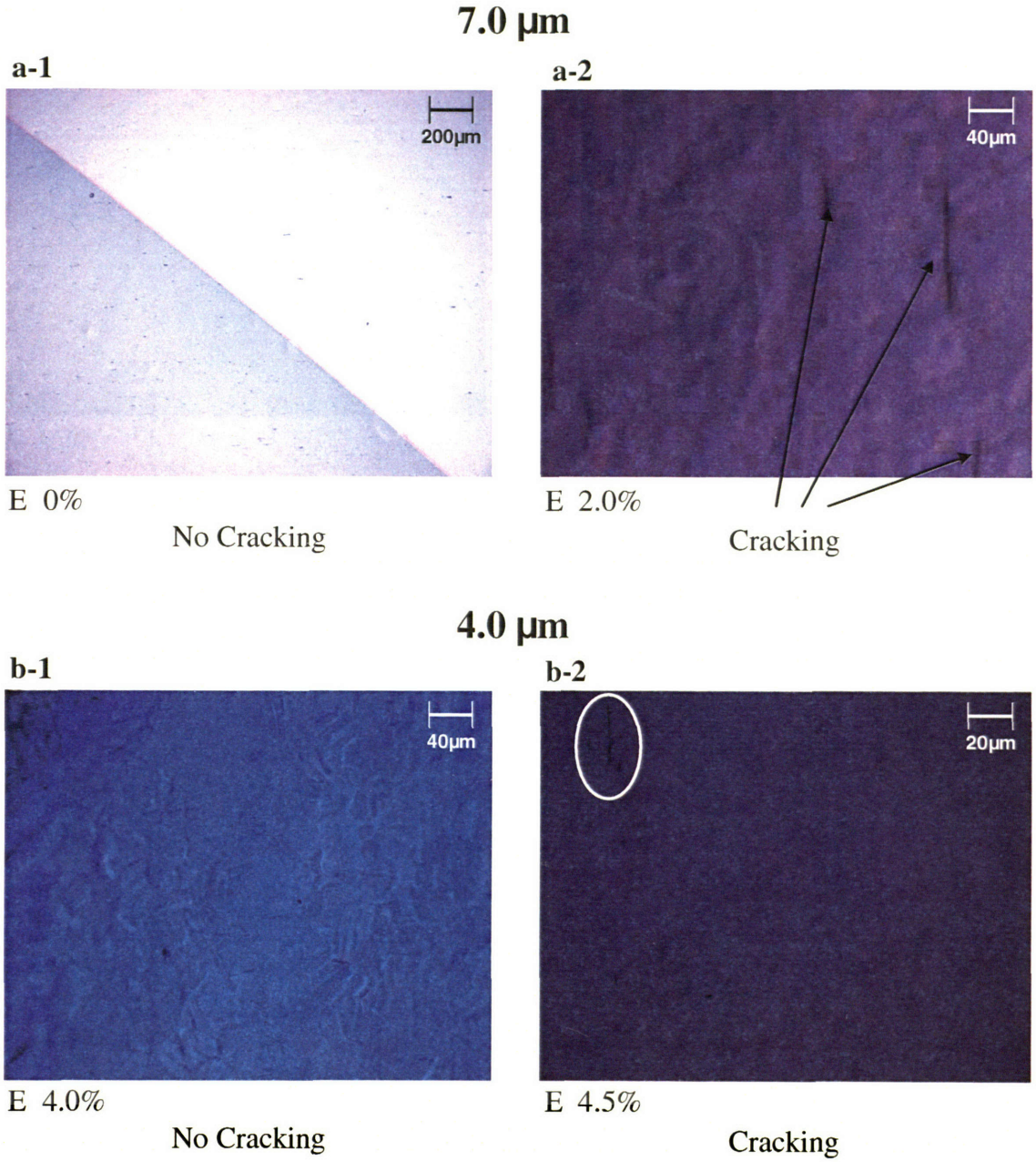

Figure 6-1 Micrographs from bending tests carried out on engineered 4-3136 cured at a temperature of 200°C. A stainless steel substrate is used. (a-1) Film edge shown for 7µm film prior to strain application. (a-2) Brittle cracking observed in the 7µm thick film at 2.0% strain. Several cracks are observed amongst which three are labeled. Crack length is ~40-60µm. Grain structure of the deformed stainless steel is visible. (b-1) No cracking observed in 4µm film at 4.0% strain. Regions on the left side as well as the right side are not in focus. Grain structure of the stainless steel is visible. (b-2) Cracking observed in 4µm film at 4.5% strain. The crack is on the top left corner. Crack length is ~20µm.

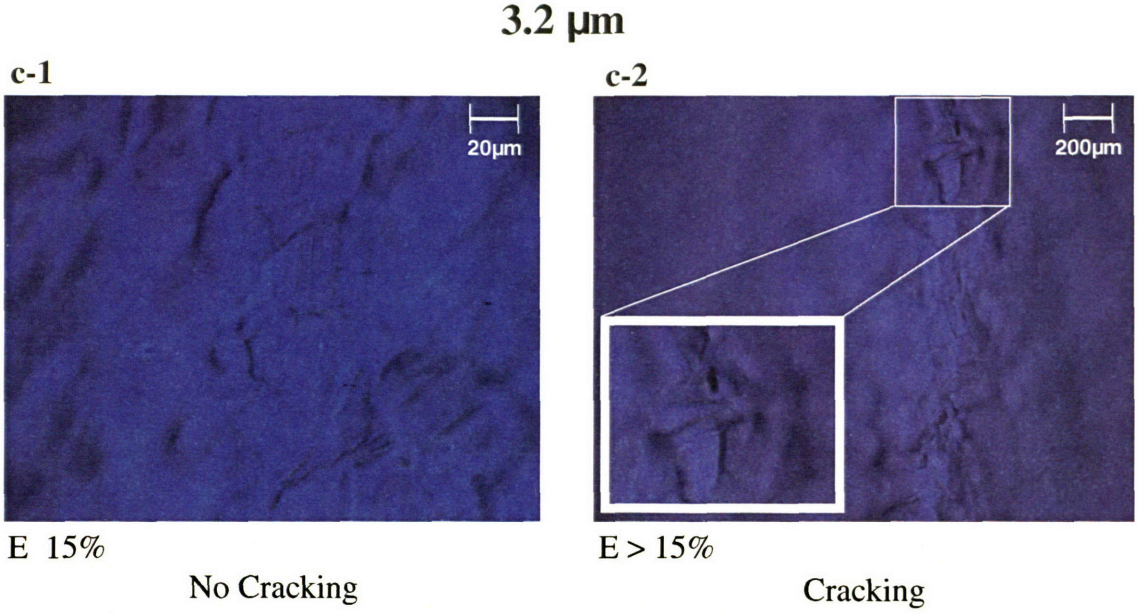

Figure 6-1 Engineered 4-3136 films cured at 200°C. (c-1) No cracking observed in a 3.2µm thick film under 15% strain. Only the middle region of the picture is in focus. The regions on the left and right are not in focus. Stainless steel deformation features dominate the view field. (c-2) Ductile cracks observed in a 3.2µm thick film with a failure strain >15%. Only a vertical strip through the middle section of the micrograph is in focus. A magnified region is shown in the inset which identifies the crack. The crack length is ~50µm.

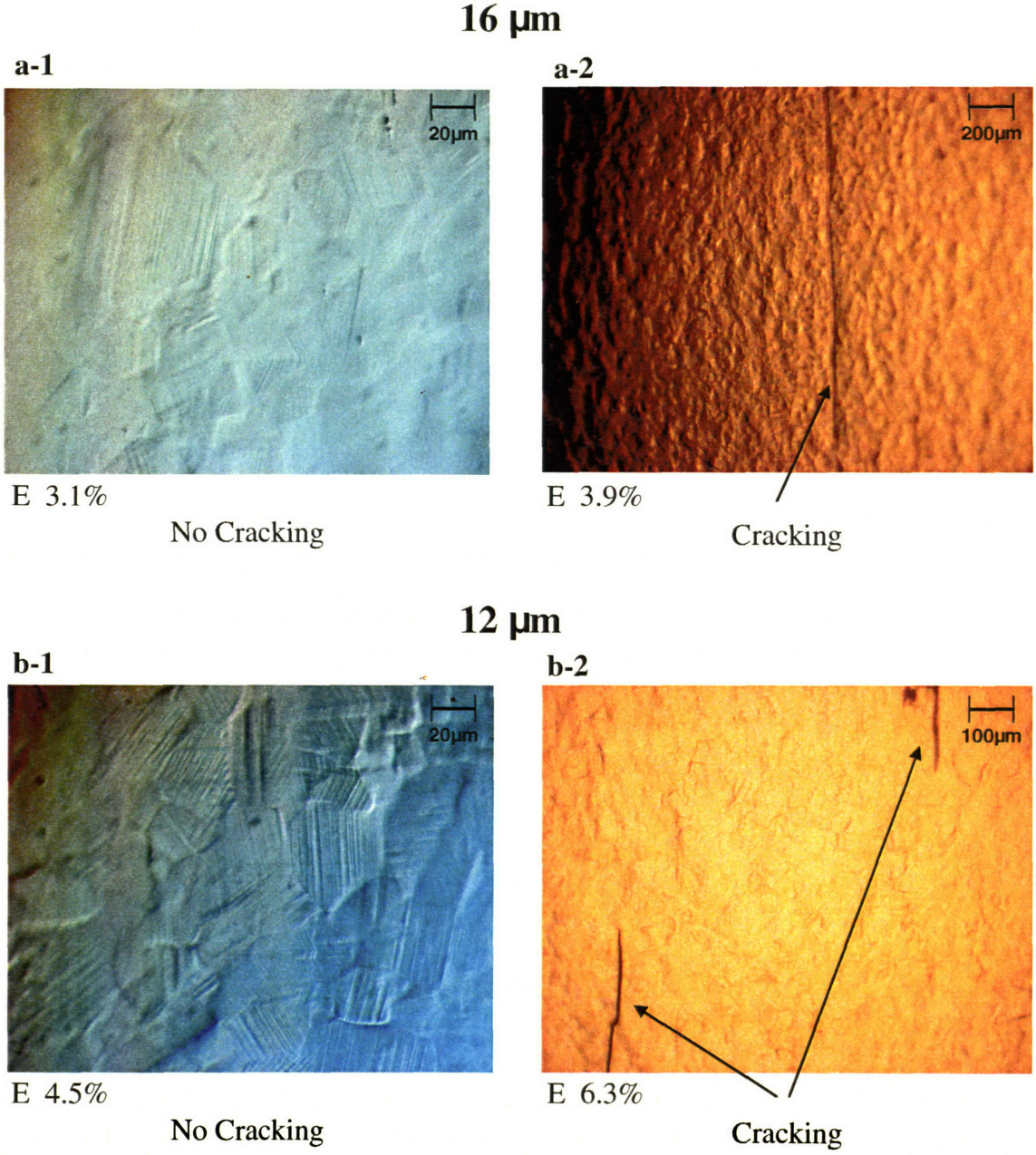

Figure 6-2 Micrographs from bending tests carried out on engineered 4-3136 cured at a temperature of 300°C. A stainless steel substrate is used. (a-1) No cracking observed in a 16µm thick film at 3.1% strain. Stainless steel features are visible. (a-2) Brittle cracking observed in a 16µm thick film at 3.9% strain. The crack spans the entire vertical dimension of the micrograph and has a length of at least 1 mm. Stainless steel features are visible. (b-1) No cracking observed in 12µm film at 4.5% strain. Stainless steel substrate features dominate the view field. (b-2) Cracking observed in a 12µm film at 6.3% strain. The two cracks are on the top right and the bottom left. Crack length is ~100µm.

10 µm

c-1

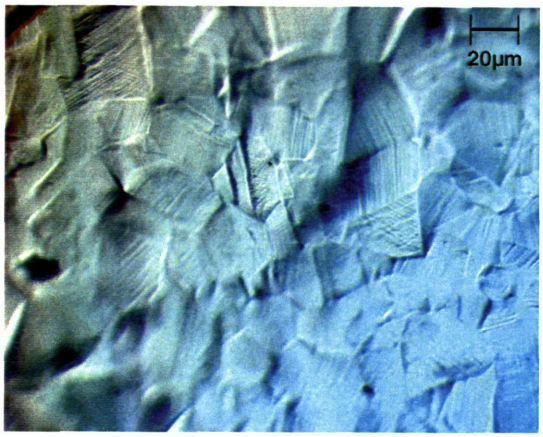

E 10.5%

No Cracking

c-2

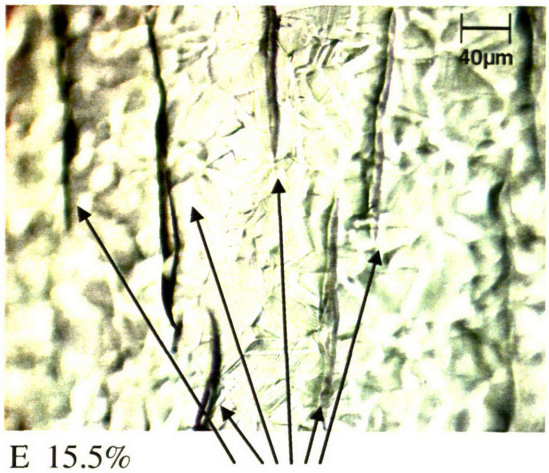

E 15.5%

Cracking

Figure 6-2 Engineered 4-3136 cured at a temperature of 300°C. (c-1) No cracking observed in a 10µm thick film under 10.5% strain. Stainless steel features dominate the view field. (c-2) Ductile cracks observed in a 10µm thick film at a 15.5% strain. Several cracks have been labeled.

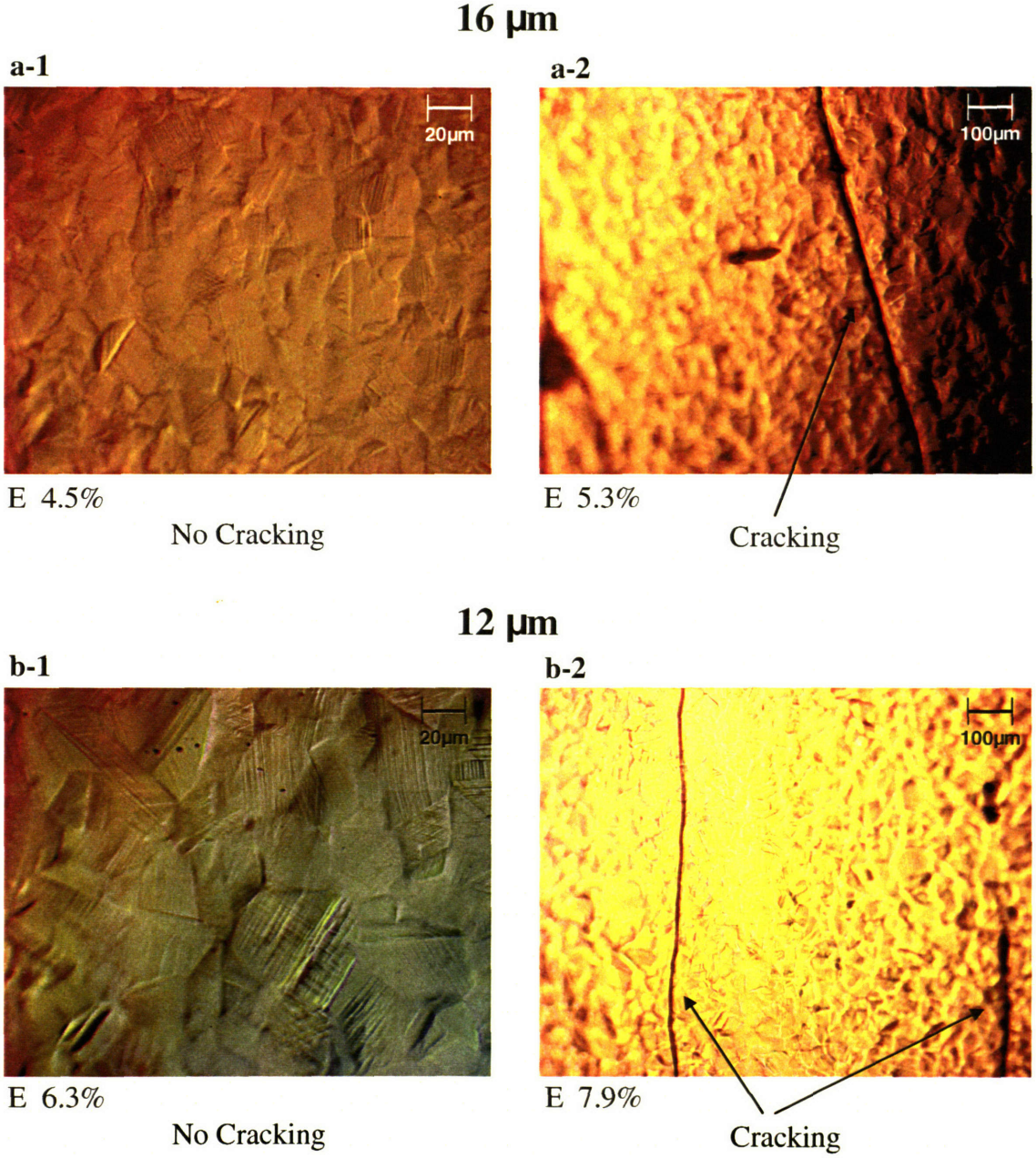

Figure 6-3 Micrographs from bending tests carried out on engineered 4-3136 cured at a temperature of 350°C. A stainless steel substrate is used. (a-1) No cracking observed in a 16µm thick film at 4.5% strain. Stainless steel features are visible. (a-2) Brittle cracking observed in a 16.0µm thick film at 5.3% strain. The crack spans the entire vertical dimension has a length greater 1mm. (b-1) No cracking observed in 12µm film at 6.3% strain. Stainless steel grain structure is visible. (b-2) Brittle cracking observed in a 12µm film at 7.9% strain. Two cracks are labeled. Crack length is at least 1mm.

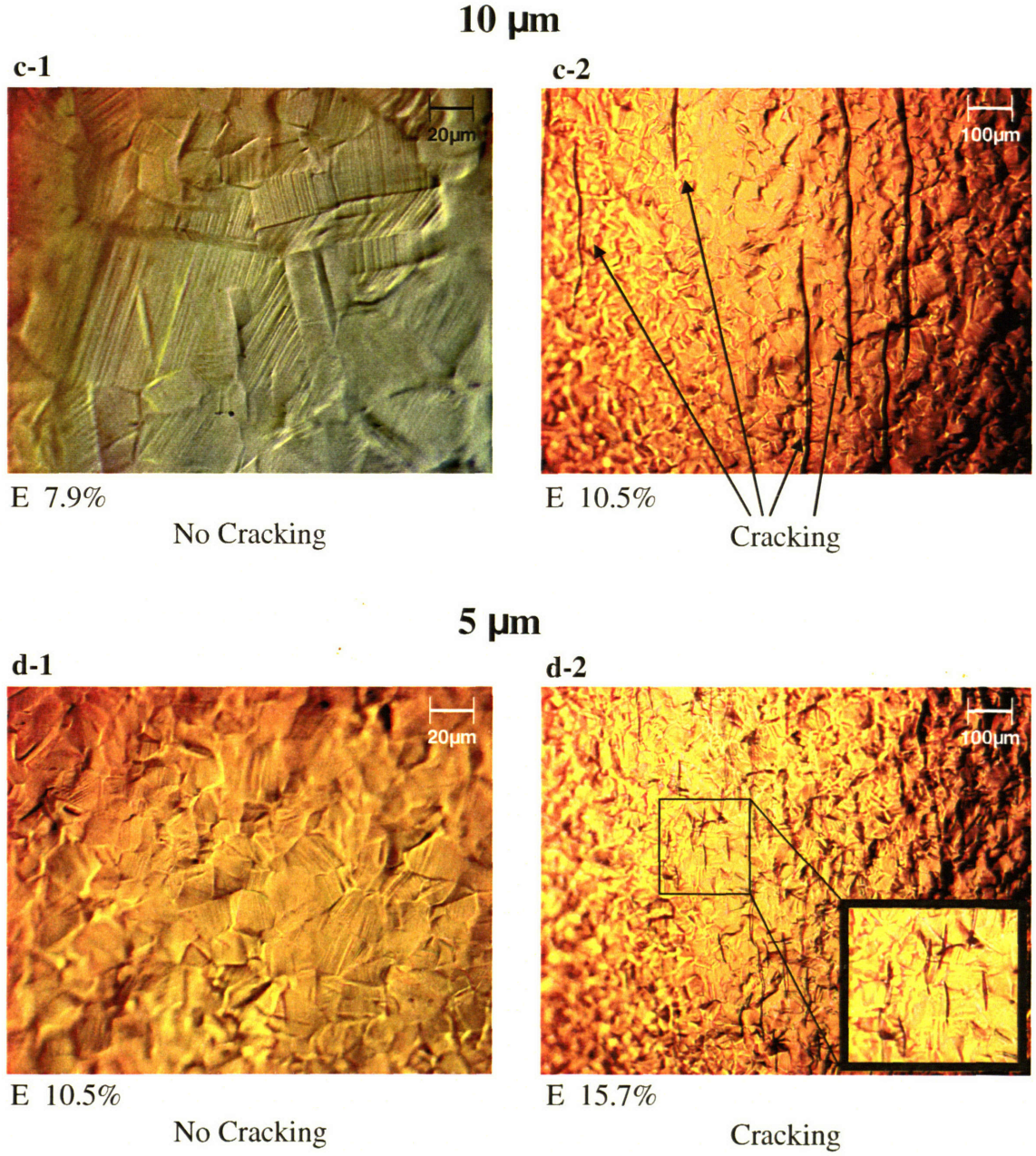

Figure 6-3 Engineered 4-3136 cured at a temperature of 350°C. (c-1) No cracking observed in a 10µm thick film at 7.9% strain. Grain structure of stainless steel dominates view field. (c-2) Ductile cracks are observed in a 10µm thick film at a 10.5% strain. Several cracks are labeled. Crack length is ~100µm. (d-1) No cracking observed in a 5µm thick film at 10.5% strain. (d-2) Ductile cracks observed in a 5µm film at 15.7% strain. In the inset a magnified view is shown. The crack length is ~50µm.

15 µm

a

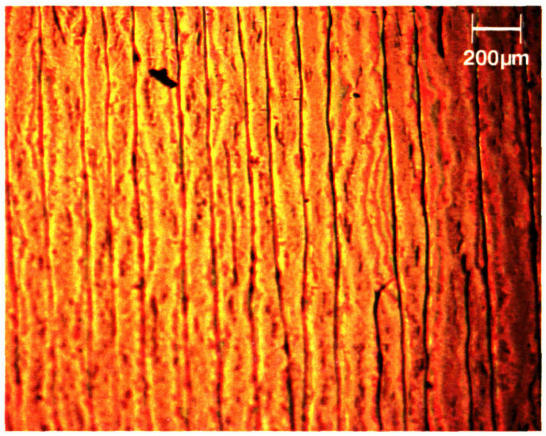

E 1.2%

Cracking

4 µm

b

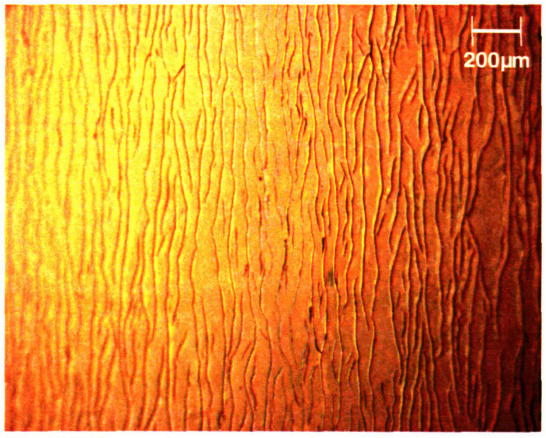

E 1.2%

Cracking

Figure 6-4 Micrographs from bending tests carried out on engineered 4-3136 cured at a temperature of 400°C. A stainless steel substrate is used. (a) Brittle cracking in a 15µm thick film at 1.2% strain. Crack length is at least 1mm. (Note: This micrograph is previously discussed in Section 3.1.3.) (b) Brittle cracking observed in a 4µm thick film at 1.2% strain. Numerous cracks are observed throughout the sample.

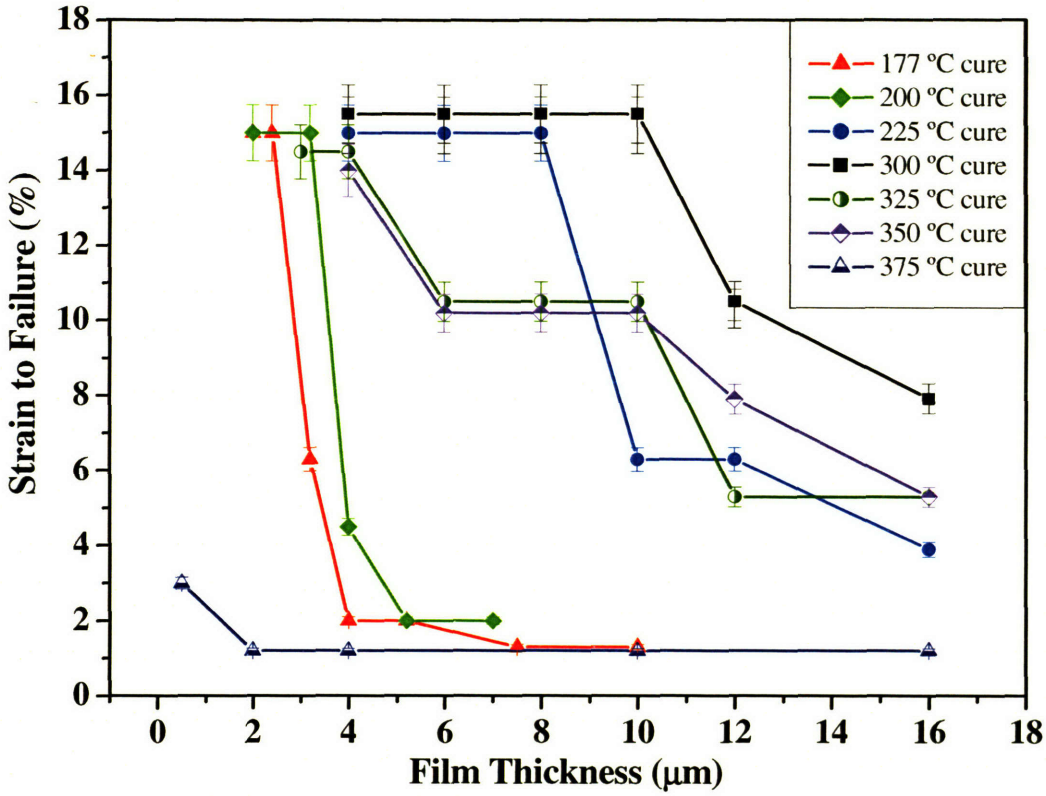

Figure 6-5 Strain to failure vs. thickness for engineered 4-3136 resin for several cure temperatures. For a cure temperature of 177°C, the observed critical thickness is ~3μm with a strain to failure of approximately 15%. For films cured at 200°C, the observed critical thickness is ~4μm with a strain to failure of 15%. For 225°C cure temperature a critical thickness of ~9-10μm is observed and for 300°C cure temperature a critical thickness of ~10-11μm is observed. A gradual transition in the strain to failure as a function of film thickness is observed when the films are cured at 325°C and 350°C. When cured at 400°C, the material exhibits a very low strain to failure for the entire thickness range. (Error bars for all plots are according to the analysis presented in Section 3.1.2.)

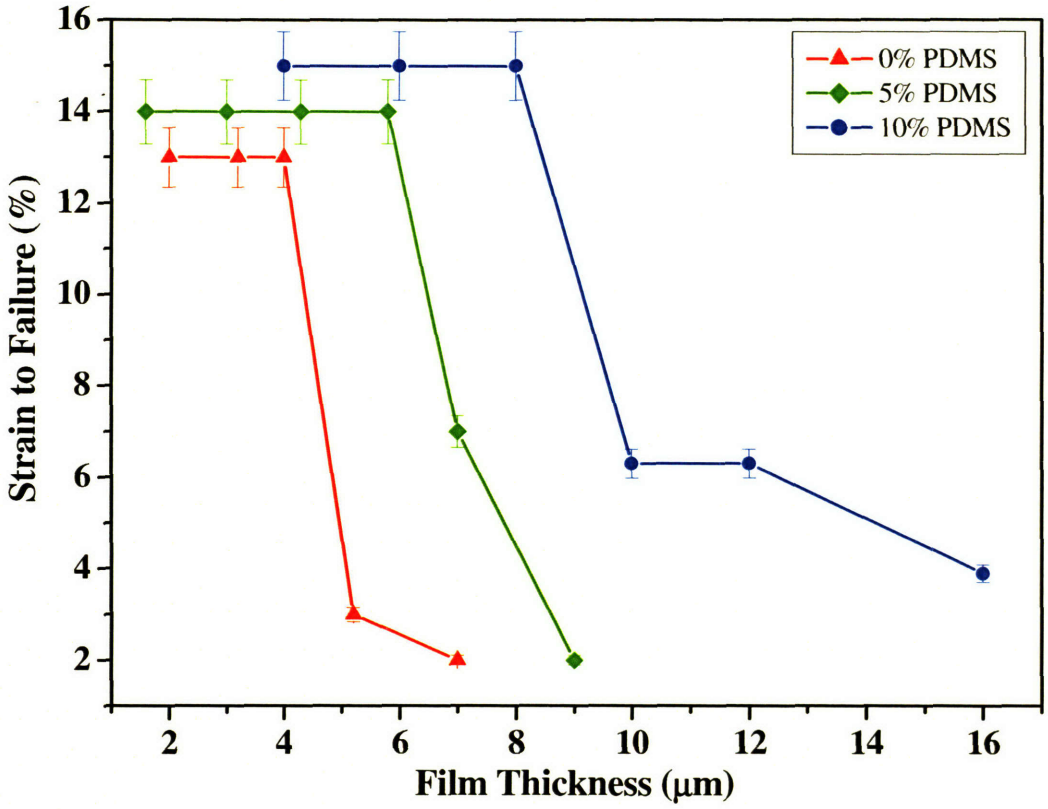

Figure 6-6 Effect of PDMS concentration on the critical thickness of 4-3136. The films are cured at 225°C. The strain to failure as a function of film thickness is plotted for three resins: neat 4-3136, 4-3136 modified with 5% PDMS and 4-3136 modified with 10% PDMS. A critical thickness of ~4-5μm is observed for the neat resin with a 13% strain to failure. A critical thickness of 6μm is observed for the 5% PDMS modified 4-3136 resin with a 14% strain to failure. A critical thickness of 9-10μm is observed for the 10% PDMS modified 4-3136 resin with a 15% strain to failure. (Error bars for all plots are according to the analysis presented in Section 3.1.2.)

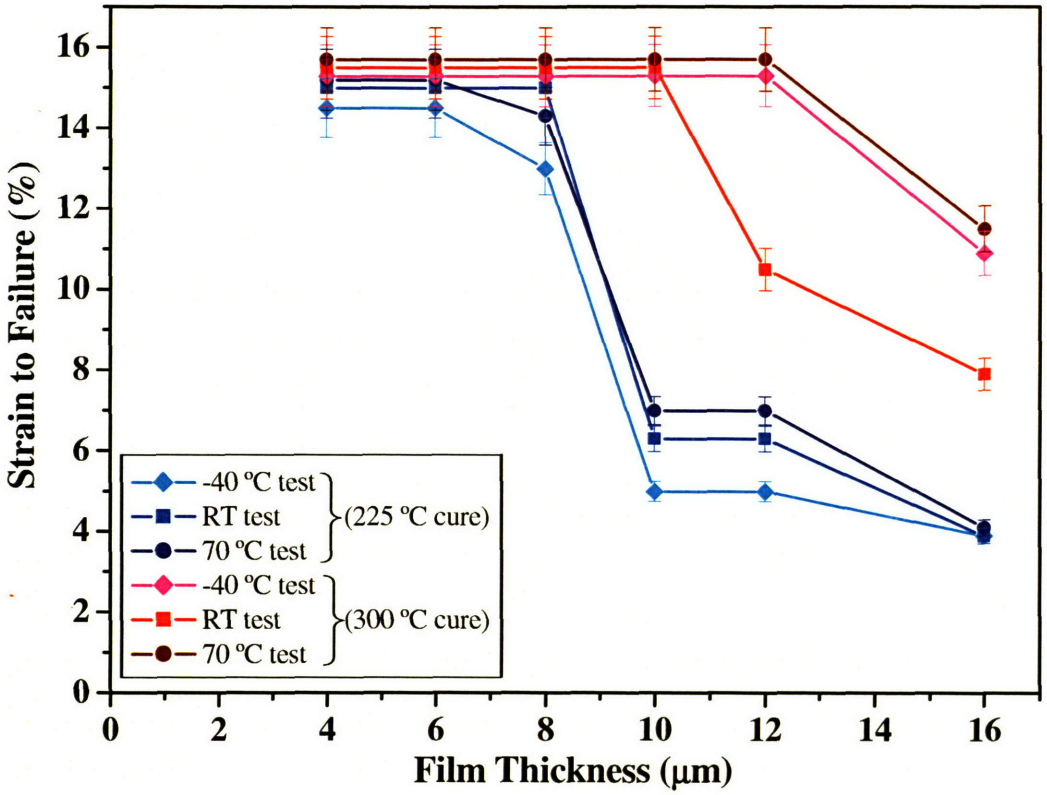

Figure 6-7 Effect of test temperature on critical thickness for engineered 4-3136 resin films prepared at two cure temperatures (225°C and 300°C). The strain to failure as a function of the film thickness is plotted for three different test temperatures -40°C, room temperature and 75°C. The critical thickness is nearly independent of test temperature. For films cured at 225°C, the observed critical thickness is ~7-8μm for the three test temperatures. For films cured at 300°C, the observed critical thickness is ~10-11μm for the three test temperatures. (Error bars for all plots are according to the analysis presented in Section 3.1.2.)

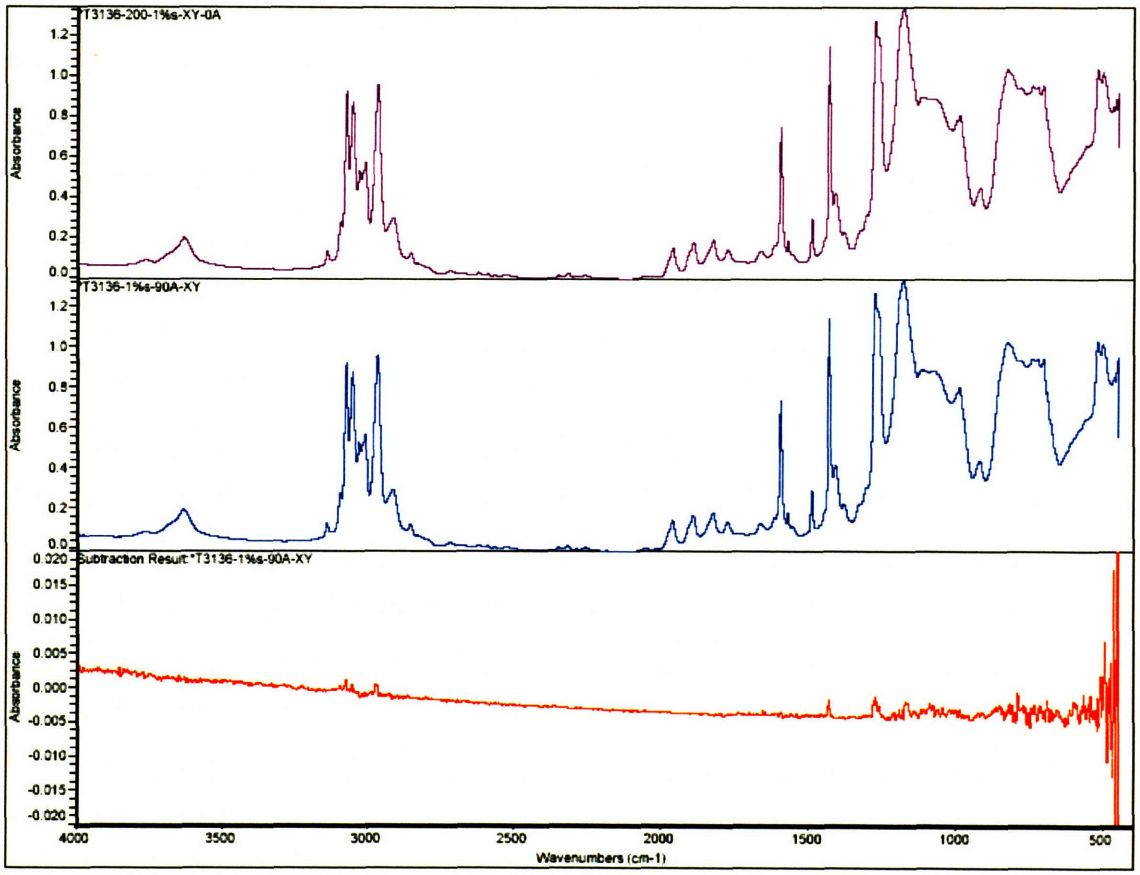

Figure 6-8 Results of orientation study in carried out on engineered 4-3136 thick film (15μm). No strain is applied. The top two graphs show the IR spectra for the two different polarizations. The bottom curve is the resultant difference obtained upon subtraction of the first graph from the second.

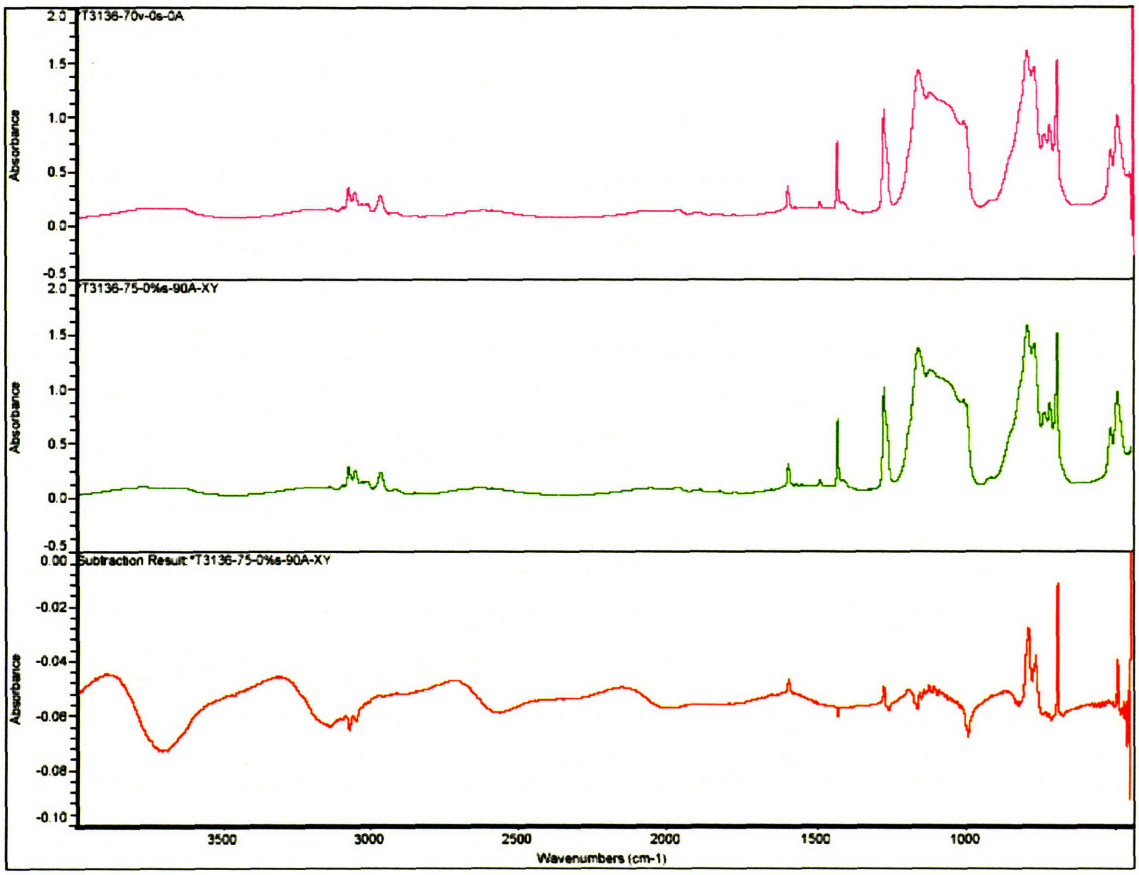

Figure 6-9 Results of orientation study carried out on engineered 4-3136 thin film (7.5μm). No strain is applied. The top two graphs show the IR spectra for the two different polarizations. The bottom curve is the resultant difference obtained upon subtraction of the first graph from the second.

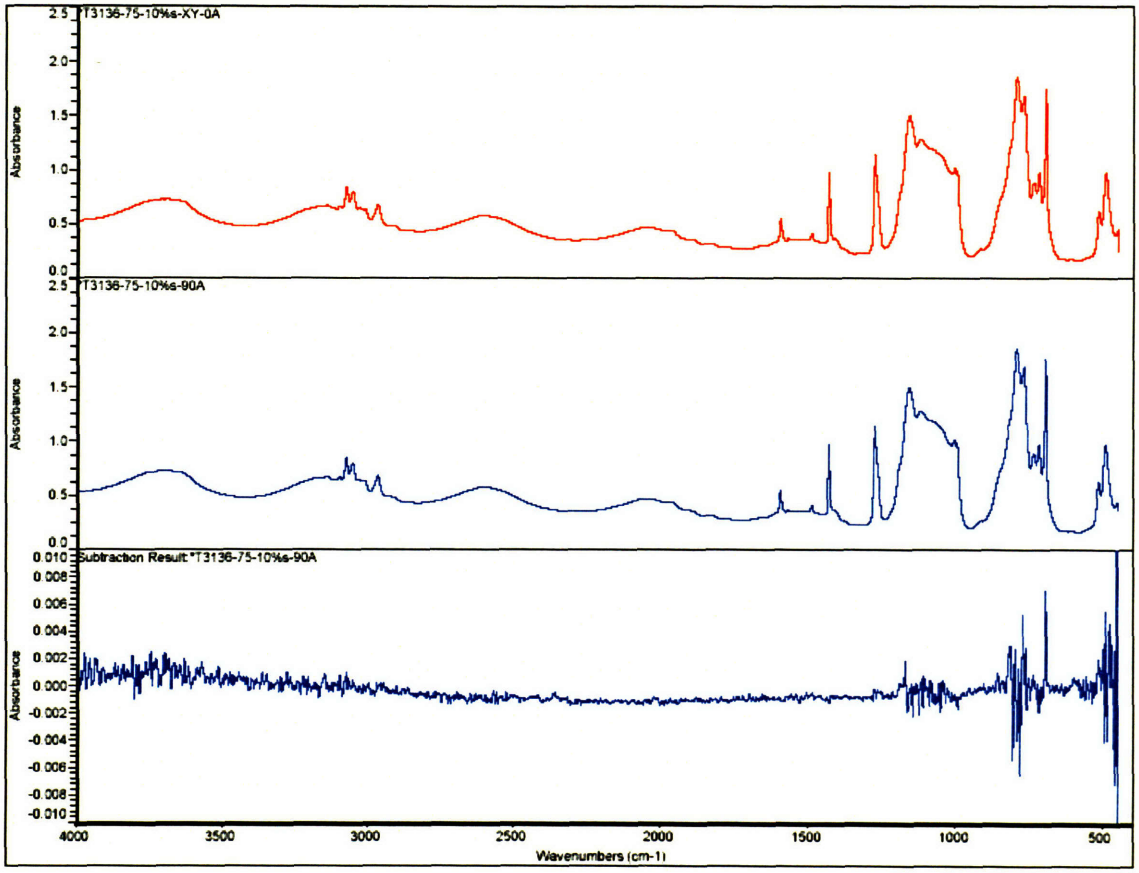

Figure 6-10 Results of orientation study carried out on engineered 4-3136 thin film (7.5μm). The film-substrate combination is elongated to 10%. The top two graphs show the IR spectra for the two different polarizations. The bottom curve is the resultant difference obtained upon subtraction of the first graph from the second.

7 Methyl-T-silsesquioxane Results

The Methyl-T* resin is an experimental silicone thermoset obtained from Dow Corning Corporation. This resin has been developed as a potential candidate for a specific commercial application - to replace silica as an interlayer dielectric in integrated circuits. Methyl-T resin has excellent thermal resistance at very high temperatures. However, it is extremely brittle which has prohibited its use in practical applications. Previous methods to increase fracture toughness of bulk Methyl-T resin have met with limited success. Therefore there exists a need to develop a robust method to increase fracture toughness of Methyl-T resin. Hence, critical thickness investigation is being carried out for this resin.

The Methyl-T resin has a structure of $(MeSiO_{3/2})_n$. The resin is synthesized by the hydrolysis of methyltrichlorosilane. Mechanical properties of Methyl-T resin in the bulk form have been studied previously.[57]

7.1 Critical Thickness Results

7.1.1 Thin Film Fabrication

Methyl-T resin films of different thicknesses (thickness range 0.1μm – 2.3μm) are prepared on stainless steel substrates using spin coating. The solvent used is methyl-isobutyl-ketone. Spin coating is carried out for one minute at a spin speed of 1300 RPM. An acceleration of 425 revolutions/min^2 is utilized. The film thickness is measured using

* From this point on, the methyl-T silsesquioxane resin will be identified as Methyl-T.

a profilometer; the values for film thickness and the corresponding solution concentrations are presented in Appendix E.

After this step, the films undergo a curing cycle. Multiple curing temperatures are utilized to investigate influence of curing temperature on mechanical properties. In the curing cycle, first, the temperature is increased from room temperature to 80°C at a rate of 10°C/min. At 80°C the film is allowed to pre-cure for 30 minutes. Next, the temperature is increased at 5°C/min to reach the final cure temperature. The films are then allowed to stay at the cure temperature for one hour. Subsequently, the film is allowed to cool to room temperature at a rate of 3°C /min.

7.1.2 Bending Test Results

The range of temperature used for curing the Methyl-T resin is from 200°C to 450°C. This range is selected based on prior information available for curing of the Methyl-T resin in bulk form.[57] Optical micrographs of bending tests carried out on samples prepared at three chosen cure temperatures: 250°C, 275°C and 450°C are presented in this section.

In Figure 7-1, the micrographs from the bending tests carried out for samples cured at 250°C are presented. The range of film thickness tested is from 0.4μm to 2.3μm. All films sustain a strain of 11% without fracture and subsequently fail at a 15% strain. The micrographs of the intact and fractured 2.3μm film are shown in Figure 7-1(a-1) and (a-2) respectively. The crack length as observed in Figure 7-1(a) is ~50μm. The micrographs of the intact and fractured 0.4μm film are shown in Figure 7-1(b-1) and (b-2) respectively.

The crack length as observed in Figure 7-1(b) is ~ 20μm. Critical thickness of Methyl-T resin at this cure temperature would therefore be higher than 2.3μm. Further bending tests for films of thickness beyond 2.3μm have not been conducted since reasonable quality films could not be prepared using spin coating.

In Figure 7-2, the optical micrographs from bending tests carried out on Methyl-T resin films cured at 275°C are presented. A 1.3μm film is observed to sustain a strain of 2.3% (Figure 7-2(a-1)) and fails at 3.1% strain (Figure 7-2(a-2)). The cracks are observed to be brittle and have a crack length of at least 1mm. A thinner film of 0.6μm is observed to sustain a higher strain of 4.5% (Figure 7-2(b-1)) and fails at 5.3% strain (Figure 7-2(b-2)). The cracks observed in this film are much smaller having a length of ~20μm. Further, for a 0.4μm film no fracture is observed till 6.3% strain (Figure 7-2(c-1)) with failure occurring at 7.9% strain (Figure 7-2(c-2)). A magnified view of the crack is shown in the inset. The length of the crack is ~20μm. Finally, a 0.2μm film can sustain 11% strain (Figure 7-2(d-1)) and subsequently fails at 14.5% strain (Figure 7-2(d-2)). According to these experiments, the critical thickness value for Methyl-T resin cured at 275°C is ~0.2-0.3μm.

In Figure 7-3, optical micrographs of two Methyl-T resin films of thickness 1.3 and 0.4μm cured at 450°C are presented. For both thickness values, the maximum attainable strain is 1.2% as seen in Figure 7-3(a-1) and (b-1) respectively. Both these films crack at 2% strain as seen in Figure 7-3(a-2) and (b-2) respectively. Cracks in these films are observed to be brittle with a characteristic length scale of over 50μm.

The results of the bending tests for the Methyl-T resin films are summarized in a plot (Figure 7-4). At the 200°C cure temperature, a consistent 25% strain to failure is achieved for the entire thickness range tested. At the 250°C cure temperature, the strain to failure across all thicknesses tested is also consistent at a lower value of 15%. According to the bending test results, the critical thickness for Methyl-T resin cured at 200°C and 250°C is above 2.3μm. For 275°C cure temperature, a critical thickness value of ~0.2μm is observed with strain reaching 15% before failure. For cure temperatures above 275°C the Methyl-T resin properties deteriorate severely as shown in the strain to failure vs. thickness plot for 300°C and 450°C cure temperatures.*

7.2 Summary

According to the bending test results, the Methyl-T resin demonstrates a critical thickness of over 2.3μm when cured at a temperature below 250°C. Since it fractures at a fairly high strain value (>15%), Methyl-T in the thin film form essentially qualifies as a ductile material. In comparison, fracture strain for bulk Methyl-T resin cured at similar temperatures is approximately 2.5%.[57] Therefore as long as a cure temperature of less than 250°C is selected, the Methyl-T resin can be utilized for practical applications like inter layer dielectrics in which the thickness requirement is in sub-micron range. Structural applications may also be considered. When cured at a temperature of 275°C, the critical thickness value of Methyl-T resin reduces substantially to 0.2μm. Although the 0.2μm value is fairly low, it may be possible to use such a film in integrated circuits as well. Further increase in the curing temperature leads to a very low fracture strain for

* An analysis along the lines of what is presented in Section 5.1.3 can be used to understand the influence of cure temperature on critical thickness for Methyl-T resin.

films across the entire thickness range. The low fracture strain in these cases may be associated with chemical degradation of the material. In the future, to access superior properties at higher cure temperatures for Methyl-T resin, molecular engineering by PDMS incorporation can be pursued to increase its inherent deformation ability. PDMS based toughening has been previously carried out for bulk Methyl-T resin.[57]

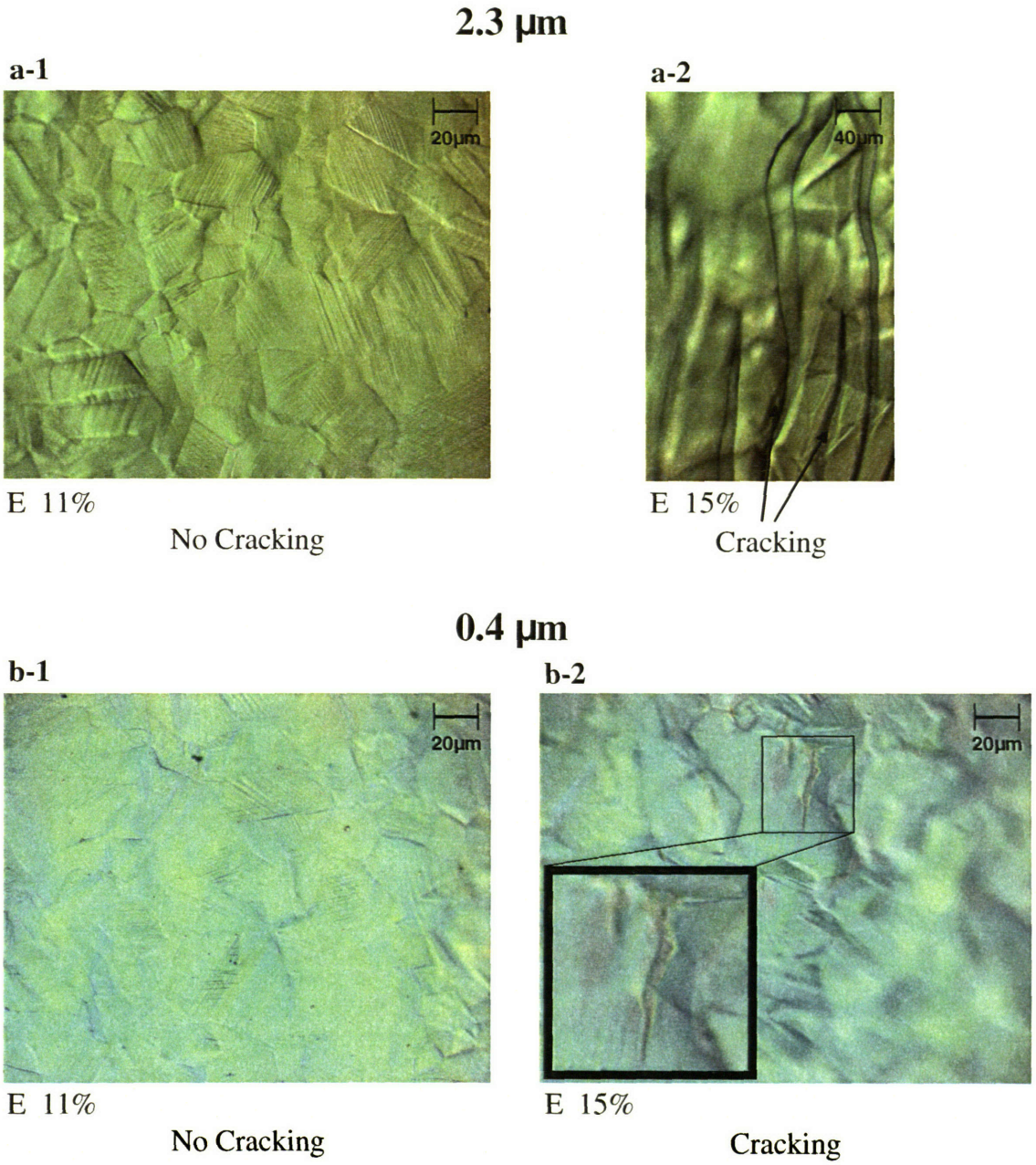

Figure 7-1 Micrographs from bending tests carried out on Methyl-T resin films cured at a temperature of 250°C. A stainless steel substrate is used. (a-1) No cracking is observed in a 2.3µm thick film at 11% strain. Stainless steel grain structure is visible. (a-2) Ductile cracks observed in 2.3µm film at 15.0% strain. Cracks extend ~100µm across. (b-1) No cracking observed in 0.4µm film at 11.0% strain. Stainless steel grain structure is visible. (b-2) Ductile cracks observed in a 0.4µm film at 15.0% strain. A magnified picture of the crack is shown in the inset.

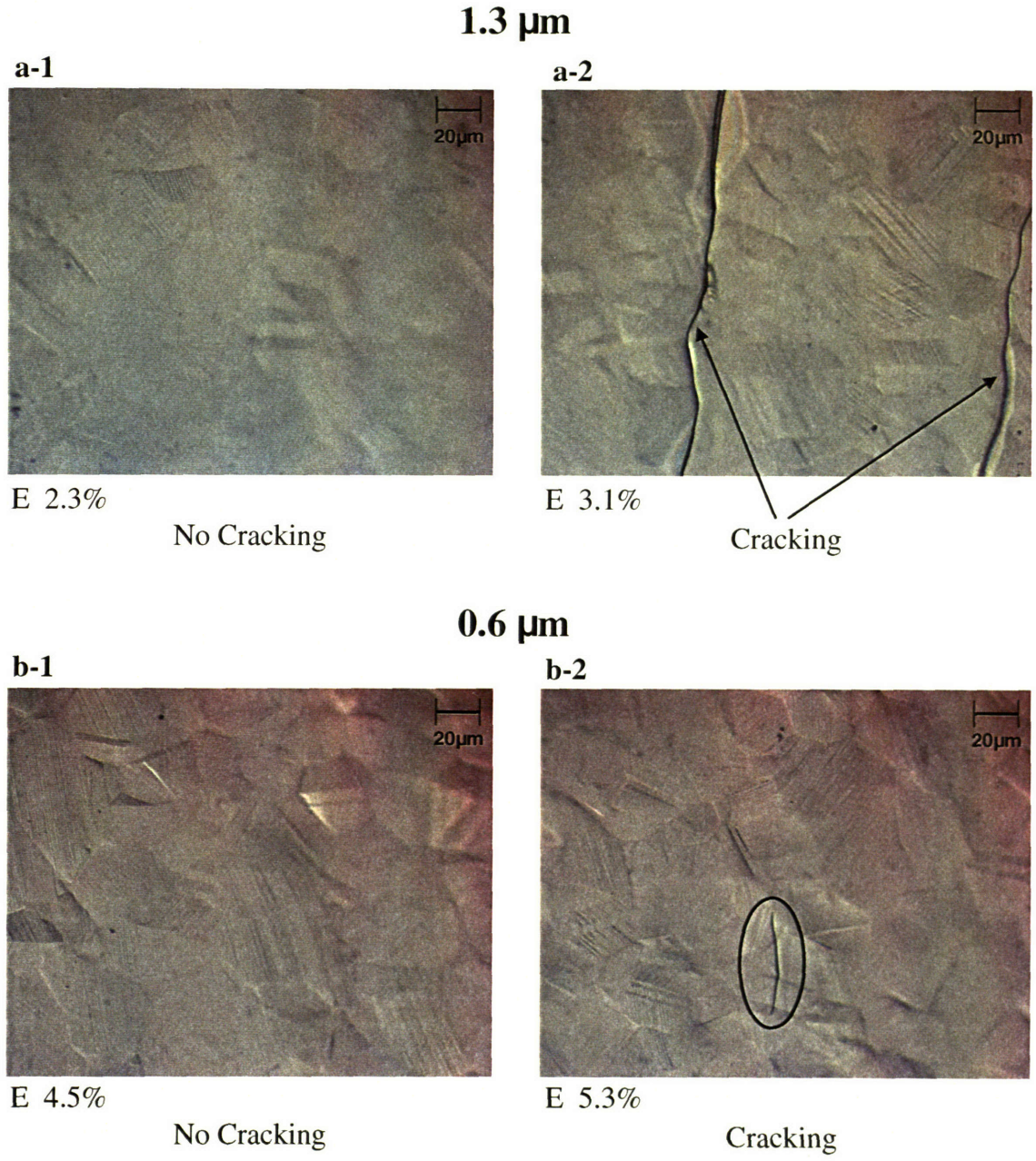

Figure 7-2 Micrographs from bending tests carried out on Methyl-T resin films cured at a temperature of 275°C. A stainless steel substrate is used. (a-1) No cracking observed in a 1.3µm thick film at 2.3% strain. Stainless steel grain structure is visible. (a-2) Brittle cracking observed in a 1.3µm thick film at 3.1% strain. Crack spans the entire vertical dimension of the micrograph with a length of at least 1mm. (b-1) No cracking observed in 0.6µm film at 4.5% strain. Stainless steel grain structure is visible. (b-2) Cracking observed in a 0.6µm film at 5.3% strain. Crack length is ~20-30µm.

0.4 μm

c-1

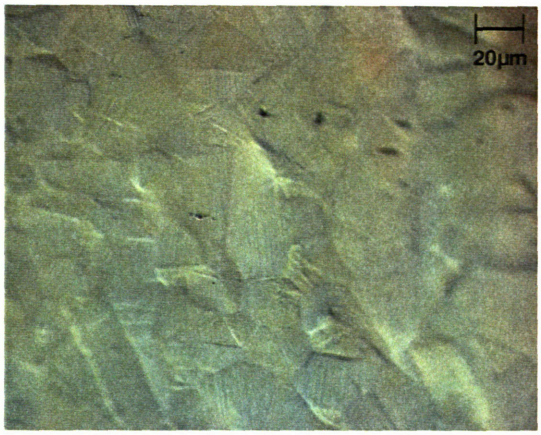

E 6.3%

No Cracking

c-2

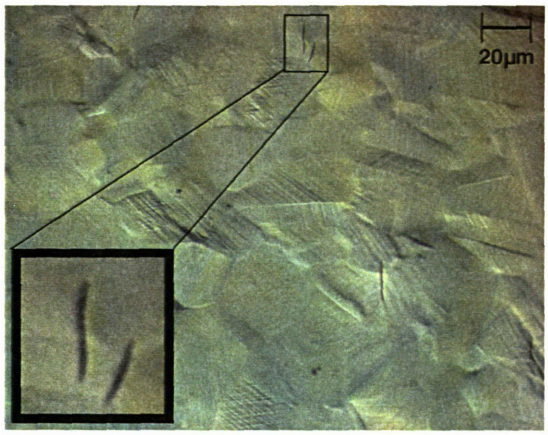

E 7.9%

Cracking

0.2 μm

d-1

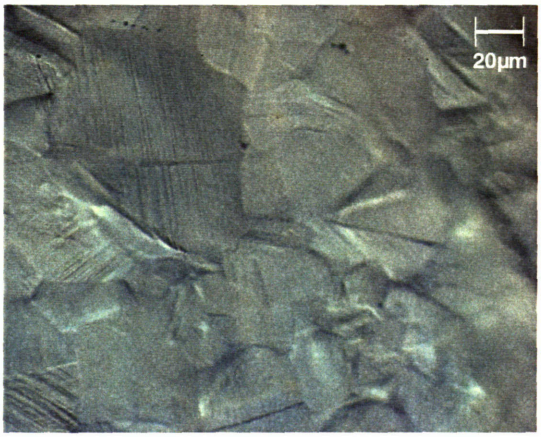

E 11.0%

No Cracking

d-2

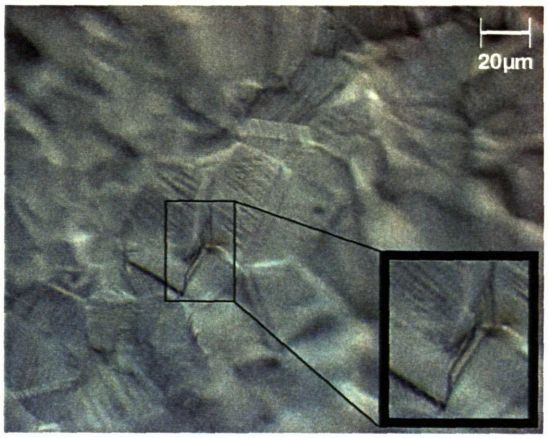

E 14.5%

Cracking

Figure 7-2 Methyl-T resin films cured at a temperature of 275°C. (c-1) No cracking observed in a 0.4μm thick film at 6.3% strain. Stainless steel grain structure is visible. (c-2) Cracking observed in a 0.4μm thick film at 7.9% strain. A magnified view of the cracks is shown in the inset. Crack length is ~10-20μm. (d-1) No cracking observed in 0.2μm film at 11% strain. Stainless steel grain structure is visible. (d-2) Ductile cracks observed in a 0.2μm film at 14.5% strain. Crack length is ~20μm.

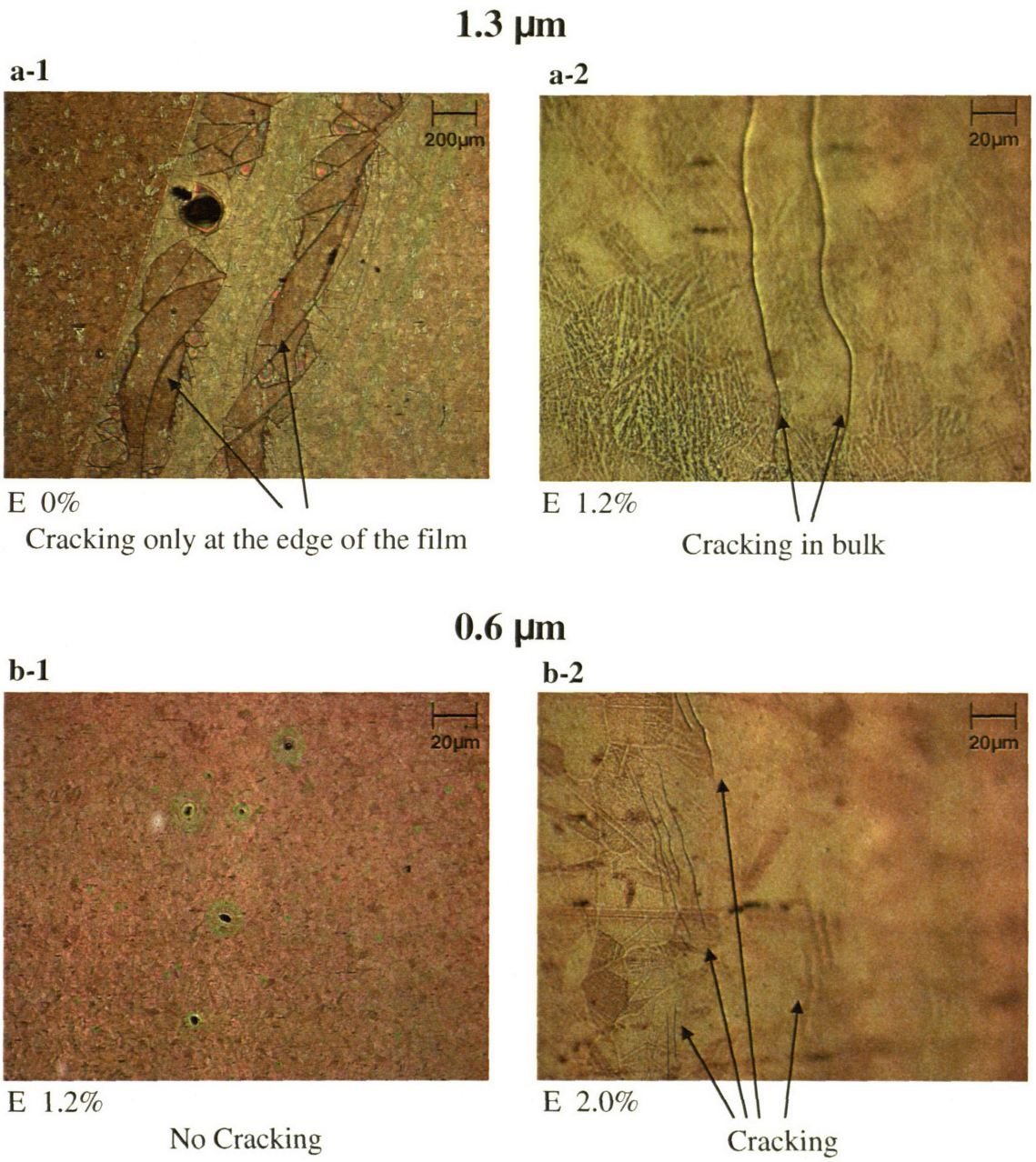

Figure 7-3 Micrographs from bending tests carried out on Methyl-T resin films cured at a temperature of 450°C. A stainless steel substrate is used. (a-1) Micrograph shows the film edge for a 1.3µm film prior to strain application. No cracking is observed in the inner region of the film. Cracks are observed at the film edge. (a-2) Brittle cracking observed in the inner region of the 1.3µm thick film at 1.2% strain. Crack length is at least 100µm. (b-1) No cracking observed in 0.6µm film at 1.2% strain. Grain structure of the stainless steel is visible. (b-2) Cracking observed in a 0.6µm film at 2.0% strain. The region on the right side of the film is out of focus. Crack length is ~40µm.

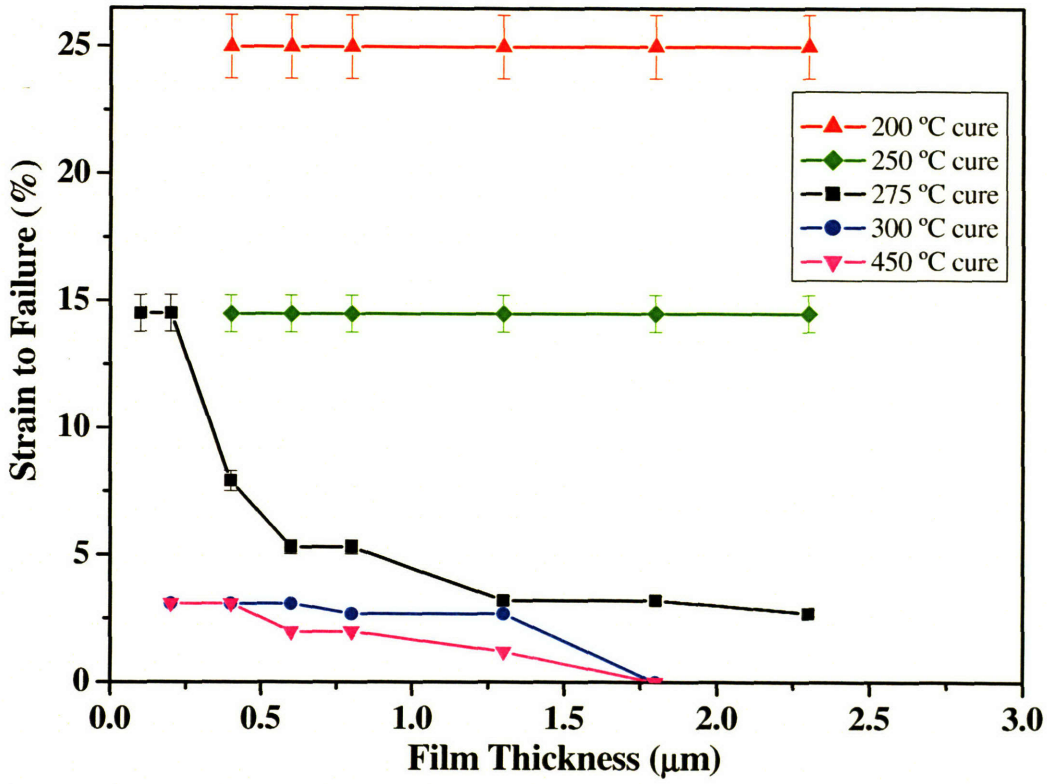

Figure 7-4 Strain to failure as a function of film thickness for Methyl-T resin cured at five different cure temperatures. For films cured at 200°C, a consistent 25% strain to failure is observed for the entire thickness range tested. For films cured at 250°C, the observed strain to failure across all thicknesses is 15%. For 275°C cure temperature, a critical thickness value of ~0.2μm is observed with a strain to failure of 15%. No critical thickness effects are observed in films cured at 300°C and 450°C. (Error bars for all plots are according to the analysis presented in Section 3.1.2.)

8 C-resin Results

The C-resin is a group of commercial optical coatings manufactured by SDC Technologies Corporation. These optical coatings are used in several industrial applications for abrasion resistance, impact resistance, index matching and optical clarity. The C-resin can be applied on a number of substrate materials including polycarbonate, stainless steel and acrylic materials for applications such as safety glasses, contact lenses and automotive parts.

Detailed information on composition and structure of C-resin is not available.* C-resin structure is known[85] to be a silicone thermoset matrix (polysiloxane) with a large amount of silica particles embedded within. Since the structure of the C-resin is rather similar to silica, these polymers are optically transparent. With regard to mechanical properties, the C-resin is highly brittle. The fracture toughness of C-resins, when used in bulk form, is nearly equal to that of silica. However, the C-resin shows excellent mechanical properties in thin film form. C-resin is being studied to ascertain whether the high film fracture toughness for this material can be ascribed to the critical thickness phenomenon.

8.1 Critical Thickness Results

8.1.1 Thin Film Fabrication

Two C-resins are being studied. The first resin is named the MP-101 resin. The other resin is named PF-1202. Both these resins are available pre-dissolved in a volumetrically

* C-resin is a proprietary commercial coating.

known mixture of organic liquids/acids.* To dilute the solution appropriate solvents in the same volumetric ratio as present in the original mixture are added. Film samples of different thickness (range of thickness is 0.1μm – 3μm) of these resins are prepared on two different substrates: stainless steel and polycarbonate. Spin coating is carried out for one minute at 1300 RPM for films prepared on stainless steel substrate. For films prepared on polycarbonate substrate a spin speed of 2500 RPM is used. An acceleration of 425 revolutions/min^2 is used in both cases. The film thickness is measured using a profilometer; the values for film thickness and the corresponding dilution ratios are presented in Appendix F.

The film is cured according to the following temperature cycle: First, the temperature is increased at a rate of 5°C/min to reach the final desired cure temperature. The films are then allowed to stay at this temperature for three hours. The films are then cooled to room temperature at a rate of 3°C /min.

8.1.2 Bending Test Results for PF-1202

The curing temperature used for PF-1202 resin is 130°C. This curing temperature is selected based on the recommendation provided by the manufacturer. Optical micrographs of the bending tests carried out for PF-1202 are presented in this section.

First, the bending test results of the PF-1202 resin on polycarbonate substrate are presented (Figure 8-1). A 1.2μm film is observed to sustain a strain of 2.9% as seen in

* MP-101 solution composition: Water:12-14%, Methanol:30-32%, Isopropanol:20-22%, Acetic Acid: 3-4%, (Solids 31-33%).
PF-1202 solution composition: Water:12-15%, Methanol:7-9%, Ethanol:28-31%, PM Glycol Ether: 21-24%, (Solids 21-23%).

Figure 8-1(a-1) and fails at a strain of 4% (Figure 8-1(a-2)). Large brittle cracks which span at least 1mm are observed. Next, a 0.3μm film is observed to sustain a 4.8% strain (Figure 8-1(b-1)) and fails at 6% strain (Figure 8-1(b-2)). Cracks in this film are much smaller than those observed in the 1.2μm film. The crack length in this case is ~100μm. Finally, a 0.1μm film is observed to sustain a strain of 6.8% (Figure 8-1(c-1)). Fracture in this film occurs at 7.9% strain with a crack length of ~50μm (Figure 8-1(c-1)).

In Figure 8-2, the optical micrographs for the bending tests of PF-1202 fabricated on stainless steel are presented. A 1.2μm film prior to the application of strain is shown in Figure 8-2(a-1). This film is observed to crack at 3.6% strain (Figure 8-2(a-2)). A thinner film of 0.3μm is observed to sustain a much higher strain of 6.1% (Figure 8-2(b-1)). This film fails at 7.1% strain (Figure 8-2(b-2)). The observed crack length is ~50μm.

The bending test results for the PF-1202 resin are summarized in Figure 8-3. The strain to failure is plotted as a function of film thickness. Measured strain to failure values properties are observed to be similar for PF-1202 films prepared on either of the two substrates. For both cases, the solid line depicts the highest strain sustained at a particular film thickness. The dashed line depicts the next incremental strain level at which failure is observed. At higher thicknesses (0.5μm and beyond), the strain to failure is low (<2%) indicating brittle behavior. In the 0.2-0.5μm thickness range, the strain to failure value increases from 3% to about 7-8%. Below 0.2μm, the strain to failure is much higher (>8%). Based on these results, a critical thickness of ~0.2μm is determined for PF-1202.

8.1.3 Bending Test Results for MP-101

MP-101 critical thickness measurements are carried out using bending tests. For MP-101, the influence of cure temperatures on the fracture strain is also investigated. Cure temperatures range from room temperature to 400°C. The bending results are presented in Figure 8-4. For room temperature cure, the strain to failure value increases gradually from 1-2% for a 1μm film to ~8% for a 0.2μm film. When cured at a temperature of 50°C, the fracture performance of the MP-101 improves significantly. The strain to failure reaches 8-9% for a film thickness of 0.6μm. A critical thickness value of 0.6μm is therefore determined based on the bending tests. When the curing temperature is increased further, to 100°C, the fracture performance slightly deteriorates. At this temperature, a gradual increase in failure strain takes place, from 2% for a 3μm film to about 7-8% for a 0.3μm film. As the curing temperature is increased to 200°C and beyond, progressively further degradation in fracture properties is observed. The critical thickness at a 200°C cure temperature is approximately 0.1-0.2μm with a 4-5% failure strain. At 300°C and 400°C cure temperatures, the fracture strain values are greatly diminished over the entire range of film thickness.*

8.2 Summary

The C-resin experimental results have shown that a critical thickness of ~0.2μm is observed for the PF-1202 resin. For the MP-101 resin a critical thickness of ~0.6μm is achieved. In both PF-1202 and MP-101, the strain to failure below the critical thickness is

* An analysis along the lines of what is presented in Section 5.1.3 can be used to analytically understand the influence of cure temperature on critical thickness of MP-101.

approximately 8-10%. This high strain to failure is a significant improvement over thick films by a factor of ~4-5. These results confirm that the C-resin thin film fracture properties make them suitable materials for commercial coatings.

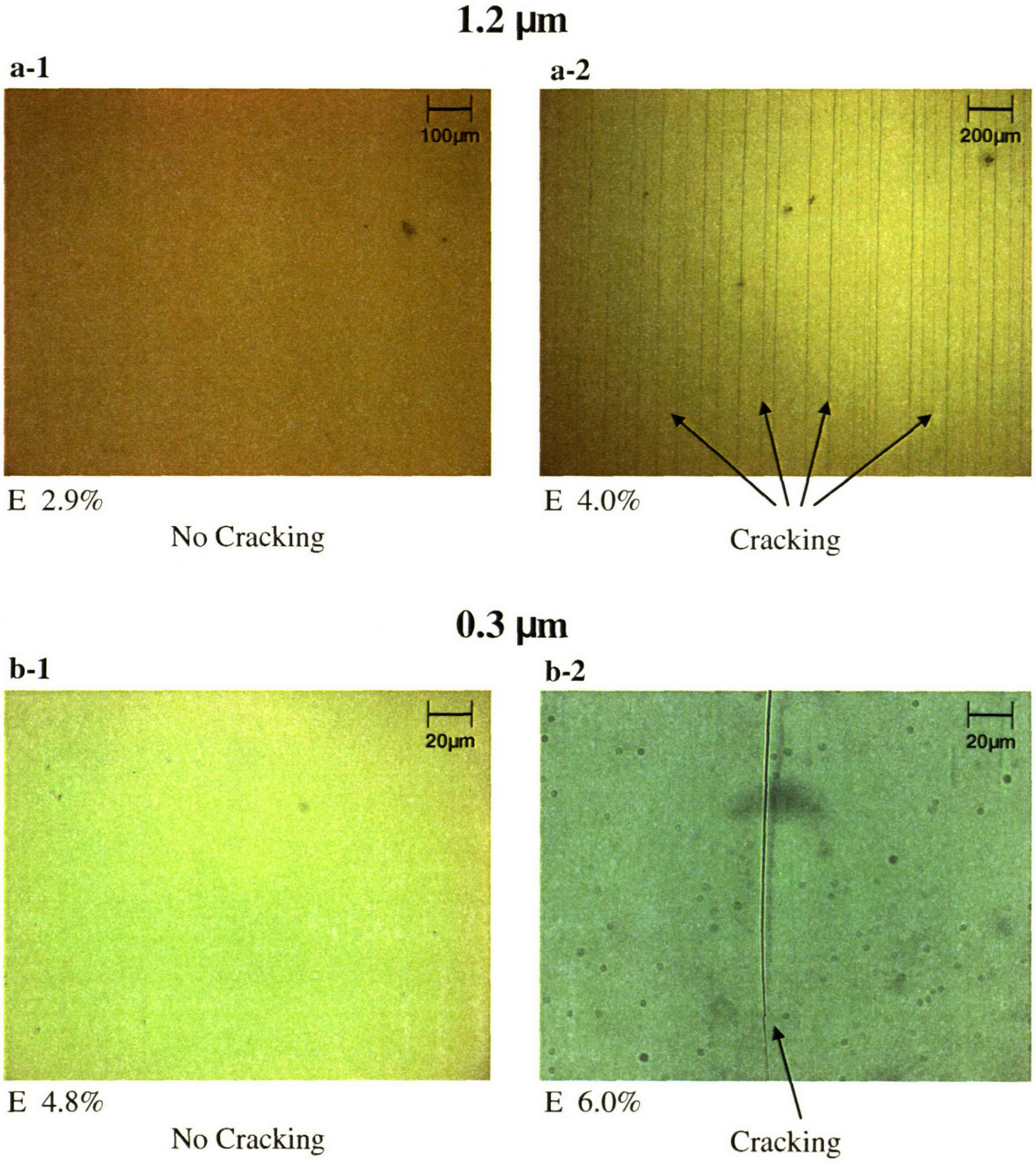

Figure 8-1 Micrographs from bending test results for PF1202 resin cured at 130°C. A polycarbonate substrate is used. (a-1) No cracking in a 1.2μm thick film at 2.9% strain. Small black spots in the micrographs are dust particles. (a-2) Brittle cracking observed in a 1.2μm thick film at 4.0% strain. Crack length is at least 1mm. (b-1) No cracking observed in 0.3μm film at 4.8% strain. (b-2) Cracking observed in a 0.3μm film at 6.0% strain.

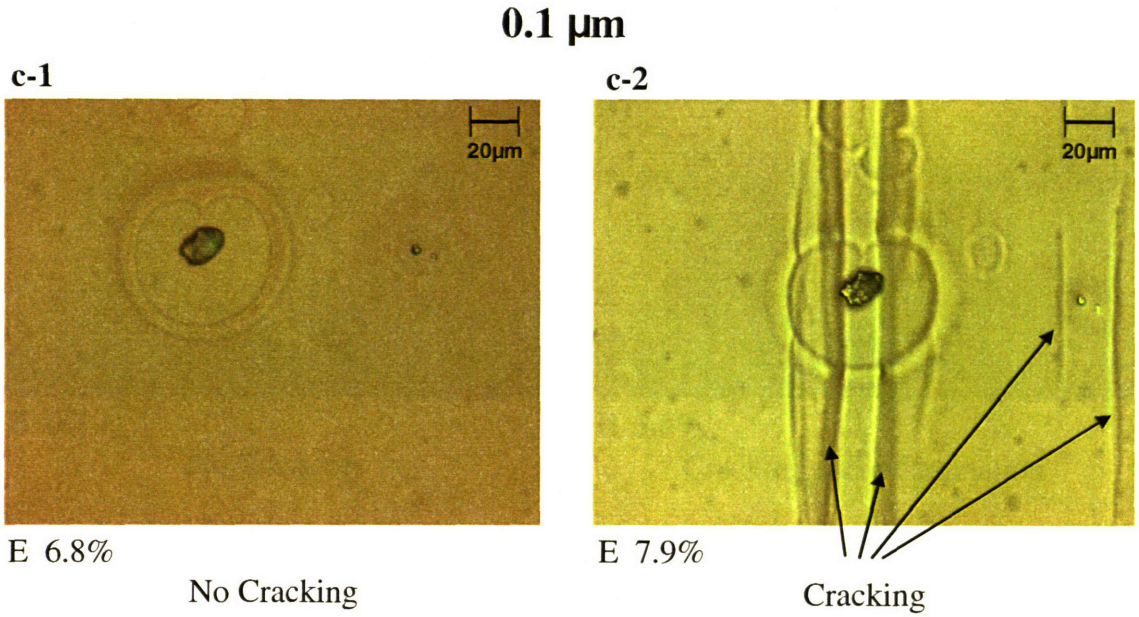

Figure 8-1 PF1202 resin cured at 130°C. (c-1) No cracking in a 0.1μm thick film at 6.8% strain. A large dust particle is observed within the film. (c-2) Cracking observed in a 0.1μm thick film at 7.9% strain. (Note: This picture is discussed previously in Section 3.1.3.)

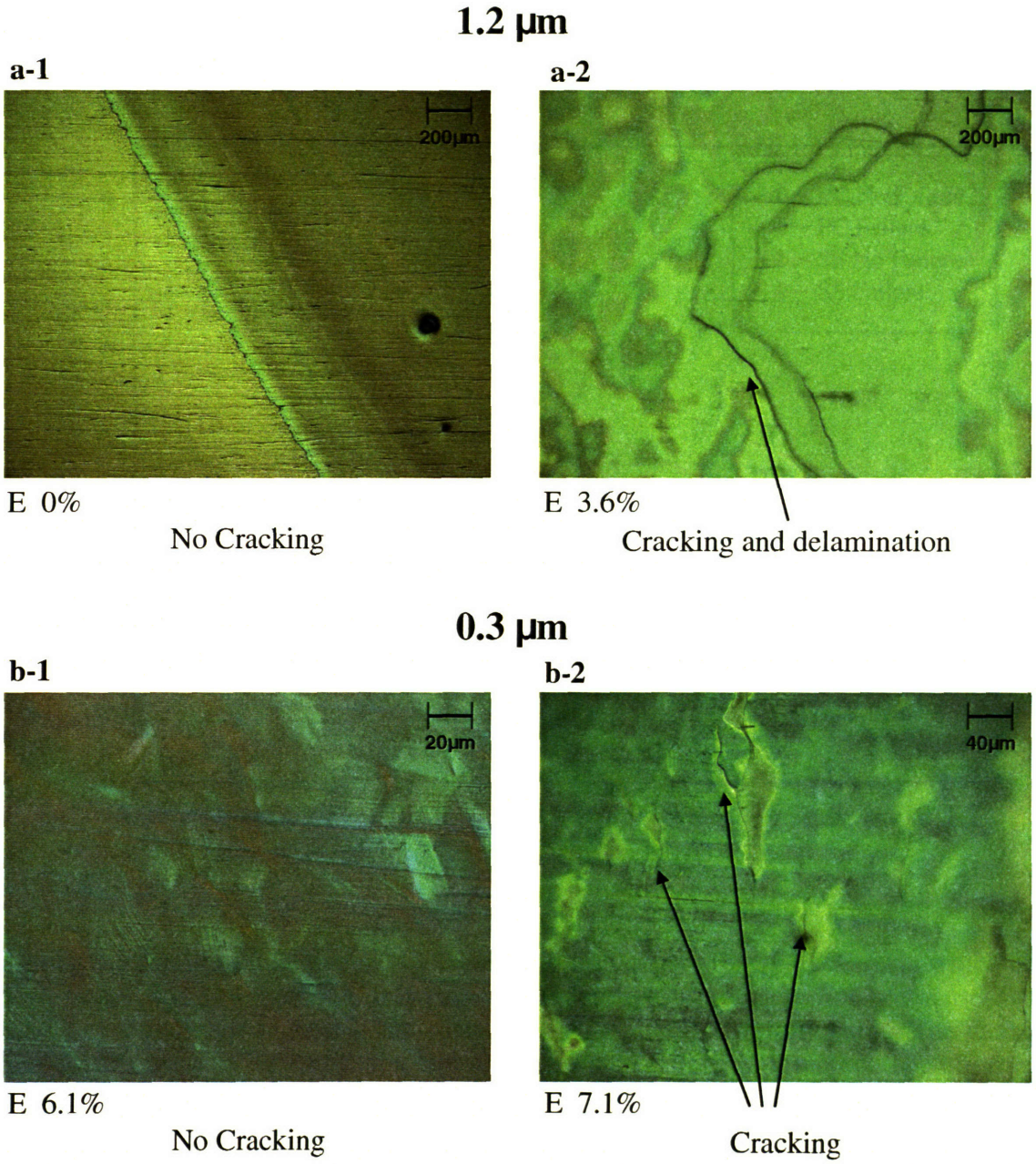

Figure 8-2 Micrographs from bending test results for PF1202 resin cured at 130°C. A stainless steel substrate is used. (a-1) A 1.2µm film is shown prior to strain application. (a-2) Brittle cracking observed in a 1.2µm film at a strain of 3.6%. Delamination of the film is also observed. (b-1) No cracking observed in 0.3µm film at 6.1% strain. Stainless steel grain structure is visible. (b-2) Cracking is observed in a 0.3µm film at 7.1% strain. The crack length is ~40µm.

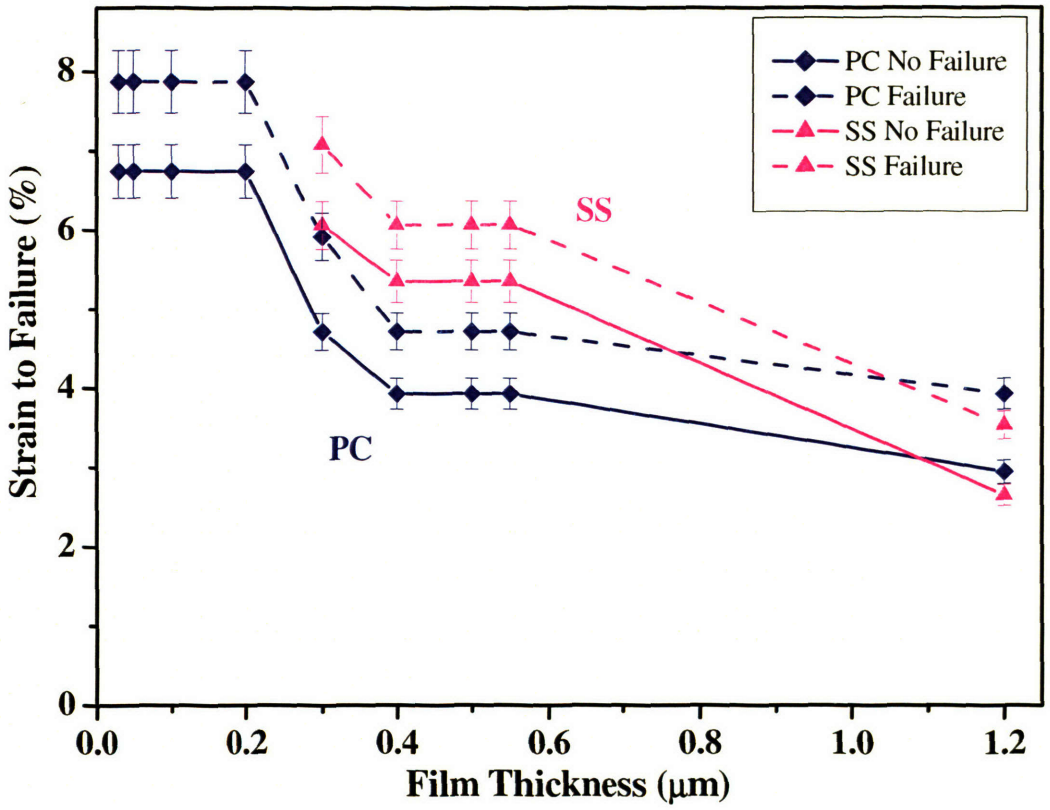

Figure 8-3 Strain to fracture as a function of film thickness for PF-1202 resin which has been tested using two substrates: stainless steel and polycarbonate. For both cases, the solid line depicts the highest strain sustained at a particular film thickness. The dashed line depicts the next incremental strain level at which failure is observed. The observed critical thickness is 0.2μm. The highest value of fracture strain as observed on films (below critical thickness) prepared on stainless steel is ~8%. (Error bars for all plots are according to the analysis presented in Section 3.1.2.)

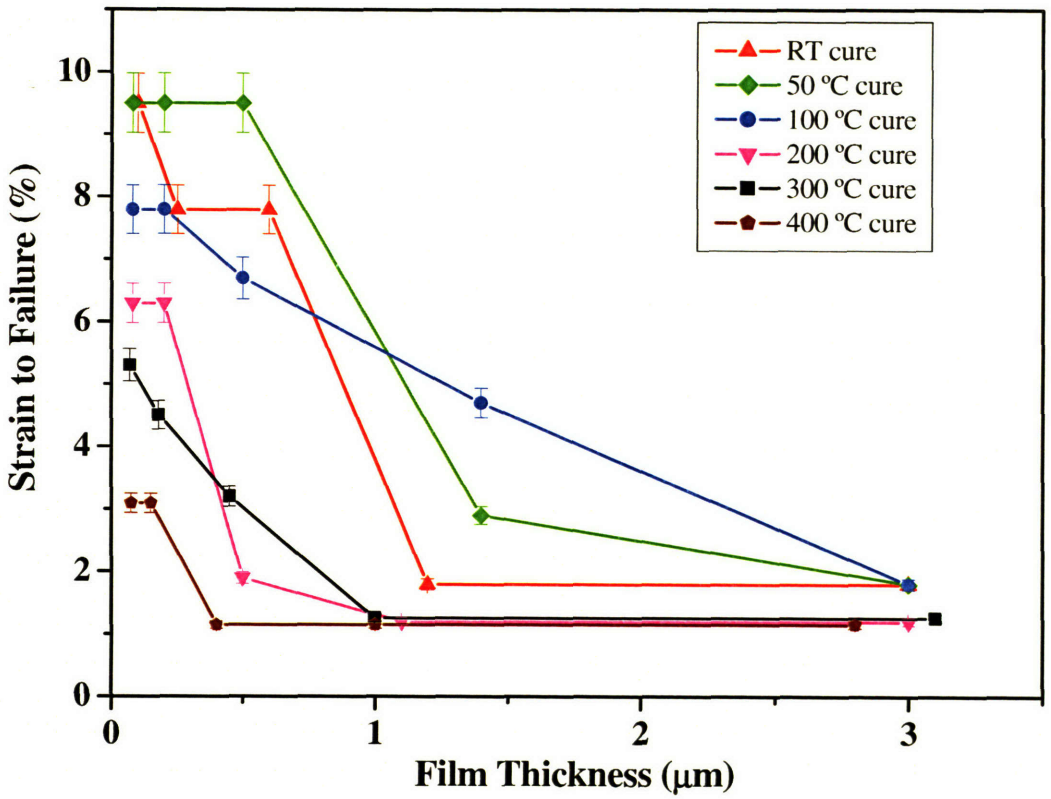

Figure 8-4 Strain to failure as a function of film thickness for MP-101 resin for several cure temperatures. For room temperature cure, the strain to failure shows a gradual transition across the entire range of film thickness. At a cure temperature of 50°C, the observed critical thickness is ~0.6μm with a strain to failure of ~9-10%. For 100°C curing, a gradual transition in failure strain is observed as a function of film thickness. The critical thickness at a 200°C cure temperature is observed to be ~0.1-0.2μm with a 4-5% failure strain. At 300°C and 400°C cure temperatures, the fracture strain values are observed to greatly reduce over the entire range of film thickness. (Error bars for all plots are according to the analysis presented in Section 3.1.2.)

9 Conclusions

The focus of this thesis has been to use critical thickness effects to achieve high fracture toughness in macroscopically brittle polymers. The most significant outcome of this work has been the direct validation of critical thickness phenomenon using thin films of several chosen brittle polymers. In previously published results, critical thickness is inferred through indirect experimental methods in which local thinning of polymers is achieved within a bulk polymer. With the direct experimental evidence presented in this thesis, the critical thickness hypothesis is substantiated to a much greater extent. This work has not only opened up several new avenues for research relating to critical thickness and polymer intrinsic deformation mechanisms but is also expected to impact polymer toughening approaches in industry. Commercially, critical thickness can be exploited to achieve fracture toughness in brittle polymers since this technique is generalized and not material specific unlike current techniques. The non-material specificity of critical thickness can greatly eliminate detailed materials chemistry studies and provide a simplified approach to polymer toughening.

To analytically describe critical thickness, two models are developed in this thesis. The first model utilizes an energy approach according to which a crack does not initiate if the crack driving force is less than the crack resistance. Such a condition is shown to be true for a brittle polymer at critical thickness. The second model is based on mechanics and is a refinement of a previously presented model. The criterion of critical thickness according to this model is that a minimum film thickness is required for typical fracture features like crazes to exist within it. These models predict a fairly accurate value for the

critical thickness when compared against experimental data. According to these models, critical thickness is a monotonically increasing function of network density. This trend is opposite to what is typically observed in bulk materials where fracture toughness decreases with increase in network density. Such a result is of significance in thermosets since they have an extremely high network density and are therefore expected to have a high critical thickness. Also, using models, it is shown that critical thickness has very little dependence on temperature below the softening temperature of the polymer.

In this thesis, critical thickness has been experimentally determined for polystyrene and silicone thermosets. A new method to measure critical thickness has been developed. The experimentally determined critical thickness for polystyrene is ~0.1μm with a strain to failure >15% (bulk failure strain is 2%). For silicones, it is shown that the critical thickness is much higher. A silicone resin which is commercially used as a laminate binder (4-3136) is experimentally determined to have a critical thickness of ~5μm with a strain to failure of ~13% (bulk strain to failure <2%). Molecular modification of this resin using functionalized PDMS is shown to increase the critical thickness of the resin to ~10μm. A high temperature silicone resin (Methyl-T) is shown to have a critical thickness of over 2.3μm with a strain to failure of 15% when cured at 250°C. Commercial optical coatings called C-resins are also shown to exhibit critical thickness. Although, these results are not surprising since critical thickness is postulated as a fundamental polymer property, the detailed characterization of critical thickness on a number of polymers affirms that the postulate is valid and applicable to brittle polymers in general. In the future extensive experimental investigations may not be necessary to

quantify critical thickness for every brittle polymer. Analytical models can be used to predict critical thickness.

Through this study several aspects of silicone resins come to light. The intrinsic deformation ability of these polymers is much superior to what has been ascribed to them in past. Clearly, with critical thickness in the 10μm range and a >15% strain to failure, 4-3136 qualifies as a ductile material. Therefore it suggests that bulk fracture properties of these materials are dominated more so by extrinsic fracture features thereby causing them to be much more brittle than typical carbon chain polymers. The significant improvement in fracture toughness for these silicones by a simple reduction in the size scale has several implications. Till now, the low fracture toughness of these silicones has not allowed them to be used widely. With the demonstration of high failure strains in these materials, it will now be possible to utilize these polymers for commercial applications. Now truly, the silicone thermosets can be championed as materials which combine heat and oxidation resistance of glass with the versatility of plastics. The most direct use of these materials is as coatings. Use of these materials in fibers, multilayers and structural plastics is also envisioned.

In the future, several potential avenues for research exist. The next step would be to test for critical thickness phenomenon on unsupported polymer films. Such a task is extremely challenging because of difficulty in fabrication of unsupported films at these thicknesses, handling of such films as well as failure strain measurements. Another major avenue for research is to study variation of characteristic properties (designated as secondary properties in this thesis) like glass transition temperature, crosslink density, molecular orientation and birefringence as a function of film thickness. Studying these

properties would improve understanding of the intrinsic deformation mechanisms in polymers at length scales below the critical thickness. Engineering tasks include designing methods so that critical thickness effects can be used in practical applications. Suggested applications are formation of fibers and multilayers. Another engineering task would be to devise new methods to improve deformation capability within polymers through molecular engineering methods described in this thesis.

Appendix A

Substrate Material and Substrate Thickness Selection

There are several criteria which govern substrate selection amongst which the following are the most important:

1. The ability of the substrate to flex to a reasonable strain value is a necessary requirement for bending and elongation experiments. This requirement precludes the choice of certain commonly used substrates like silicon and glass.
2. The substrate must be inert to the solvent being used for spin coating. For all the materials in this study (except the C-resin), toluene and methyl-isobutyl-ketone (MIBK) are been determined as the most appropriate solvents. Most polymers are not inert to these two solvents and are therefore not suitable. An exception is polysulfone which is inert to MIBK. Polysulfone has been used as a substrate for making polystyrene thin films. C-resin solvents are a combination of organic liquids and acids which are inert to stainless steel as well as polycarbonate.
3. Fabrication of high quality uniform thickness thin films in the micron to sub micron range should be possible atop the selected substrate.

Based on these requirements, a high deformation stainless steel (#8 mirror polish) is chosen as a suitable substrate. Stainless steel is inert to organic solvents and mild acids. Stainless steel, as experimentally determined, allows fabrication of high quality films atop it. The other substrates that have been chosen are polysulfone and silver which have been exclusively used in polystyrene critical thickness experiments. For C-resin, polycarbonate has been used as a substrate in addition to stainless steel.

Substrate thickness is another important factor for these experiments. The following points must be considered:

1. The substrate should be easily bent by hand for bending experiments. For example, a stainless steel coupon with a thickness greater than 1.5mm would be extremely difficult to bend by hand.
2. The substrate should be thick enough to provide sufficient strain when bent partially or fully. For example, a 1mm thick material allows for the application of approximately 25-30% strain when fully bent.

Based on these two requirements, a 1mm thick stainless steel substrate is chosen. A 1.5mm thick polycarbonate, silver and polysulfone substrates are chosen.

Appendix B

Polystyrene Thin Films: Solution Concentration vs. Film Thickness

Table 1: Polystyrene film thickness as a function of the solution concentration used for spin coating

Substrate: Stainless Steel
Solvent: Toluene

Solution Conc. (gm/l)	Film Thickness (μm)
1.0	0.07
1.5	0.11
2.0	0.18
2.5	0.21
3.0	0.28
3.5	0.34
4.0	0.45
6.0	1.5

Substrate: Polysulfone
Solvent: MIBK

Solution Conc. (gm/l)	Film Thickness (μm)
1.0	0.08
1.5	0.13
2.0	0.17
2.5	0.21
3.0	0.25
3.5	0.29
4.0	0.33

Substrate: Silver
Solvent: MIBK

Solution Conc. (gm/l)	Film Thickness (μm)
1.0	0.08
2.0	0.15
4.0	0.3

Appendix C

4-3136 Thin Films: Solution Concentration vs. Film Thickness

Table 2: 4-3136 film thickness as a function of the solution concentration used for spin coating

Substrate: Stainless Steel
Solvent: MIBK

Solution Conc. (gm/l)	Film Thickness (μm)
10	0.7
20	1.5
30	2.5
40	3.2
50	4.0
75	7.0
100	8.0
150	12.0

Appendix D

Engineered 4-3136 Thin Films: Solution Concentration vs. Film Thickness

Table 3: Engineered 4-3136 film thickness as a function of the solution concentration used for spin coating

Substrate: Stainless Steel
Solvent: MIBK

Solution Conc. (gm/l)	Film Thickness (μm)
10	0.7
20	1.6
30	2.5
40	3.2
50	4.0
75	7.2
100	8
125	10
150	12
200	16

Appendix E

Methyl-T Resin Thin Films: Solution Concentration vs. Film Thickness

Table 4: Methyl-T resin film thickness as a function of the solution concentration used for spin coating

Substrate: Stainless Steel
Solvent: Toluene

Solution Conc. (gm/l)	Film Thickness (μm)
5	0.1
10	0.2
20	0.4
30	0.6
40	0.8
50	1.3
75	1.8
100	2.3

Appendix F

C-Resin Thin Films: Solution Concentration vs. Film Thickness

Table 5: C-resin film thickness as a function of the solution concentration used for spin coating

Substrate: Polycarbonate
Material: PF1202

Dilution ratio (%)	Film Thickness (μm)
100	6.0
50	3.0
16	1.0
9	0.55
4.5	0.28
1.0	0.06

Substrate: Stainless Steel
Material: MP 101

Dilution ratio (%)	Film Thickness (μm)
100	3.0
50	1.2
25	0.65
10	0.24
5	0.12

References

1 Young R.J., Introduction to Polymers, Chapman and Hill, 1982.

2 Jaffe M., Chenevey E., Cooper W., Glick M., Haider M.I. and Rafalko J., Makromolekulare Chemie-Macromolecular Symposia, 53, 1992, p163.

3 Ulrich D.R., Polymers for Nonlinear Optical Applications: Molecular Crystals and Liquid Crystals, 189, 1990, p3.

4 Dawson D.J., Fleming W.W., Lyerla J.R. and Economy J., ACS Symposium Series, 282, 1985, p63.

5 Yoda N. and Hiramoto H., Journal of Macromolecular Science-Chemistry, A21 (13-1), 1984, p1641.

6 Langer R., MRS Bulletin, 20, 1995, p18.

7 Peppas N.A. and Sefton M.Y., Polymers as Biomaterials - Preface Biomaterials, 11 (9), 1990, p611.

8 Shahinpoor M. and Kim K.J., Journal of Ionic Polymer-Metal Composites: i. Fundamentals Smart Materials & Structures, 10 (4), 2001, p819.

9 Ellis W.D., Wood-Polymer Composites, 353, 2000, p75.

10 Krevelen, D.W.V., Properties of Polymers, New York, Elsevier, 1976.

11 Tadmor Z. and Gogos C.G., Principles of Polymer Processing, Wiley, New York, 1979.

12 Tadmor Z., Plastics Rubber and Composites, 33 (1), 2004, p3.

13 Vandersanden M.C.M., Meijer H.E.H. and Lemstra P.J., Polymer, 34 (10), 1993, p2148.

14 Vandersanden M.C.M., Ultimate Toughness of Amorphous Polymers, PhD thesis, Eindhoven University of Technology, Eindhoven, Netherlands, 1993.

15 An Introduction to Silicon Based Materials, http://www.dowcorning.com, Dow Corning Corporation.

16 Arends C.B., Polymer Toughening, Marcel Dekker Inc., New York, 1989.

17 Keith R. and Kinloch A.J., Toughened Plastics I : Novel Approaches in Science and Engineering, Advances in Chemistry Series, 233, 1996.

18 Keith R. and Kinloch A.J., Toughened Plastics II : Novel Approaches in Science and Engineering, Advances in Chemistry Series, 252, 1996.

19 Ham S., Plastics engineering, 57 (6), 2001, p46.

20 Ashbee K.H.G., Fundamental Principles of Fiber Reinforced Composites, Lancaster, Technomic Publishing Company, c1989.

21 Mcgarry F.J. and Rosner R.B., Rubber Toughened Plastics, ACS Advances in Chemistry Series, 233, 1993, p305.

22 Sultan J.N. and Mcgarry F.J., Polymer Engineering Science, 13, 1973, p29.

23 Yanagese A., Ito M., Yamamoto N. and Ishikawa M., Journal of Applied Polymer Science, 62, 1996, p1387.

24 Gebizlioglu O.S., Argon A. S. and Cohen R.E., Polymer, 26, 1985, p529.

25 Lowell P.A., Mcdonald J., Saunders D.E.J. and Young R.J., Polymer, 34, 1993, p61.

26 Das B., Gangopadhyay T. and Sinha S., Journal of Applied Polymer Science, 54, 1994, p367.

27 Tanrattanakul V., Baer E., Hiltner A., Hu R., Dimonie V.L., Elaasser M.S., Sperling L.H. and Mylonakis S.G., Journal of Applied Polymer Science, 62 (12), 1996, p2005.

28 Bucknall C.B., Soares V.L.P., Yang H.H. and Zhang X.C., Macromolecular Symposia, 101, 1996, p265.

29 Dear J.P., Journal of Materials Science, 38 (5), 2003, p891.

30 Thom H., Composites part A-Applied Science and Manufacturing, 29 (8), 1998, p869.

31 Meyer L.H., Cherney E.A. and Jayaram S.H., IEEE Electrical Insulation Magazine, 20 (4), 2004, p31.

32 Alan S.W., Plasticizers: Principles and Practice, The Institute of Materials, The University Press, Cambridge, 1995.

33 Kinloch A.J. and Shaw S.J., Polymer, 24, 1983, p1355.

34 Yamini S. and Young R.J., Journal of Materials Science, 15, 1980, p1823.

35 Williams J.G., Stress Analysis of Polymers, Longman, London, 1977, p242.

36 Griffith A.A., Philosophical Transactions Royal Society, A221, 1920, p163.

37 Zhu B., Toughening of Rigid Silicone Resins, PhD thesis, Massachusetts Institute of Technology, Cambridge, 1997.

38 Kaji M., Nakahara K. and Ogami K., Journal of Applied Polymer Science, 75 (4), 2000, p528.

39 Angola J.C., Fujita Y. and Sakai T., Journal of Polymer Science part B-Polymer Physics 26 (4), 1988, p807.

40 Karger-Kocsis J., Polymer Bulletin, 36, 1996, p119.

41 Kramer E.J., Advances in Polymer Science, 52-53, 1983, p1.

42 Vandersanden M.C.M., Meijer H.E.H. and Tervoort T.A., Polymer, 34 (14), 1993, p2961.

43 Vandersanden M.C.M. and Meijer H.E.H., Polymer, 34 (24), 1993, p5063.

44 Vandersanden M.C.M., Buijs L.G.C., Debie F.O. and Meijer H.E.H., Polymer, 35 (13), 1994, p2783.

45 Vandersanden M.C.M. and Meijer H.E.H., Polymer, 35 (13), 1994, p2774.

46 Vandersanden M.C.M. and Meijer H.E.H., Polymer, 35 (14), 1994, p2991.

47 Vandersanden M.C.M., Dekok J.M.M. and Meijer H.E.H., Polymer, 35 (14), 1994, p2995.

48 Krupenkin T.N. and Fredrickson G.H., Macromolecules, 32 (15), 1999, p5029.

49 Krupenkin T.N. and Fredrickson G.H., Macromolecules, 32 (15), 1999, p5036.

50 Rascio V.J.D., Corrosion Reviews, 18 (2-3), 2000, p133.

51 Lork A. and Vissac T., Surface Coatings International part B-Coatings Transactions, 87 (1), 2004, p41.

52 Warrick E.L., Forty Years of Firsts: The Recollections of a Dow Corning Pioneer, Mcgraw-Hill, New York, 1990, p20.

53 Arimitsu K., Kobayashi H., Furutani M., Gunji T., Abe Y. and Ichimura K., Journal of Photopolymer Science and Technology, 17 (1), 2004, p19.

54 Colombo P., Perini K., Bernardo E., Capelletti T. and Macagnan G., Journal of the American Ceramic Society, 86 (6), 2003, p1025.

55 Zhu B., Katsoulis D.E., Keryk J.R. and Mcgarry F.J., Polymer, 41, 2000, p7559.

56 Li Z., High Fracture Toughness and High Modulus Silicone Resins, PhD thesis, Massachusetts Institute of Technology, 2000.

57 Zhu B., Katsoulis D.E., Keryk J.R. and Mcgarry F.J., Macromolecules, 37 (4), 2004, p1455.

58 Prevorse D.C., Harget P.J., Sharma R.K. and Reimschu A.C., Journal of Macromolecular Science-Physics B, 8 (1-2), 1973, p127.

59 Brody H., Journal of Macromolecular Science-Physics B, 22 (1), 1983, p19.

60 Donald A.M. and Kramer E.J., Journal of Polymer Science Part B-Polymer Physics, 20 (5), 1982, p899.

61 Henkee C.S. and Kramer E.J., Journal of Polymer Science Part B-Polymer Physics, 22 (4), 1984, p721.

62 Ward I.M., Mechanical Properties of Solid Polymers, New York, Wiley, 1983.

63 Haward R.N., The Physics of Glassy Polymers: Materials Science and Technology, New York, London, Applied Science Publishers, 1973.

64 Lauterwasser B.D. and Kramer E.J., Philosophical Magazine A-Physics of Condensed Matter Structure Defects and Mechanical properties, 39 (4), 1979, p469.

65 Suo Z., Fracture in Thin Films, Encyclopedia of Materials: Science & Technology, Second Edition, Elsevier Science, 2001.

66 Prest W.M. and Porter R.S., Journal of Polymer Science, (A-2) 10, 1972, p1639.

67 Miller P. and Kramer E.J., Journal of Materials Science, 26, 1991, p1459.

68 Kramer E.J. and Berger L.L., Advances in Polymer Science, 91/92, 1990, p1.

69 Eyring H., Journal of Chemical Physics, 4, 1936, p283.

70 Bhushan B., Nanomechanical Properties of Solid Surfaces and Thin Films, Handbook of Micro/Nanotribology, CRC Press, 1999.

71 Bartczak Z., Argon A.S., Cohen R.E., and Weinberg M., Polymer, 40, (1999), p2331.

72 Conner R.D., Johnson W.L., Paton N.E. and Nix W.D., Journal of Applied Physics, 94 (2), 2003, p904.

73 Chen Z., Cotterell B. and Wang W., Engineering Fracture Mechanics, 69 (5), 2002, p597.

74 Chen Z., Cotterell B., Wang W., Guenther E. and Chua S.J., Thin Solid Films, 394 (1-2), 2001, p202.

75 Suo Z., Ma E.Y., Gleskova H. and Wagner S., Applied Physics Letters, 74 (8), 1999, p1177.

76 Timoshenko S. and Woinowsky-Kreiger S., Theory of Plates and Shells, McGraw-Hill, New York, 1959.

77 Technical Data Sheet, Allegheny Ludlum Corporation, Pittsburgh, PA.

78 Crist B., Annual Review of Materials Science, 25, 1995, p295.

79 Ree M., Chu C.W. and Goldberg M.J., Journal of Applied Physics, 75 (3), 1994, p1410.

80 Mirabella F.M., Applied Spectroscopy 42 (7), 1988, p1258.

81 Zbinden R., Infrared Spectroscopy of High Polymers, Academic Press, New York and London, 1964.

82 Fakhraai Z., Sharp J.S. and Forrest J.A., Journal of Polymer Science part B–Polymer Physics, 42 (24), 2004, p4503.

83 Cusano A., Persiano G.V., Russo M. and Giordano M., IEEE Sensors Journal, 4 (6), 2004, p837.

84 Satorius A., Critical Thickness in Silicone Polymers, SM thesis, Massachusetts Institute of Technology, 2003.

85 Mcgarry F.J., Personal Communication.